**Doctoral Dissertation**

# Development of Photo-induced Ultrafast DNA Duplex Invasion and its Applications

# （光誘起形超高速 DNA 二重鎖侵入法の開発とその応用）

ZUMILA Hailili

Supervisor: Fujimoto Kenzo

Division of Advanced Science and Technology

Japan Advanced Institute of Science and Technology

Materials Science

March 2026

## Abstract

In this dissertation, I investigated the engineering of novel photochemical strategies for the sequence-specific recognition and manipulation of double-stranded DNA. Accessing genetic information within the stable DNA double helix remains a primary challenge in molecular biology due to the significant thermodynamic and kinetic barriers presented by Watson-Crick base pairing. While existing technologies like PNA and LNA can invade the duplex, they often require prolonged incubation times, elevated temperatures, or complex designs to achieve high efficiency.

The research centers on the application of 3-cyanovinylcarbazole nucleoside, $^{CNV}$K, an ultra-fast photo-cross-linker capable of forming a covalent bond with a complementary pyrimidine base within one second of UV irradiation at 366 nm. First, focusing on Photo-induced Double Duplex Invasion (pDDI), a pair of invasion probes containing both $^{CNV}$K and 5-cyanouridine ($^{C}$U) was utilized as the photo-cross-linker and photo-cross-linking inhibitor. The result showed successful invasion of the probes. However, with the unexpected discovery of the invasion difference between the paired Forward and Reverse probe, we speculate the possibility of achieving Photo-induced Duplex Invasion (pDI) with a single invasion probe. With a systematic analysis via Job's plots , we confirmed the invasion independence of the paired invasion probes. This discovery led to the development of Photo-induced Duplex Invasion (pDI). And the result showed that pDI achieved superior invasion efficiencies, exceeding 90% in just 60 seconds of photo-irradiation.

Finally, we further applied the photochemical principles to dynamic DNA nanotechnology by constructing a Photo-induced DNA Memory Gate. Driven by toehold-mediated strand displacement (TMSD), this device utilizes the rapid cross-linking of $^{CNV}$K to lock the gate into specific "Written" or "Blocked" states based on the order of data inputs. By converting reversible equilibrium reactions into irreversible kinetic traps, this motif overcomes the inherent instability of traditional DNA logic circuits.

Overall, this work establishes $^{CNV}$K -mediated photo-cross-linking as a versatile kinetic driver for DNA manipulation. These findings lay the groundwork for a new class of photo-antigene therapeutics and stateful molecular robotics capable of recording complex biological events with high spatiotemporal precision.



Keywords: 3-cyanovinylcarbazole nucleoside, photo-cross-linker, double-duplex invasion, duplex-invasion, DNA logic circuit, DNA computing

**Acknowledgment**

First, I would like to express my great gratitude to my honorable supervisor Professor Dr. Fujimoto Kenzo for his valuable notes and remarks, continuous support, great patience, and supervision throughout my Masters' and Doctoral' study. I want to thank him for introducing me to this topic, providing me guidance through the whole learning and researching process. I cannot have accomplished my thesis without him. I greatly acknowledge the academic support and constructive advice of my second supervisor Professor Dr. Takamura Yuzuru, and my supervisor for the minor research project Associate Professor Dr. Hamada Tsutomu, for their support and guidance.

I would also like to thank Dr. Nakamura Shigetaka, Dr. Watanabe Yasuha, Dr. Sethi Siddhant, Dr. Mo Junling for teaching me all the essential techniques, providing me advice during my research process. And lots of thanks to all my seniors and Lab-mates for helping me out whenever I had problems, and for their company during my stay.

Finally, I would like to thank my family for their emotional and financial support during my research life in a foreign country. I could not have come this far without their support and encouragement. Thank you.

ZUMILA HAILILI

JAIST, Ishikawa, Japan

List of Figures:

Figure 1. The structure of DNA helix. ..... 13
Figure 2. Zinc Finger Nucleases (ZFNs), Transcription Activator-Like Effector Nucleases (TALENs), and CRISPR/Cas9..... 15
Figure 3. Triplex forming oligonucleotides (TFOs)..... 16
Figure 4. Chemical structure of Peptide Nucleic Acids (a) and Locked Nucleic Acids (b)..... 17
Figure 5. DNA molecular engineering. ..... 19
Figure 6. Reversible photoisomerization of azobenzene. ..... 20
Figure 7. The reversible photoisomerization between the closed-loop form spiropyran and the open-loop form merocyanine. ..... 21
Figure 8. Photoisomerization of diarylethenes and stilbenes. ..... 21
Figure 9. Chemical structure of Psoralen (a) and Coumarin (b). ..... 22
Figure 10. 3-cyanovinylcarbazole nucleoside ($^{CNV}$K). ..... 23
Figure 11. 3-cyanovinylcarbazole nucleoside ($^{CNV}$K). a). Chemical structure of 3-cyanovinylcarbazole nucleoside ($^{CNV}$K). b). Photo-chemical properties of $^{CNV}$K: $^{CNV}$K can photo-cross-link with the pyridine base in its complementary strand at -1 position under 366 nm UV-irradiation in 1 second and can photo-split under 312 nm UV-irradiation. ..... 36
Figure 12. Schematic of photo-induced double duplex invasion (pDDI). $^{C}$U prohibits inter-probe cross-linking between the paired invading probes. ..... 38
Figure 13. Chemical structure of 5-cyanouridine ($^{C}$U). ..... 38
Figure 14. The recognition areas and photo-cross-linking sites of KU invasion probes. K is $^{CNV}$K and U is $^{C}$U, the lightening mark denotes photo-cross-linking, cross-linking site in the template strand is underlined. ..... 41
Figure 15. pDDI efficiency of KU invading probes towards 400-mer template DNA. a). 8% denaturing PAGE reflecting the pDDI efficiency of both sets of probes. Lane M: 100-bp DNA ladder; lane 1: 400-mer template DNA with 100 molar access of Set1-KU-Fw and Set1-KU-Rev probes incubated at 37°C for 60 mins; lane 2: Lane 1 with photo-irradiated at 385 nm for 1 min; ; lane 3: 400-mer template DNA with 100 molar access of Set2-KU-Fw and Set2-KU-Rev probes incubated at 37°C for 60 mins; lane 4: Lane 3 with photo-irradiated at 385 nm for 1 min;. b). pDDI efficiency of the probes. Data are presented as the mean ± SD. ..... 43
Figure 16. Inter- and intra- probe cross-linking of the KU probes. a). Lane 1: Marker; Lane 2: Set 1-KU Fw and Set1-KU-Rev probes incubated at 37 °C for 60 min; Lane 3: lane 2+0.1 sec 385 nm irradiation; Lane 4: lane 2+0.2 sec 385 nm irradiation; Lane 5: lane 2+0.5 sec 385 nm irradiation; Lane 6: lane 2+1 sec 385 nm irradiation; Lane 7: lane 2+10 sec 385 nm irradiation; Lane 8: lane 2+60 sec 385

nm irradiation; Lane 9: lane 2+300 sec 385 nm irradiation. b). same as a) of Set2-KU probes. ..... 44
Figure 17. Ultra-fast feature of pDDI with Set 2-KU probes. a). 8% denaturing PAGE reflecting the ultra-fast feature of pDI using Set 2-KU probes with a photo-irradiation time-course analysis. Invasion conditions: [template DNA] = 25 nM, [probe ODN] = 2.5 μM (100-eq. relative to template DNA) at 37°C for 60 minutes then photo irradiated at 385 nm. b). Ultra-fast kinetics of the $^{CNV}$K-mediated pDI. The pDI reaction with Set 1-KT-Fw probe is monitored over a time interval of (0 s, 0.1 s, 0.2 s, 0.5 s, 1s, 10 s, 60 s and 300 s) with other conditions unchanged. The invasion efficiency is reflected by the conversion rate of 400- mer Template DNA. The result showed the invasion efficiency of Set 2-KU probes reached 80% after only 1 second of photo-irradiation. Data are presented as the mean ± SD. ..... 45
Figure 18. pDDI efficiency of KU invading probes. a). 8% denaturing PAGE reflecting the pDDI efficiency of Set 1-KU probes. Lane M: 100-bp DNA ladder; lane 1-2: 200-mer//190-mer template only; lane 3-4: 200-mer template DNA with Set1-KU-Fw probe; lane 5-6: 190-mer template DNA with Set1-KU-Rev probe; lane 7-8: 200-mer//190-mer dsDNA with both Set1-KU-Fw and Set1-KU-Rev probes. Invasion conditions: [template DNA] = 100 nM, [probe ODN] = 10 μM (100-eq. with respect to the template DNA) at 37°C for 60 mins then photo-irradiated at 385 nm for 1 min. b). Same as (a), reflecting the pDDI efficiency of Set 2-KU probes. c). pDDI efficiency of the probes. Data are presented as the mean ± SD. ..... 46
Figure 19. Job's plot investigating the invasion independence of pDDI. a). 8% denaturing PAGE reflecting the invasion independence of the Set1-KU probes. Lane M: 100-bp DNA ladder; lane 1-2: 200-mer//190-mer template only; lane 3-4: 200-mer//190-mer dsDNA with Forward:Reverse probe at 100:0 ratio; lane 5-6: 200-mer//190-mer dsDNA with Forward:Reverse probe at 75:25 ratio; lane 7-8: 200-mer//190-mer dsDNA Forward:Reverse probe at 50:50 ratio; lane 9-10: 200-mer//190-mer dsDNA with Forward:Reverse probe at 25:75 ratio; lane 11-12: 200-mer//190-mer dsDNA with Forward:Reverse probe at 0:100 ratio. 100 nM ds template DNA incubated at 37°C for 60 minutes after adding the probes, then photo-irradiated at 385 nm for 1 min. b). Same as (a), reflecting that of Set2-KU probes. c). Job's plot reflecting the invasion independence of KU probes. Data are presented as the mean ± SD. ..... 48
Figure 20. Schematic of photo-induced duplex invasion (pDI) with single invading probe containing only the photo-cross-linker $^{CNV}$K. ..... 55
Figure 21. The recognition areas and photo-cross-linking sites of KT invasion probes. KT probes share the same recognition area and cross-linking site as KU probes, $^{C}$U in KU sets replaced by T in KT sets. K is $^{CNV}$K and the lightening mark

denotes photo-cross-linking, cross-linking site in the template strand is underlined. ..... 56
Figure 22. pDI efficiency. a). 8% denaturing PAGE reflecting the pDI efficiency of Set 1-KT and Set 1-KU probes. Lane M: 100-bp DNA ladder; lane 1-2: 200-mer // 190-mer template only; lane 3-4: 200-mer // 190-mer ds DNA with Set1 KT-Fw probe; lane 5-6: 200-mer // 190-mer ds DNA with Set 1-KU-Fw probe; lane 7-8: 200-mer // 190-mer ds DNA with Set 1-KT-Rev probe; lane 9-10: 200-mer // 190-mer ds DNA with Set 1-KU-Rev probe. Invasion conditions: [template DNA] = 100 nM, [probe ODN] = 10 uM (100-eq. relative to template DNA) at 37°C for 60 minutes then photo irradiated at 385 nm for 1 min. b). Same as (a), reflecting the pDI efficiency of Set 2. c). pDI efficiency of the probes. Data are presented as the mean ± SD. ..... 58
Figure 23. Normalized Abs. at 260 nm and the calculated melting temperature of both sets. ODN-Fw is natural ODN that does not contain $^{CNV}$K or $^{C}$U..... 59
Figure 24. Ultra-fast feature of pDI (Set 1-KT-Fw). a). 8% denaturing PAGE reflecting the ultra-fast feature of pDI using Set 1-KT-Fw probe with a photo-irradiation time-course analysis. Invasion conditions: [template DNA] = 100 nM, [probe ODN] = 10 μM (100-eq. relative to template DNA) at 37°C for 60 minutes then photo irradiated at 385 nm. b). Ultra-fast kinetics of the $^{CNV}$K-mediated pDI. The pDI reaction with Set 1-KT-Fw probe is monitored over a time interval of (0 s, 0.1 s, 0.2 s, 0.5 s, 1s, 10 s, 30 s, 60 s and 300 s) with other conditions unchanged. The invasion efficiency is reflected by the conversion rate of Fw-Template (200 mer). The result showed the invasion efficiency of Set 1-KT-Fw probe exceeded 75% after only 1 second of photo-irradiation. Data are presented as the mean ± SD. ..... 60
Figure 25. Ultra-fast feature of pDI (Set 2-KT-Fw). a). 8% denaturing PAGE reflecting the ultra-fast feature of pDI using Set 2-KT-Fw probe with a photo-irradiation time-course analysis. Invasion conditions: [template DNA] = 100 nM, [probe ODN] = 10 μM (100-eq. relative to template DNA) at 37°C for 60 minutes then photo irradiated at 385 nm. b). Ultra-fast kinetics of the $^{CNV}$K-mediated pDI. The pDI reaction with Set 2-KT-Fw probe is monitored over a time interval of (0 s, 0.1 s, 0.2 s, 0.5 s, 1s, 10 s, 30 s, 60 s and 300 s) with other conditions unchanged. The invasion efficiency is reflected by the conversion rate of Fw-Template (200 mer). The result showed the invasion efficiency of Set 2-KT-Fw probe exceeded 40% after only 1 second of photo-irradiation. Data are presented as the mean ± SD. ..... 61
Figure 26. Incubation time-course analysis using Set 1-KT-Fw. a). 8% denaturing PAGE reflecting the ultra-fast feature of pDI using Set 1-KT-Fw probe with incubation time-course analysis. Invasion conditions: [template DNA] = 100 nM, [probe ODN] = 10 μM (100-eq. relative to template DNA) at 37°C for a various time

intervals, then photo irradiated at 385 nm for 1 s. b). Ultra-fast kinetics of the $^{CNV}$K-mediated pDI. The incubation duration after adding Set 1-KT-Fw probe is monitored over a time interval of (0 min, 1 min, 5 min, 10 min, 30 min and 60 min), following 1 s of photo-irradiation under 385 nm. The invasion efficiency is reflected by the conversion rate of Fw-Template (200 mer). Data are presented as the mean ± SD. ..... 62
Figure 27. pDI concentration analysis of Set 1-KT-Fw probe. a). 8% denaturing PAGE reflecting the pDI efficiency over a varies of probe concentration using Set 1-KT-Fw probe. Invasion conditions: [template DNA] = 100 nM, after adding the probe the mixture is incubated at 37°C for 60 min, then photo irradiated at 385 nm for 1 s. b). The invasion efficiency of Set 1-KT-Fw probe at different concentration condition. Invasion efficiency is reflected by the conversion rate of Fw-Template (200 mer). Data are presented as the mean ± SD. ..... 63
Figure 28. Comparison of probe length in pDI. a). 8% denaturing PAGE result. Invasion conditions: [template DNA] = 100 nM, [probe ODN] = 10 μM (100-eq. of template DNA) at 37°C for 60 minutes then photo irradiated at 385 nm for 1 min. b). Conversion rate of invasion probes of different length. Data are presented as the mean ± SD..... 64
Figure 29. 8% denaturing PAGE Demonstrating the reversibility of pDI. Concentration conditions: [template DNA] = 100 nM, [probe ODN] = 10 μM (100-eq. of template DNA). a). Invasion (photo-cross-linking) and photo-splitting condition: ds template DNA and probe ODN was incubated at 37°C for 60 minutes then photo irradiated at 385 nm for 1 min, photo-splitting group underwent 312 nm photo-irradiation after the photo-cross-linking. b). Invasion (photo-cross-linking) after photo-splitting. Lane 2: pDI procedure; Lane 3: 20 min of 312 nm photo-irradiation of Lane 2; Lane 4: 1 min of 385 nm photo-irradiation of Lane 3. ..... 65
Figure 30. Ion dependence of the probe. 8% denaturing PAGE demonstrating the pDI efficiency under different buffer condition using Set 2-KT-Fw probe. Invasion conditions: [template DNA] = 100 nM, [probe ODN] = 10 μM (100-eq. of template DNA) at 37°C for 60 minutes then photo irradiated at 385 nm for 1 min. ..... 66
Figure 31. Photo-induced DNA memory gate transition..... 71
Figure 32. Toehold mediated strand displacement reaction. ..... 72
Figure 33. $^{CNV}$K in accelerating toehold mediated strand displacement reaction. a). DNA strand displacement reaction accelerated by ultrafast DNA photo-cross-linking through inhibition of the backward branch migration. b). The effect of photo energy on photo-cross-linking rate. c). The effect of insertion position of $^{CNV}$K on strand displacement reaction. ..... 73

Figure 34. Schematic of the simple 2-input photo-induced memory gate transition. a). When Data strands were added into the Memory gate in sequential order, both Data 1 and Data 2 cross-links with the hairpin structure under photo-irradiation, fully opens the hairpin gate and transit from the Unwritten State to the Written State. b). When Data strands were added into the Memory gate in reverse order, Data 2 cross-links with the hairpin structure and inhibits the cross-linking of Data 1 to the memory gate, transiting the gate to the Blocked State..... 74
Figure 35. 15% denaturing PAGE result of the photo-induced gate transition at 1:1 Gate: Data ratio. Lane 1: Memory gate only; Lane 2: Memory gate + Data 1; Lane 3: Memory gate + Data 2; Lane 4: Data strands added in sequential order; Lane 5: Data strands added in reverse order. ..... 76
Figure 36. 15% denaturing PAGE result of the photo-induced gate transition at 1:2 Gate: Data ratio. Lane 1: Memory gate only; Lane 2: Memory gate + Data 1; Lane 3: Memory gate + Data 2; Lane 4: Memory gate + mixture of both Data strands; Lane 5: Data strands added in sequential order; Lane 6: Data strands added in reverse order. ..... 77
Figure 37. 15% Native PAGE result of Photo-ON and Photo-OFF experiments. Lane 1: Memory gate only. Lane 2 ~ Lane 6 are Photo-ON condition. Lane 2: Memory gate + Data 1; Lane 3: Memory gate + Data 2; Lane 4: Memory gate + mixture of both Data strands; Lane 5: Data strands added in sequential order; Lane 6: Data strands added in reverse order. Lane 7 ~ Lane 11 are same as Lane 2 ~ Lane 6, under Photo-OFF condition..... 79
Figure 38. Photo-induced memory gate transition under short photo-irradiation. a). 15% Denaturing PAGE result. Lane 1: Memory gate only; Lane 2: Memory gate + Data 1; Lane 3: Memory gate + Data 2; Lane 4: Data strands added in sequential order; Lane 6: Data strands added in reverse order. Same for Lane 6 and 7, Lane 8 and 9, Lane 10 and 11. Mixtures were photo-irradiated every time after adding the corresponding Data strand, photo-irradiation duration is noted on each lane. b). 15% Native PAGE result. ..... 80

List of Tables:

Table 1. Template DNA sequence. ..... 40
Table 2. pDDI invading probe sequence. ..... 41
Table 3. pDI invading probe sequence. ..... 56
Table 4. Probes used for comparison of probe length in pDI ..... 64
Table 5. Buffer Conditions. ..... 66
Table 6. Sequences used in this section. ..... 75

# Table of Contents


*Chapter 1 General Introduction ..... 12*

**1.1 Deoxyribonucleic Acid (DNA) ..... 12**

**1.2 Strategies for Sequence-Specific Recognition of Double-Stranded DNA ... 13**

1.2.1 Protein-Based Recognition ..... 14

1.2.2 Oligonucleotide-Based Recognition ..... 15

**1.3 Dynamic DNA Nanotechnology ..... 17**

**1.4 Photo-Responsive DNA Technologies ..... 19**

1.4.1 Azobenzene ..... 19

1.4.2 Spiropyran ..... 20

1.4.3 Diarylethene and Stilbene ..... 21

1.4.4 Psoralen and Coumarin ..... 22

1.4.5 3-Cyanovinylcarbazole Nucleoside ($^{CNV}$K) ..... 23

**1.5 Research Objectives and Outline ..... 23**

**1.6 Reference: ..... 25**

*Chapter 2 Photo-induced Double Duplex Invasion (pDDI) ..... 34*

**2.1 Background ..... 34**

**2.2 3-Cyanovinylcarbazole nucleoside ($^{CNV}$K) ..... 36**

**2.3 Schematic of photo-induced double duplex invasion (pDDI) ..... 37**

**2.4 Material and methods ..... 38**

**2.5 Result and Discussion ..... 42**

2.5.1 pDDI towards 400-mer Template DNA ..... 42

2.5.2 pDDI efficiency of the KU invasion probes ..... 45

2.5.3 Invasion independence of the probes in photo-induced double-duplex invasion (pDDI) 47

2.5.4 Discussion ..... 49

**2.6 Reference: ..... 50**

*Chapter 3 Photo-induced Duplex Invasion (pDI) ..... 54*

**3.1 Background ..... 54**

**3.2 Schematic of photo-induced duplex invasion (pDI) ..... 54**

**3.3 Material and methods ..... 55**

**3.4 Result and Discussion ..... 57**

3.4.1 pDI efficiency of the invasion probes ..... 57

3.4.2 The ultra-fast kinetics of pDI ..... 59

3.4.3 Concentration analysis of pDI ..... 62

3.4.4 Probe Length ..... 63
3.4.5 Reversibility and Reusability ..... 64
3.4.6 Ion Dependence ..... 65
3.4.7 Discussion ..... 66
**3.5 Reference: ..... 68**
***Chapter 4 Photo-induced DNA Memory Gate Transition ..... 70***
**4.1 Background ..... 70**
**4.2 Schematic of photo-induced DNA Memory Gate Transition ..... 71**
**4.3 Material and Methods ..... 74**
**4.4 Results and discussions ..... 75**
4.4.1 Photo-induced memory gate transition ..... 75
4.4.2 The significance of $^{CNV}$K in memory gate transition ..... 78
4.4.3 Ultra-fast kinetics of photo-induced memory gate transition ..... 79
4.4.4 Discussion ..... 80
**4.5 Reference: ..... 82**
***Chapter 5 Conclusion ..... 84***
**5.1 General Conclusion ..... 84**
**5.2 Future Perspectives ..... 85**
***List of Publications ..... 87***
**Articles: ..... 87**
**International Conferences (7 presentations): ..... 87**
**Domestic Conferences (21 presentations): ..... 88**
***Appendix ..... 91***
**I. Experiment Instruments ..... 91**
**II. Experiment Reagents ..... 92**
**III. Scheme for synthesizing of $^{CNV}$K-amidite ..... 97**
**IV. Scheme for synthesizing of Trifluorothymidine ($^{TF}$T) / $^{C}$U-amidite ..... 99**
**V. ODN Purification ..... 100**

# Chapter 1 General Introduction

## 1.1 Deoxyribonucleic Acid (DNA)

Deoxyribonucleic Acid (DNA) serves as the fundamental repository of genetic information for all life organisms. Its sequence encodes the instructions required for the development, function, growth, and reproduction of all cellular life. The central dogma of molecular biology describes the directional flow of this genetic information: DNA is transcribed into Ribonucleic Acid (RNA), which is subsequently translated into proteins—the functional effectors of cellular life. Mutations, abnormal expression or dysregulation of these sequences of genomic DNA can lead to genetic disorders and serious diseases. Therefor the ability of sequence-specific recognition and access of genomic sequences within the double-stranded DNA is a crucial cornerstone of genetic manipulations and molecular engineering. Strategies such as antisense technology [1-5], RNA interference (RNAi) [6-10], and more recently, genome editing tools, have all been developed to intervene in this flow of information.

DNA naturally forms right-handed double-helix structure in the life organisms. It is consists of two strands of nucleotides linked by a sugar-phosphate backbone. Each nucleotide is composed of a deoxyribose sugar residue, a phosphoryl group, and one of four bases: Adenine (A), Thymine (T), Guanine (G), or Cytosine (C). Following the Watson-Crick base pairing rules, Adenine (A) pairs with Thymine (T) via two hydrogen bonds, and Guanine (G) pairs with Cytosine (C) via three hydrogen bonds, creating a thermodynamically stable duplex. This stability is further reinforced by base-stacking interactions between adjacent hydrophobic nucleobases and the screening of phosphate charges by metal ions in the physiological environment.

While this stability is essential for preserving genetic fidelity, it presents a formidable barrier for external agents attempting to access the sequence information within the helix. Unlike single-stranded RNA, which is often accessible for

hybridization, the bases in double-stranded DNA (dsDNA) are sterically occluded and energetically protected. Therefore, any strategy designed to target and manipulate double-stranded DNA must overcome this significant thermodynamic and kinetic barrier.

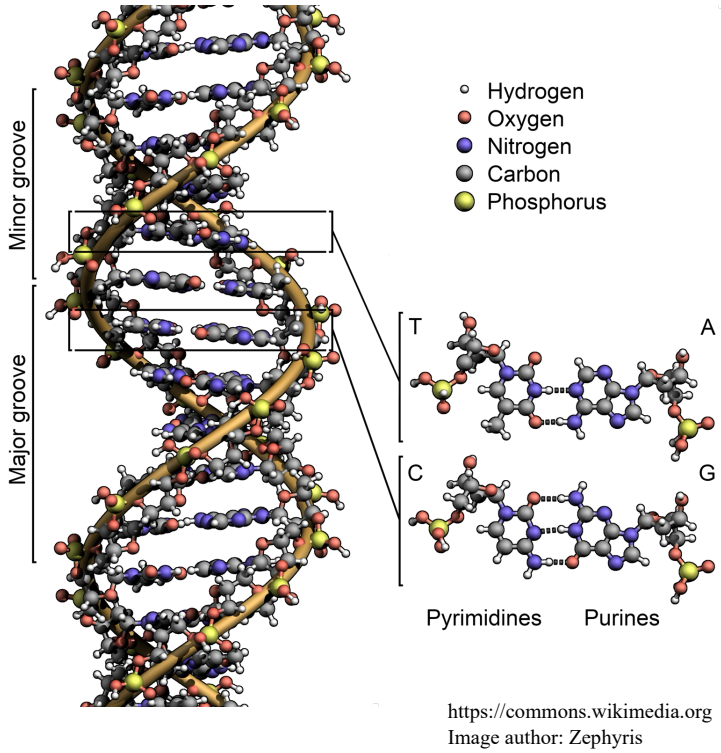


*Figure 1. The structure of DNA helix.*

## 1.2 Strategies for Sequence-Specific Recognition of Double-Stranded DNA

Recognition technologies for specific sequences within the dsDNA helix has evolved from the utilization of naturally occurring proteins to sophisticated synthetic analogues.

### 1.2.1 Protein-Based Recognition

A wide spectrum of protein-based genetic manipulation strategies a under active development, DNA-binding proteins like Zinc Finger Nucleases (ZFNs) [11-17], Transcription Activator-Like Effector Nucleases (TALENs) [11,18,19], Cas9 [20-25] along with other DNA-recognizing small molecules are investigated [18,19].

Zinc Finger Nucleases (ZFNs) [11-17] is one of the first-generation gene-editing tools. ZFNs use zinc-coordinated modules to recognize DNA. Each zinc finger module recognizes a specific 3-base pair triplet. By fusing these domains to the FokI cleavage domain, researchers created ZFNs capable of targeted gene correction. However, the zinc fingers are significantly influenced by its neighboring fingers, making the engineering difficult and prone to failure.

Transcription Activator-Like Effector Nucleases (TALENs) [11,18,19] represented a significant leap forward, offering a modular recognition code where specific amino acid repeats correspond one-to-one with DNA bases, in which one TALE repeat recognizes exactly one DNA base. This modularity simplified the design process compared to ZFNs. However, the major drawback of TALENs is their size. A typical TALEN pair requires a large coding sequence. It complicates its delivery into cells and packaging into viral vectors.

The discovery of Clustered Regularly Interspaced Short Palindromic Repeats (CRISPR) revolutionized the field [20-25]. By utilizing a guide RNA (gRNA) to direct the Cas9 nuclease, CRISPR bypasses the need for complex protein engineering. However, despite its widespread adoption, its target range is restricted by the requirement for a Protospacer Adjacent Motif (PAM) sequence. And its tolerance for mismatches between the guide RNA and the target genomic DNA leads to a higher frequency of off-target mutations [23].

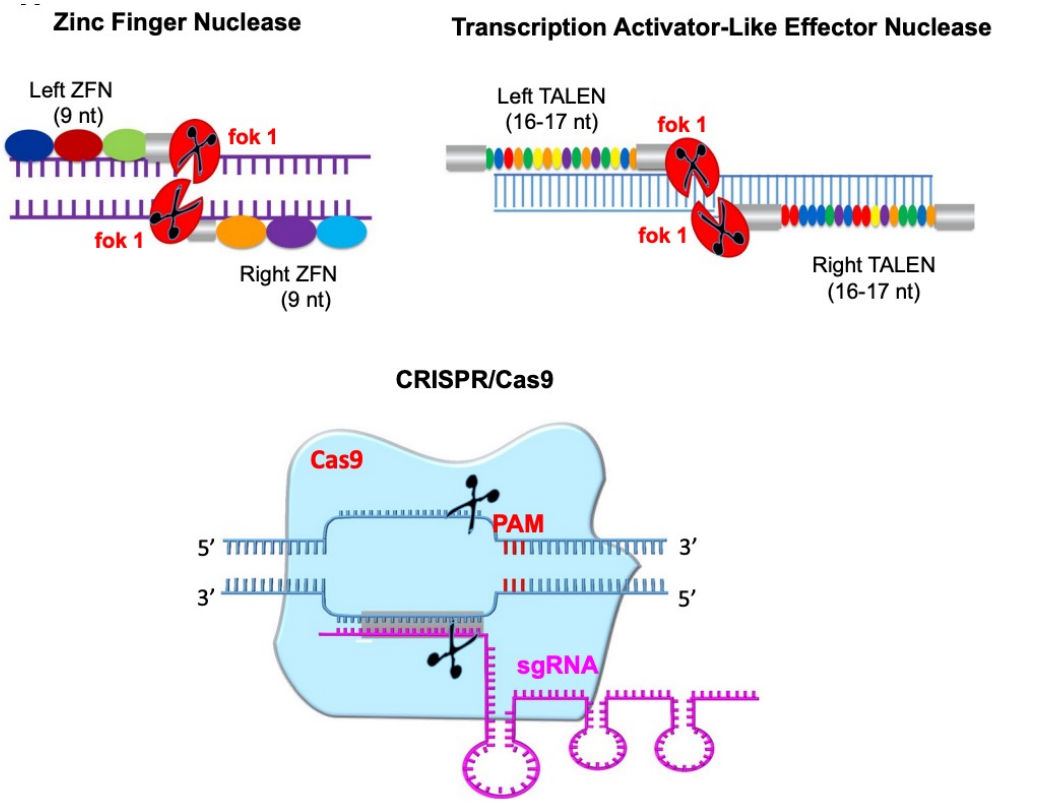


*Mol Biotechnol.* **2018**, 60, 329–338

*Figure 2. Zinc Finger Nucleases (ZFNs), Transcription Activator-Like Effector Nucleases (TALENs), and CRISPR/Cas9*

## 1.2.2 Oligonucleotide-Based Recognition

While protein-based tools are effective, they are large, structurally complex, and susceptible to enzymatic degradation. Consequently, their practical application is often constrained by environmental factors such as pH, temperature, and delivery barriers. Chemical approaches, utilizing small molecules or modified oligonucleotides, offer an alternative for these protein-based dsDNA recognition strategies.

The concept of DNA recognition by oligonucleotides dates back to 1957, when Felsenfeld et al. reported the formation of a triple-stranded structure in poly-A and poly-U oligonucleotides [26]. Triplex forming oligonucleotides (TFOs) bind to the major groove of the double helix via Hoogsteen or reverse-Hoogsteen hydrogen bonds [27-29]. This allows for recognition without disrupting the underlying Watson-Crick base pairs

[30]. However, the binding mechanism restricts the targets to polypurine/polypyrimidine sequences. Furthermore, TFOs has a strict requirement of acidic pH conditions for protonation of cytosines to form the C+:G-C triplet. These specific requirements limit the general applications of TFOs for genomic targeting [30-33]. Dervan et.al developed pyrrole-imidazole polyamides that could recognize the minor groove of double-stranded DNA [32, 33]. These molecules can distinguish between G-C and A-T base pairs based on their specific hydrogen bonding patterns. While being highly specific, recognition of long, unique genomic sequences still remain a challenge.

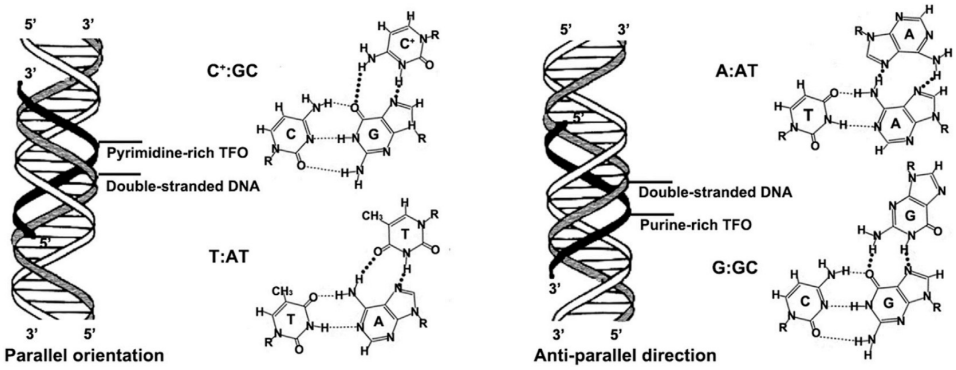


*Front. Pharmacol.* **2022**, *13*, 1007723

*Figure 3. Triplex forming oligonucleotides (TFOs)*

In 1991, Nielsen et al. introduced Peptide Nucleic Acids (PNA) [34]. PNA replaces the minus charged sugar-phosphate backbone with a neutral pseudo-peptide backbone. The neutral backbone eliminates the electrostatic repulsion between the probe and its target DNA, resulting in exceptionally high binding affinity [35]. PNA can invade the DNA duplex, displacing the non-complementary DNA strand to form a stable PNA-DNA hybrid [36, 37]. However, the high hydrophobicity of PNA often leads to poor solubility and self-aggregation [38]. Furthermore, the stability of PNA:PNA self-duplexes is significantly high and can kinetically trap the probe duplex. Strategies such as pseudo-complementary PNA (pcPNA) [39, 40] and cationic modifications (e.g., $G^{+}$-

PNA) [41, 42] have been developed to mitigate this, but they still require pro-longed incubation for the diplex recognition.

Locked Nucleic Acids (LNA), developed independently by Obika et al. [43, 44] and Wengel et al. [45-48] in the late 1990s. It is a backbone modification, featuring a methylene bridge connecting the 2'-O and 4'-C of the ribose ring. This methylene bridge lock results in profound thermal stability and nuclease resistance. Given their high binding affinity to DNA and RNA, therapeutic strategies employing LNA-modified oligonucleotides such as LNA-containing antisense oligonucleotides (ASOs) [49] , and double-stranded DNA recognition strategies such as LNA-Triplex-Forming Oligonucleotides (LNA-TFOs) and Zorro-LNA [50-53] have been investigated. However, this high binding affinity also makes LNAs prone to form secondary structure which decrease the active probe concentration. Also, double-duplex invasion using the LNA-modified probe always requires hours to days of reaction duration [53].

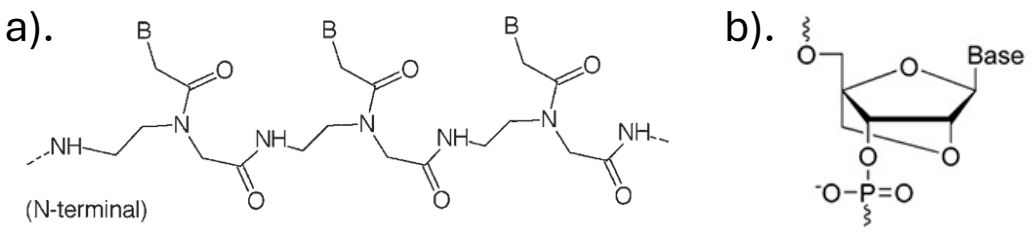


*Science*. **1991**, *254*, 1497–1500

*J. Am. Chem. Soc.* **1998**, *120*, 13252–13253

*Figure 4. Chemical structure of Peptide Nucleic Acids (a) and Locked Nucleic Acids (b).*

## 1.3 Dynamic DNA Nanotechnology

Beyond its role as a genetic information carrier, DNA has emerged as a biological material for building dynamic molecular machines and programmable logic circuits. DNA Nanotechnology exploits the predictable thermodynamics of Watson-Crick base

pairing to engineer nano-scale non-equilibrium systems that can sense, compute, and actuate.

The DNA molecular devices are usually driven by either enzyme or Toehold-Mediated Strand Displacement (TMSD) [54-56]. TMSD relies entirely on Watson-Crick base pairing thermodynamics and does not require enzymes, therefor it is programmable and less restricted in its application compared to the enzyme-driven nano machines. In TMSD process, an invader strand binds to a short, single-stranded overhang region (toehold) on its target. This binding initiates a branch migration process where the invader strand gradually displaces the pre-bounded complementary strand.

The programmability of TMSD has led to its extensive application in molecular engineering and biomedical diagnostics. TMSD can be engineered to detect diverse biomarkers, from specific microRNA sequences to single-nucleotide polymorphisms (SNPs) [57]. By coupling the strand displacement event to a fluorescent output, these systems can provide signal amplification, allowing for the detection of low-abundance targets. Moreover, TMSD allows the construction of logic gates (AND, OR, NOT), amplifiers, and molecular circuits [58-63]. These DNA molecular devices use the free energy of hybridization to perform mechanical work, such as processing input informations or reconfiguring the structure of DNA origami scaffolds [64-66]. A major challenge in DNA computing is the kinetics and reversibility of these reactions. Because TMSD is an equilibrium process, the "output" of a DNA logic gate can often reverse itself if the concentration of waste products accumulates [59-61].

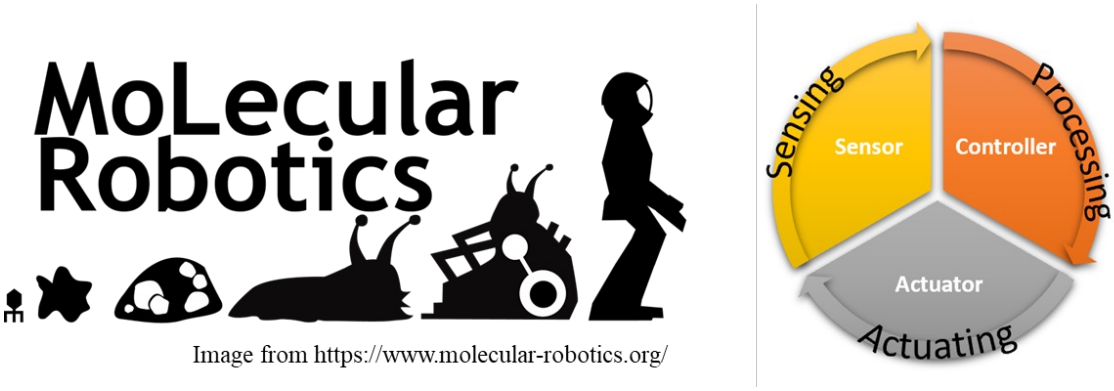


*Figure 5. DNA molecular engineering.*

## 1.4 Photo-Responsive DNA Technologies

In the regulation of DNA-based biomedical strategies and nano devices, to overcome the limitations of slow invasion kinetics, researchers have turned to light as an external regulatory trigger. Photo-regulation provides spatiotemporal control and allows for tunability through wavelength selection [67]. A variety of photoreactive moieties have been integrated into DNA to modulate its structure and function. These can be broadly categorized based on their mechanism of action: photo-switches, which alter conformation, and photo-cross-linkers, which form covalent bonds.

### 1.4.1 Azobenzene

Azobenzene is arguably the most widely utilized photo-switch in DNA nanotechnology [68, 79]. It operates by reversible *trans-cis* isomerization mechanism. In the dark or under visible light, azobenzene exists in the planar *trans* form capable of intercalating between base pairs and can stabilizes the DNA duplex. Upon 300 nm - 400 nm UV irradiation, it isomerizes to the non-planar *cis* form. This steric bulk conformation disrupts base stacking and destabilizes the double helix, effectively lowering the melting temperature [69, 78]. This property has been extensively used to reversibly associate and dissociate DNA nanostructures, allows it to function as a reversible switch for DNA machines [70]. Azobenzene relies on introducing steric hindrance to push strands apart. the *cis* state is thermally unstable and will slowly relax back to *trans* in the dark [67].

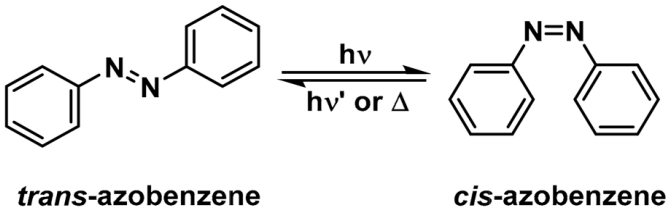


*Crystals*, **2021**, *11*(7), 840

*Figure 6. Reversible photoisomerization of azobenzene.*

## 1.4.2 Spiropyran

Spiropyran is a photochromic molecule that undergo chemical polarity change upon UV irradiation. The hydrophobic, closed spiro-form of spiropyran undergoes C-O bond cleavage upon UV irradiation, and forms the hydrophilic charged merocyanine form [67, 70, 80]. This mechanism has been utilized to control the assembly of DNA-based hydrogels. The pH-sensitivity of the open merocyanine form allows it to modulate DNA binding in response to pH changes. These mechanisms can applied to designing sensors capable of single-molecule analysis of RNA:spiropyran interactions [70, 77]. However, its hydrolytic instability in aqueous solutions limits its applications for precise sequence-specific gene manipulation. Also, the spiropyran molecule can degrade and lose its functionality in prolonged biological applications [67].

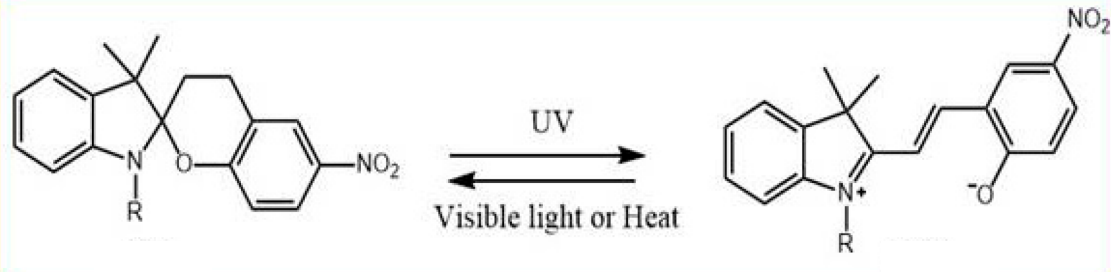


*Molecules*, **2023**, *29*(11), 2536

*Figure 7. The reversible photoisomerization between the closed-loop form spiropyran and the open-loop form merocyanine.*

## 1.4.3 Diarylethene and Stilbene

Diarylethene and stilbene derivatives are renowned for their thermal bi-stability, these molecules undergo a reversible electrocyclic ring-closing/ring-opening reaction upon different wavelengths of UV irradiation. Unlike azobenzene, both isomers are thermally stable and do not spontaneously revert in the dark [67, 71]. Diarylethene is frequently used as fluorescence switches, it generally function as a modification within the backbone or as a base surrogate.

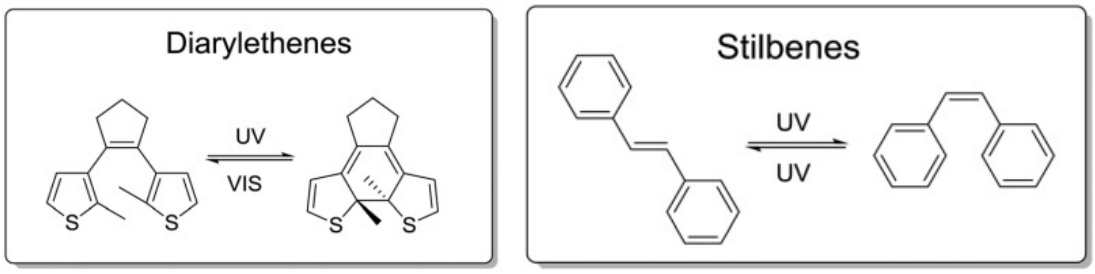


*Chemical Society Reviews*, **2017**, *46*(4), 1052–1079

*Figure 8. Photoisomerization of diarylethenes and stilbenes.*

## 1.4.4 Psoralen and Coumarin

Psoralen is one of the earliest DNA photo-cross-linkers discovered and developed as a standard tool for DNA photo-regulation[72]. Upon 320 nm – 400 nm UV irradiation, psoralen undergoes a [2+2] photocycloaddition with thymine bases on its complementary strands, creates a robust covalent bond [72]. It is widely used for chemically stabilizing DNA nanostructures such as DNA origami, to prevent thermal denaturation [73]. The major drawback of psoralen is its reaction kinetics. High cross-linking rate typically requires up to hours of irradiation [72]. Furthermore, the reversal of psoralen adducts requiring short-wavelength UV (<254 nm), and it causes significant UV-induced DNA damage, makes it unsuitable for reversible *in vivo* manipulation.

Coumarin is also capable photo-cross-linking upon >300 nm photo-irradiation. Like psoralen, coumarin derivatives intercalate into the duplex and undergo a [2+2] photocycloaddition with an adjacent pyrimidine base upon UV irradiation. It has been used successfully for DNA cross-linking and as a fluorescent probe to monitor hybridization status [74]. While effective, coumarin cross-linking kinetics are generally slower than the vinyl-derivatives utilized in our work.

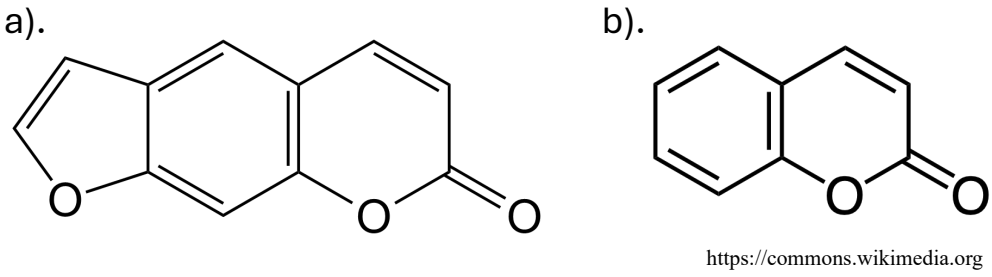


*Figure 9. Chemical structure of Psoralen (a) and Coumarin (b).*

### 1.4.5 3-Cyanovinylcarbazole Nucleoside ($^{CNV}$K)

This dissertation centers on the application of 3-cyanovinylcarbazole nucleoside ($^{CNV}$K), an ultra-fast photo-cross-linker developed by the Fujimoto laboratory [82]. $^{CNV}$K, Unlike psoralen or coumarin, undergoes a [2+2] photocycloaddition with an adjacent pyrimidine base within a second of 366 nm UV irradiation. The cross-link can be efficiently reversed (photo-split) by irradiation at 312 nm, enabling a reversable spatiotemporal control. And unlike the non-covalent switching of azobenzene, $^{CNV}$K forms a covalent bond that thermodynamically stabilizes the cross-linked duplex.

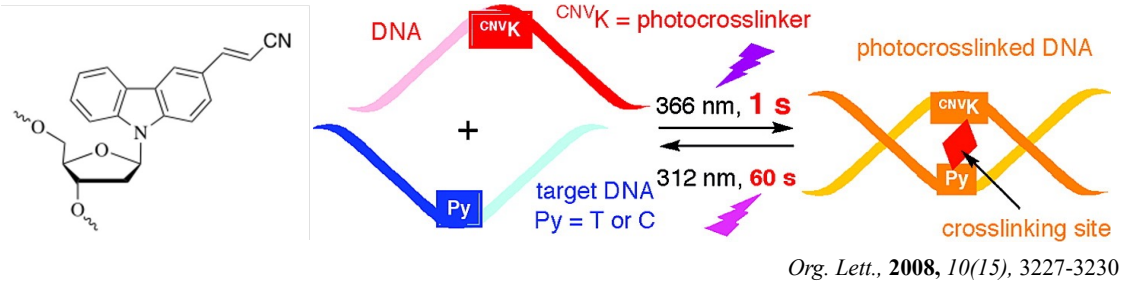


*Org. Lett.*, **2008,** *10(15),* 3227-3230

*Figure 10. 3-cyanovinylcarbazole nucleoside ($^{CNV}$K).*

## 1.5 Research Objectives and Outline

Despite the advances in double-duplex recognition and invasion approaches like PNA, LNA, several problems remain that limits their broader application. First, conventional double-duplex invasion strategies are often kinetically slow, which limits their utility in real-time applications. Second, many Double Duplex Invasion methods require paired probes, which tend to form probe-duplex [83] that reduces overall invasion efficiency. In our previous work, we proposed a photo-induced double duplex invasion approach using $^{CNV}$K [84]. While investigating the invasion mechanism of this particular approach, we discovered the invasion independence of pDDI probes and proposed a photo-induced duplex invasion (pDI) that achieves fast invasion using only $^{CNV}$K while

still maintaining a high invasion efficiency. This rapid pDI approach provides a powerful new tool for site-specific manipulation of genomic DNA. However, we also realized a limitation of the pDI strategy is that ion condition has a strong impact on its invasion efficiency. We believe the generally well-studied modification methods for enhancing the invasion affinity of double-duplex invasion[31-35] might also be applied to pDI as well, so that pDI can be used in biological relevant buffer conditions.

From a DNA engineering perspective, however, the thermodynamic stability of the double helix under high-salt conditions serves a distinct and valuable function when the invasion process is facilitated by Toehold-Mediated Strand Displacement (TMSD). The toehold provides the necessary nucleation site to bypass the high-salt barrier. In this context, we designed a photo-induced memory gate transition motif functioned by the toehold-mediated strand displacement reaction using $^{CNV}$K.

This dissertation describes the development of photo-induced DNA manipulation strategies using $^{CNV}$K.

Chapter 2 details Photo-induced Double Duplex Invasion (pDDI), a strategy using a set of paired probes to invade long-range dsDNA targets.

Chapter 3 introduces Photo-induced Duplex Invasion (pDI), a streamlined single-probe method discovered through the analysis of pDDI mechanism. and focusing on its ultra-fast kinetics.

Chapter 4 applies this photochemical strategy to DNA nanotechnology, demonstrating a DNA Memory Gate that uses photo-cross-linking to lock logic states.

Chapter 5 provides a general conclusion and future perspectives.

## 1.6 Reference:


1. P. C. Zamecnik and M. L. Stephenson, “Inhibition of Rous sarcoma virus replication and cell transformation by a specific oligodeoxynucleotide” *Proc. Natl. Acad. Sci. U.S.A.* **1978**, *75*, 280–284.
2. Monia, B. P. et al. Evaluation of 2′-modified oligonucleotides containing 2′-deoxy gaps as antisense inhibitors of gene expression. J. Biol. Chem. 268, 14514–14522 (1993).
3. Stephenson, M. L. & Zamecnik, P. C. “Inhibition of Rous sarcoma viral RNA translation by a specific oligodeoxyribonucleotide”. *Proc. Natl Acad. Sci. USA,* **1978** ,75, 285–288.
4. Crooke, S. T. Antisense therapeutics. Biotechnol. Genet. Eng. Rev. 15, 121–157 (1998)
5. Crooke, S. T., Witztum, J. L., Bennett, C. F. & Baker, B. F. RNA-targeted therapeutics. Cell Metab. 27, 714–739 (2018)
6. Fire, S. Xu, M. K. Montgomery, S. A. Kostas, S. E. Driver and C. C. Mello, “Potent and specific genetic interference by double-stranded RNA in Caenorhabditis elegans“ *Nature*. **1998**, *391*, 806–811.
7. M. K. Montgomery, S. Xu and A. Fire, “RNA as a target of double-stranded RNA-mediated genetic interference in Caenorhabditis elegans“ *Proc. Natl. Acad. Sci. U.S.A.* **1998**, *95*, 15502–15507.
8. S. M. Elbashir, J. Harborth, W. Lendeckel, A. Yalcin, K. Weber and T. Tuschl, “Duplexes of 21-nucleotide RNAs mediate RNA interference in cultured mammalian cells“ *Nature*. **2001**, *411*, 494–498.
9. R. C. Lee, R. L. Feinbaum and V. Ambros, “The C. elegans heterochronic gene lin-4 encodes small RNAs with antisense complementarity to lin-14“ *Cell*. **1993**, *75*, 843–854.
10. M. Jinek, K. Chylinski, I. Fonfara, M. Hauer, J. A. Doudna and E. Charpentier, “The C. elegans heterochronic gene lin-4 encodes small RNAs with antisense complementarity to lin-14“ *Science*. **2012**, *337*, 816–821.

11. T. Gaj, C. A. Gersbach and C. F. Barbas, “ZFN, TALEN, and CRISPR/Cas-based methods for genome engineering“ *Trends Biotechnol.* **2013**, *31*, 397–405.
12. J. Miller, A. McLachlan and A. Klug, “Repetitive zinc-binding domains in the protein transcription factor IIIA from Xenopus oocytes“ *EMBO J.* **1985**, *4*, 1609–1614.
13. N. P. Pavletich and C. O. Pabo, “Zinc Finger-DNA recognition: crystal structure of a ZIF268-DNA complex at 2.1 å“ *Science*. **1991**, *252*, 809–817.
14. Y. G. Kim, J. Cha and S. Chandrasegaran, “Hybrid restriction enzymes: zinc finger fusions to Fok I cleavage domain“ *Proc. Natl. Acad. Sci. U.S.A.* **1996**, *93*, 1156–1160.
15. F. D. Urnov, J. C. Miller, Y.-L. Lee, C. M. Beausejour, J. M. Rock, S. Augustus, A. C. Jamieson, M. H. Porteus, P. D. Gregory and M. C. Holmes, “Highly efficient endogenous human gene correction using designed zinc-finger nucleases“ *Nature*. **2005**, *435*, 646–651.
16. F. D. Urnov, E. J. Rebar, M. C. Holmes, H. S. Zhang and P. D. Gregory, “Genome editing with engineered zinc finger nucleases“ *Nat. Rev. Genet.* **2010**, *11*, 636–646.
17. Song, M., Ramakrishna, S. Genome Editing in Stem Cells for Disease Therapeutics. *Mol Biotechnol* **60**, 329–338 (2018).
18. J. Boch, H. Scholze, S. Schornack, A. Landgraf, S. Hahn, S. Kay, T. Lahaye, A. Nickstadt and U. Bonas, “Breaking the code of DNA binding specificity of TAL-Type III effectors“ *Science*. **2009**, *326*, 1509–1512.
19. M. J. Moscou and A. J. Bogdanove, “A simple cipher governs DNA recognition by TAL effectors“ *Science*. **2009**, *326*, 1501.
20. Ishino, Y., Shinagawa, H., Makino, K., Amemura, M., & Nakata, A. (1987). Nucleotide sequence of the iap gene, responsible for alkaline phosphatase isozyme conversion in Escherichia coli, and identification of the gene product. *Journal of bacteriology*, *169*(12), 5429–5433.
21. M. Jinek, K. Chylinski, I. Fonfara, M. Hauer, J.A. Doudna, E. Charpentier, A programmable dual-RNA-guided DNA endonuclease in adaptive bacterial immunity, Science, 337 (2012), pp. 816-821

22. L. Cong, F. A. Ran, D. Cox, S. Lin, R. Barretto, N. Habib, P. D. Hsu, X. Wu, W. Jiang, L. A. Marraffini and F. Zhang, “Multiplex genome engineering using CRISPR/CAS systems“ *Science*. **2013**, *339*, 819–823.
23. H. Nishimasu, F. A. Ran, P. D. Hsu, S. Konermann, S. I. Shehata, N. Dohmae, R. Ishitani, F. Zhang and O. Nureki, “Crystal Structure of Cas9 in Complex with Guide RNA and Target DNA“ *Cell*. **2014**, *156*, 935–949.
24. Jennifer A. Doudna, Emmanuelle Charpentier, The new frontier of genome engineering with CRISPR-Cas9.*Science***346**,1258096(2014).
25. Hiroshi Nishimasu *et al.* ,Engineered CRISPR-Cas9 nuclease with expanded targeting space.*Science***361**,1259-1262(2018).DOI
26. G. Felsenfeld, D. R. Davies and A. Rich, “FORMATION OF a THREE-STRANDED POLYNUCLEOTIDE MOLECULE“ *J. Am. Chem. Soc.* **1957**, *79*, 2023–2024.
27. K. Hoogsteen, “The structure of crystals containing a hydrogen-bonded complex of 1-methylthymine and 9-methyladenine“ *Acta Crystallogr.* **1959**, *12*, 822–823.
28. K. Hoogsteen, “The crystal and molecular structure of a hydrogen-bonded complex between 1-methylthymine and 9-methyladenine“ *Acta Crystallogr.* **1963**, *16*, 907–916.
29. A. Morgan and R. Wells, “Specificity of the three-stranded complex formation between double-stranded DNA and single-stranded RNA containing repeating nucleotide sequences“ *J. Mol. Biol.* **1968**, *37*, 63–80.
30. Li, C., Zhou, Z., Ren, C., Deng, Y., Peng, F., Wang, Q., Zhang, H., & Jiang, Y. (2022). Triplex-forming oligonucleotides as an anti-gene technique for cancer therapy. *Frontiers in Pharmacology*, *13*, 1007723. https://doi.org/10.3389/fphar.2022.1007723
31. J.-C. François, T. Saison-Behmoaras and C. Hélène, “Sequence-specific recognition of the major groove of DNA by oligodeoxynucleotides via triple helix formation. Footprinting studies“ *Nucleic Acids Res.* **1988**, *16*, 11431–11440.

32. P. B. Dervan and M. M. Becker, “Molecular recognition of DNA by small molecules. Synthesis of bis(methidium)spermine, a DNA polyintercalating molecule“ *J. Am. Chem. Soc.* **1978**, *100*, 1968–1970.
33. P. Dervan, “Molecular recognition of DNA by small molecules“ *Bioorg. Med. Chem.* **2001**, *9*, 2215– 2235.
34. P. E. Nielsen, M. Egholm, R. H. Berg and O. Buchardt, “Sequence-Selective Recognition of DNA by Strand Displacement with a Thymine-Substituted Polyamide“ *Science*. **1991**, *254*, 1497–1500.
35. M. Egholm, O. Buchardt, L. Christensen, C. Behrens, S. M. Freier, D. A. Driver, R. H. Berg, S. K. Kim, B. Norden and P. E. Nielsen, “PNA hybridizes to complementary oligonucleotides obeying the Watson–Crick hydrogen-bonding rules“ *Nature*. **1993**, *365*, 566–568.
36. N. J. Peffer, J. C. Hanvey, J. E. Bisi, S. A. Thomson, C. F. Hassman, S. A. Noble and L. E. Babiss, “Strand-invasion of duplex DNA by peptide nucleic acid oligomers“ *Proc. Natl. Acad. Sci. U.S.A.* **1993**, *90*, 10648–10652.
37. J. Lohse, O. Dahl and P. E. Nielsen, “Double duplex invasion by peptide nucleic acid: A general principle for sequence-specific targeting of double-stranded DNA" *Proc. Natl. Acad. Sci. U.S.A.* **1999**, *96*, 11804–11808.
38. P. E. Nielsen, “Peptide Nucleic Acids (PNA) in chemical biology and drug discovery“ *Chem Biodivers.* **2010**, *7*, 786–804.
39. G. Lahoud, V. Timoshchuk, A. Lebedev, M. De Vega, M. Salas, K. Arar, Y.-M. Hou and H. Gamper, “Enzymatic synthesis of structure-free DNA with pseudo-complementary properties“ *Nucleic Acids Res.* **2008**, *36*, 3409–3419.
40. A. G. Olsen, O. Dahl, A. B. Petersen, J. Nielsen and P. E. Nielsen, “A novel pseudo-complementary PNA G-C base pair“ *Artificial DNA PNA XNA*. **2011**, *2*, 32–36.
41. T. Ishizuka, J. Yoshida, Y. Yamamoto, J. Sumaoka, T. Tedeschi, R. Corradini, S. Sforza and M. Komiyama, ”Chiral introduction of positive charges to PNA for double-duplex invasion to versatile sequences” *Nucleic Acids Res*. **2008**, *36*, 1464–1471.

42. M. Hibino, Y. Aiba and O. Shoji, “Cationic guanine: positively charged nucleobase with improved DNA affinity inhibits self-duplex formation” *Chem. Commun.* **2020**, *56*, 2546–2549.
43. S. Obika, D. Nanbu, Y. Hari, K.-I. Morio, Y. In, T. Ishida and T. Imanishi, “Synthesis of 2‘-O, 4‘-C-methyleneuridine and -cytidine. Novel bicyclic nucleosides having a fixed C3, -endo sugar puckering“ *Tetrahedron Lett.* **1997**, *38*, 8735–8738.
44. S. Obika, K.-I. Morio, Y. Hari and T. Imanishi, “Preparation and properties of 2‘ ,5‘-linked oligonucleotide analogues containing 3‘-O, 4‘-C-methyleneribonucleosides“ *Bioorg. Med. Chem. Lett.* **1999**, *9*, 515–518.
45. A. A. Koshkin, P. Nielsen, M. Meldgaard, V. K. Rajwanshi, S. K. Singh and J. Wengel, “LNA (Locked nucleic acid): an RNA mimic forming exceedingly stable LNA:LNA duplexes“ *J. Am. Chem. Soc.* **1998**, *120*, 13252–13253.
46. A. A. Koshkin, S. K. Singh, P. Nielsen, V. K. Rajwanshi, R. Kumar, M. Meldgaard, C. E. Olsen and J. Wengel, “LNA (Locked Nucleic Acids): Synthesis of the adenine, cytosine, guanine, 5-methylcytosine, thymine and uracil bicyclonucleoside monomers, oligomerisation, and unprecedented nucleic acid recognition“ *Tetrahedron*. **1998**, *54*, 3607–3630.
47. S. K. Singh, A. A. Koshkin, J. Wengel and P. Nielsen, “LNA (locked nucleic acids): synthesis and high-affinity nucleic acid recognition“ *Chem. Commun.* **1998**, *4*, 455–456.
48. J. Wengel, A. Koshkin, S. K. Singh, P. Nielsen, M. Meldgaard, V. K. Rajwanshi, R. Kumar, J. Skouv, C. B. Nielsen, J. P. Jacobsen, N. Jacobsen and C. E. Olsen, “LNA (Locked nucleic acid)“ *Nucleosides Nucleotides*. **1999**, *18*, 1365–1370.
49. C. Wahlestedt, P. Salmi, L. Good, J. Kela, T. Johnsson, T. Hökfelt, C. Broberger, F. Porreca, J. Lai, K. Ren, M. Ossipov, A. Koshkin, N. Jakobsen, J. Skouv, H. Oerum, M. H. Jacobsen and J. Wengel, “Potent and nontoxic antisense oligonucleotides containing locked nucleic acids“ *Proc. Natl. Acad. Sci. U.S.A.* **2000**, *97*, 5633–5638.
50. B.-W. Sun, B. R. Babu, M. D. Sørensen, K. Zakrzewska, J. Wengel and J.-S. Sun, “Sequence and pH effects of LNA-Containing Triple Helix-Forming

oligonucleotides: Physical chemistry, biochemistry, and modeling Studies“ *Biochemistry*. **2004**, *43*, 4160–4169.

51. Y. V. Pabon-Martinez, Y. Xu, A. Villa, K. E. Lundin, S. Geny, C.- H. Nguyen, E. B. Pedersen, P. T. Jørgensen, J. Wengel, L. Nilsson, C. I. E. Smith and R. Zain, “LNA effects on DNA binding and conformation: from single strand to duplex and triplex structures“ *Sci. Rep.* **2017**, *7*, 11043
52. R. Ge, J.E. Heinonen, M.G. Svahn, A.J. Mohamed, K.E. Lundin, C. I. E. Smith., “Zorro locked nucleic acid induces sequence-specific gene silencing“. *The FASEB Journal*, **2007**, *21*, 1902-1914.
53. E. M. Zaghloul, A. S. Madsen, P. M. D. Moreno, I. I.bOprea, S. El-Andaloussi, B. Bestas, P. Gupta, E. B. Pedersen, K. E. Lundin, J. Wengel, C. I. E. Smith. “Optimizing anti-gene oligonucleotide 'Zorro-LNA' for improved strand invasion into duplex DNA” *Nucleic Acids Res*. **2011**, *39*, 1142–1154.
54. D. Y. Zhang, and E. Winfree. Control of DNA Strand Displacement Kinetics Using Toehold Exchange, *J. AM. CHEM. SOC.*, 131, 17303-17314 (2009)
55. G. Seelig, D. Soloveichik, D. Y. Zhang, and E. Winfree. Enzyme-free nucleic acid logic circuits, *Science*, 314, 5805, 1585-1588 (2006)
56. N. Srinivas, J. Parkin, G. Seelig, E. Winfree, and D. Soloveichik. Enzyme-free nucleic acid dynamical systems, *Science*, 358, 6369, eaal2052 (2017)
57. Souza, K.J., Agrawal, D.K. Employing toehold-mediated DNA strand displacement reactions for biomedical applications. *Med-X* **2**, 1 (2024).
58. Yurke B, Turberfield AJ, Mills AP Jr, Simmel FC, and Neumann JL. A DNA-fuelled molecular machine made of DNA, *Nature*, 406, 605-608 (2000)
59. F. C. Simmel, and B. Yurke. A DNA-based molecular device switchable between three distinct mechanical states, *Appl. Phys. Lett.*, 80, 5, 883-885 (2002)
60. Shin, J. S., and Pierce, N. A. Rewritable memory by controllable nanopatterning of DNA, *Nano letters*, 4, 5, 905-909 (2004)
61. M. Takinoue, and A. Suyama. Hairpin-DNA memory Using Molecular Addressing, *small*, 2, 11, 1244-1247 (2006)
62. L. Qian, and E. Winfree. A simple DNA gate motif for synthesizing large-scale

circuits, *J. R. Soc.*, 8, 1281-1297 (2011)

63. Montagne K, Plasson R, Sakai Y, Fujii T, and Rondelez Y. Programming an in vitro DNA oscillator using a molecular networking strategy. *Mol Syst Biol.*, 7, 466 (2011)
64. Hagiya, M., Aubert-Kato, N., Wang, S., and Kobayashi, S. Molecular computers for molecular robots as hybrid systems. *Theoretical Computer Science*., 632, 4-20 (2016)
65. L. Qian, and E. Winfree. Scaling up digital circuit computation with DNA strand displacement cascades, Science, 332, 6034, 1196-1201 (2011)
66. X. Song, A. Eshra, C. Dwyer, and J. Reif. Renewable DNA seesaw logic circuits enabled by photoregulation of toehold-mediated strand displacement, *RSC Adv*., 7, 28130-28144 (2017)
67. Wang, C., O'Hagan, M. P., Li, Z., Zhang, J., Ma, X., Tian, H., & Willner, I. (2022). Photoresponsive DNA materials and their applications. *Chemical Society Reviews*, *51*(2), 720–760.
68. Asanuma, H., Ito, T., Yoshida, T., Liang, X., & Komiyama, M. (1999). Photoregulation of the Formation and Dissociation of a DNA Duplex by Using the cis–trans Isomerization of Azobenzene. *Angewandte Chemie International Edition*, *38*(16), 2393-2395.
69. Liang, X., Asanuma, H., & Komiyama, M. (2002). Photoregulation of DNA triplex formation by azobenzene. *Journal of the American Chemical Society*, *124*(9), 1877–1883.
70. Willner, I. (1997). Photoswitchable biomaterials: en route to optobioelectronic systems. *Accounts of Chemical Research*, *30*(9), 347–356.
71. Irie, M., Fukaminato, T., Matsuda, K., & Kobatake, S. (2014). Photochromism of diarylethene molecules and crystals: memories, switches, and actuators. *Chemical Reviews*, *114*(24), 12174–12277.
72. Cimino, G. (1985). Psoralens as photoactive probes of nucleic acid structure and function: organic chemistry, photochemistry, and biochemistry. *Annual Review of Biochemistry*, *54*(1), 1151–1193.
73. Kalra, S., Donnelly, A., Singh, N., Matthews, D., Del Villar-Guerra, R., Bemmer, V., Dominguez, C., Allcock, N., Cherny, D., Revyakin, A., & Rusling, D. A.

(2024). Functionalizing DNA Origami by Triplex-Directed Site-Specific Photo-Cross-Linking. *Journal of the American Chemical Society*, *146*(19), 13617–13628

74. Haque, M. M., Sun, H., Liu, S., Wang, Y., & Peng, X. (2014). Photoswitchable Formation of a DNA Interstrand Cross-Link by a Coumarin-Modified Nucleotide. *Angewandte Chemie International Edition*, *53*(27), 7001-7005
75. Lee, H. M., Larson, D. R., & Lawrence, D. S. (2009). Illuminating the chemistry of life: design, synthesis, and applications of "caged" and related photoresponsive compounds. *ACS chemical biology*, *4*(6), 409–427.
76. Zhang, X., Zhang, J., Ying, Y., Tian, H., & Long, Y. (2014). Single molecule analysis of light-regulated RNA: spiropyran interactions. *Chemical Science*, *5*(7), 2642.
77. Tuma, J., Tonzani, S., Schatz, G. C., Karaba, A. H., & Lewis, F. D. (2007). Structure and Electronic Spectra of DNA Mini-hairpins with Gn:Cn Stems. The Journal of Physical Chemistry B, 111(45), 13101–13106. https://doi.org/10.1021/jp072303m.
78. Asanuma H, Liang X, Nishioka H, Matsunaga D, Liu M, Komiyama M. Synthesis of azobenzene-tethered DNA for reversible photo-regulation of DNA functions: hybridization and transcription. Nat Protoc. 2007;2(1):203-12.
79. Xue, L., Pan, Y., Zhang, S., Chen, Y., Yu, H., Yang, Y., Mo, L., Sun, Z., Li, L., & Yang, H. (2021). Fluorescent Azobenzene-Containing Compounds: From Structure to Mechanism. *Crystals*, *11*(7), 840.
80. Ding, S., Lv, X., Xia, Y., & Liu, Y. (2023). Fluorescent Materials Based on Spiropyran for Advanced Anti-Counterfeiting and Information Encryption. *Molecules*, *29*(11), 2536.
81. Lubbe, A. S., Szymanski, W., & Feringa, B. L. (2017). Recent developments in reversible photoregulation of oligonucleotide structure and function. *Chemical Society Reviews*, *46*(4), 1052–1079.
82. Y. Yoshimura and K. Fujimoto, “Ultrafast Reversible Photo-Cross-Linking Reaction: toward in situ DNA manipulation” *Org. Lett*. **2008**, *10*, 3227–3230.

83. K. Fujimoto, A. Hirano, Y. Watanabe, A. Shimabara and S. Nakamura, “The Inhibition Effect of Photo-Cross-Linking between Probes in Photo-Induced Double Duplex Invasion DNA” *ChemBioChem.* **2021**, *22*, 3402–3405.
84. S. Sethi, H. Zumila, Y. Watanabe, J. Mo and K. Fujimoto, “UltraFast PhotoInduced double duplex DNA invasion into a 400-mer dsDNA target” *Bioorg. Med. Chem. Lett*. **2024**, *98*, 129597.

# Chapter 2 Photo-induced Double Duplex Invasion (pDDI)

## 2.1 Background

Aiming for specific and effective recognition and manipulation of double-stranded DNA, a large number of artificial moieties, such as Peptide Nucleic Acids (PNAs) [1, 2] and Lock Nucleic Acids (LNAs) [3-9] has been developed. Naturally, DNA possesses a double-helix structure following the Watson-Crick base pairing rules. The double-helix unwinds and disassociates during processes such as DNA replication, transcription, and cell division in a highly regulated manner. Research efforts have been increasingly focused on chemical approaches for sequence-selective recognition of the DNA double-duplex. Felsenfeld et al. (1957) first reported the formation of triplex in poly-A and poly-U oligonucleotides [10]. Triplex forming oligonucleotide (TFO) winds around the Watson-Crick double helix, forms the triplex structure via Hoogsteen or Reverse Hoogsteen hydrogen bonds [11, 12]. Morgan and Wells (1968) later demonstrated the possible application of TFO in inhibition of DNA transcription [13]. While TFOs recognize major groove of dsDNA without unwinding the duplex structure, their specific binding mechanism restricts the binding to polypurine/polypyrimidine sequences [13-15]. Obika et al. (1997) published the synthesis of a bicyclic nucleoside analogue, 2'-O,4'-C-methyleneuridine and -cytidine, with a methylene bridge over the 2'-O and 4'-C positions [16], and investigated its nuclease resistance, thermal stability and hybridization affinity towards complementary RNA and DNA when incorporated into oligonucleotide [44]. Concurrently, Koshkin, Singh and Wengel et al. (1998) also published their independent work on the detailed synthesis of Lock Nucleic Acid monomers, investigating the hybridization characteristics of LNA homoduplex, LNA:RNA duplex and LNA:DNA duplex [17-21]. Given the high binding affinity of LNA, research was carried out on therapeutic strategies employing LNA-modified oligonucleotides, including LNA-containing antisense oligonucleotides (ASOs) [22] and LNA-Triplex-Forming

Oligonucleotides (LNA-TFOs) [23-26] for enhanced double-stranded DNA recognition. Peptide Nucleic Acids (PNAs) represent another notable artificial nucleic acid analogue. Possessing a neutral peptide backbone, PNAs exhibits a significantly high binding affinity and sequence-selectivity towards complementary DNA and RNA, thereby enabling distinct recognition mechanisms, such as sequence-specific double-duplex invasion [1, 2, 27, 28]. However, the formation of stable PNA self-duplexes has always been one of the limitations in achieving high-efficiency dsDNA recognition. Various modifications have been developed to overcome this obstacle. Such strategies include introducing steric repulsion to destabilize PNA self-duplexes, as seen in pseudo-complementary PNAs (pcPNAs); or introducing chiral or charged modifications, such as chiral pcDNA and cationic $N^7$-methylguanine PNA ($G^+$-PNA) [29-32]. Despite these advancements, the process for successful double-duplex invasion requires prolonged incubation times and relatively elevated temperature conditions. These demanding reaction conditions are unsuitable for a broad range of applications.

In our previous research, we established the photo-induced double-duplex invasion (pDDI) targeting long-range double-stranded DNA facilitated by 3-cyanovinylcarbazole nucleotide ($^{CNV}K$) [33, 34]. In this chapter, we investigate the mechanism of pDDI strategy.

## 2.2 3-Cyanovinylcarbazole nucleoside ($^{CNV}$K)

The photo-cross-linker 3-Cyanovinylcarbazole nucleoside ($^{CNV}$K) (Figure 11) developed by our lab exhibits an ultra-fast cross-linking ability to the adjacent pyrimidine bases in its complementary DNA or RNA strands via [2 + 2] photocycloaddition within 1 s under 366 nm UV irradiation. The cross-linking reaction is also reversible by photo-splitting under 312 nm UV irradiation for 60 s. It does not require extra reagents but a suitable photo-irradiation method under certain experiment condition. Also, DNA probes having $^{CNV}$K present a high double-duplex invasion capability [33, 34, 35].

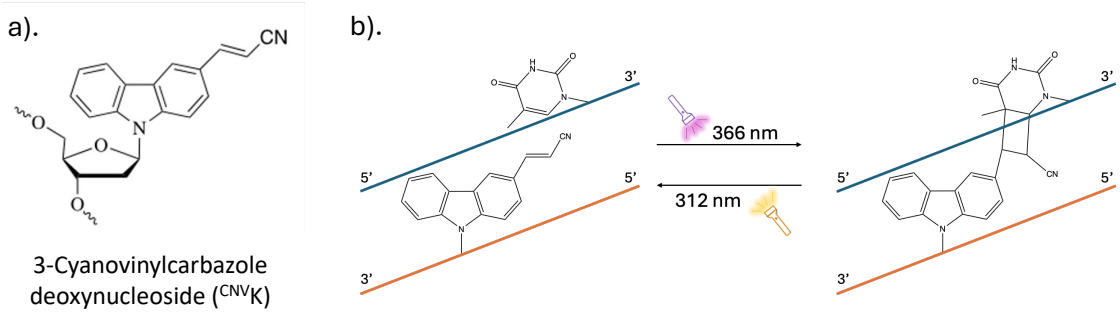


*Figure 11. 3-cyanovinylcarbazole nucleoside ($^{CNV}$K). a). Chemical structure of 3-cyanovinylcarbazole nucleoside ($^{CNV}$K). b). Photo-chemical properties of $^{CNV}$K: $^{CNV}$K can photo-cross-link with the pyridine base in its complementary strand at -1 position under 366 nm UV-irradiation in 1 second and can photo-split under 312 nm UV-irradiation.*

## 2.3 Schematic of photo-induced double duplex invasion (pDDI)

Figure 12 shows the schematic of photo-induced double-duplex invasion (pDDI). We employed distinct 200-mer and 190-mer complementary strands as templates for distinguishing and accurately quantifying the conversion rates of individual forward and reverse probes using standard Polyacrylamide gel electrophoresis (PAGE) analysis. The paired Forward and Reverse invasion probes can achieve invasion of the double-stranded Template DNA under photo-irradiation. Generally, in double-duplex invasion methods, such as PNA, LNA, the paired invasion probes always possess a complementary region, which makes their duplex formation thermodynamically more favorable than their invasion of the long dsDNA templates, consequently lowering the invasion efficiency. Incorporation of $^{CNV}K$ into the invasion probe leads to the stabilization of the probe-probe duplex through light-induced covalent bond formation. And this stabilization consequently diminishes the pool of active probes available for the invasion process. To resolve this problem, 5-cyanouridine ($^{C}U$) was also introduced to the invasion probes. $^{C}U$ modification exhibits a photo-cross-linking inhibitory effect toward $^{CNV}K$ [35]. By replacing the Thymine bases at the cross-linking site of the counter-probe, formation of undesired inter- and intra- probe cross-linking is inhibited.

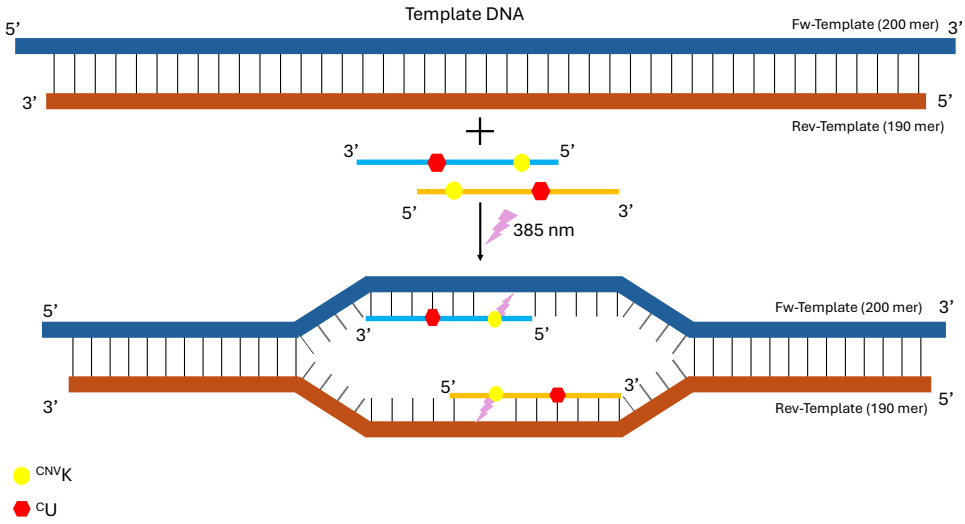


*Figure 12. Schematic of photo-induced double duplex invasion (pDDI). $^{C}U$ prohibits inter-probe cross-linking between the paired invading probes.*

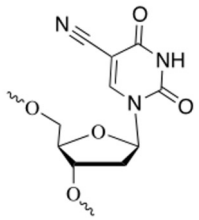


5-Cyanouridine ($^{C}U$)

*Figure 13. Chemical structure of 5-cyanouridine ($^{C}U$).*

## 2.4 Material and methods

Table 1 and Table 2 listed the template DNA sequence and invasion probe sequence used in pDDI. 400 mer Templates are the same as our previous research. While investigating the pDDI efficiency of the long-ranged 400-mer dsDNA, we unexpectedly discovered the Forward and Reverse Template might have different conversion rate, therefore, we shortened the 400-mer template and to a 200-mer Forward/ 190-mer Reverse Templates to better visualize the distinct conversion rate of

each Template strand. A total of 4 oligonucleotides (ODNs), organized into 2 Forward/Reverse probe sets, were utilized as invasion probes. The sequences of these probes were adopted from our previous study [84]. 3-cyanovinylcarbazole nucleoside ($^{CNV}$K) is incorporated as the photo-cross-linker, 5-cyanouridine ($^{C}$U) as the inter- and intra- probe photo-cross-linking inhibitor. Within each set, Forward probes were designed to target the Forward-Template strand, and Reverse probes target the Reverse-Template strand. Figure 14. illustrates the recognition areas and photo-cross-linking sites of 2 sets of KU probes. The potential cross-linking site in each paired probes are replaced by $^{C}$U.

$^{CNV}$K and $^{C}$U were synthesized, and probe oligonucleotides were prepared using DNA/RNA synthesis NTS M-Series. Probe ODNs were purified by High-Pressure Liquid Chromatography (HPLC). Purified ODNs are confirmed with MALDI-TOF mass spectrometry analysis. And their concentrations were determined by spectroscopic methods using NanoDrop 1000.

*Table 1. Template DNA sequence.*

| Template | Sequence (5'->3') |
|---|---|
| 400-mer Forward Template | ACGGACGGCGGCCCTACGATACCTTACTAGGGTCTCAGCTAATTTC ACACAGATATGTTCCTTACCCCGTTTACCACGCAGGAGAGTTAAAC GAAAGCAGCCTACGTATTTTTCGAGCTCTTTCAGCACTCTACTTGAC GGACTTTGGAATCCTAGTTGGCAGTATGGAGGCATTGTTCTCTGACC AATGAATCTGCCGAGAGAGAGGATTAACCCGCATTGGAACGAAAA GTTTGTTTTTTATGAGCCAGCCTTCGGTTGTCGATATGAGGATCTCG CGATTGAAAAGTTCATGTCTCCGTCTAATCACGATGTGAGTGGTGG GGGGTACTTCATACAAGATGCTGGATCCTTAATGAGTGGGGCTAGA GTAGCA GGCAAATACCCTAGAGCCTATTAA |
| 400-mer Reverse Template | TTAATAGGCTCTAGGGTATTTGCCTGCTACTCTAGCCCCACTCATTA AGGATCCAGCATCTTGTATGAAGTACCCCCCACCACTCACATCGTG ATTAGACGGAGACATGAACTTTTCAATCGCGAGATCCTCATATCGA CAACCGAAGGCTGGCTCATAAAAAACAAACTTTTCGTTCCAATGCG GGTTAATCCTCTCTCTCGGCAGATTCATTGGTCAGAGAACAATGCCT CCATACTGCCAACTAGGATTCCAAAGTCCGTCAAGTAGAGTGCTGA AAGAGCTCGAAAAATACGTAGGCTGCTTTCGTTTAACTCTCCTGCGT GGTAAACGGGGTAAGGAACATATCTGTGTGAAATTAGCTGAGACCC TAGTAAGGTATCGTAGGGCCGCCGTCCGT |
| Forward-Template (200 mer) | TTTGGAATCCTAGTTGGCAGTATGGAGGCATTGTTCTCTGACCAATG AATCTGCCGAGAGAGAGGATTAACCCGCATTGGAACGAAAAGTTTG TTTTTTATGAGCCAGCCTTCGGTTGTCGATATGAGGATCTCGCGATT GAAAAGTTCATGTCTCCGTCTAATCACGATGTGAGTGGTGGGGGGT ACTTCATACAAGAT |
| Reverse-Template (190 mer) | GTATGAAGTACCCCCCACCACTCACATCGTGATTAGACGGAGACAT GAACTTTTCAATCGCGAGATCCTCATATCGACAACCGAAGGCTGGC TCATAAAAAACAAACTTTTCGTTCCAATGCGGGTTAATCCTCTCTCT CGGCAGATTCATTGGTCAGAGAACAATGCCTCCATACTGCCAACTA GGATT |

*Table 2. pDDI invading probe sequence.*

| Invading Probes | Sequence 5'->3' | Target |
|---|---|---|
| Set 1-KU-Fw | GTTCCAA$^{CNV}$KGCGGGTTAATCC$^{C}$UC | Fw-Template |
| Set 1-KU-Rev | AGAGAGA$^{CNV}$KGATTAAACCCGCA$^{C}$UT | Rev-Template |
| Set 2-KU-Fw | C$^{C}$UCTCGGCAGA$^{CNV}$KTCATTGGTC | Fw-Template |
| Set 2-KU-Rev | A$^{C}$UCTGCCGAGA$^{CNV}$KAGAGGATTA | Rev-Template |

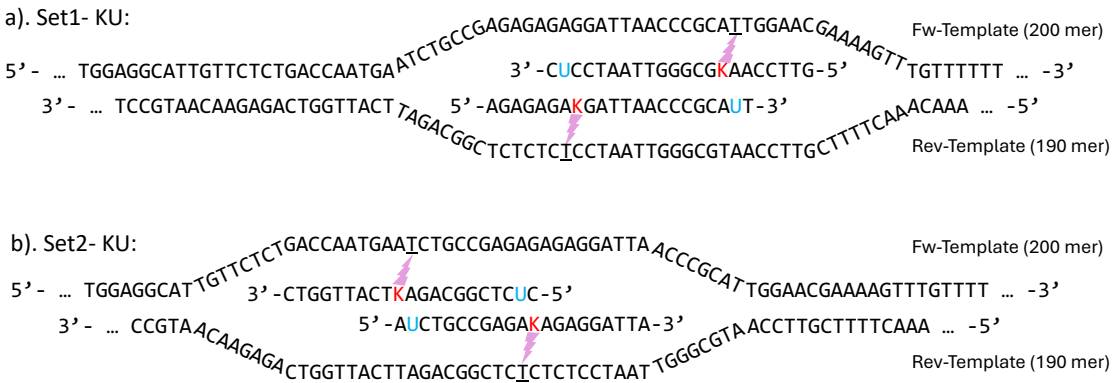


*Figure 14. The recognition areas and photo-cross-linking sites of KU invasion probes. K is $^{CNV}$K and U is $^{C}$U, the lightening mark denotes photo-cross-linking, cross-linking site in the template strand is underlined.*

Target tubes are prepared by annealing 100 nM template DNAs (200-mer and 190-mer template DNA) in 10 mM Tris-HCl buffer, pH 7.4. Target tubes were heated to 90º C for 5 mins, then gradually lower to 37ºC by -1ºC/min to form double-strand. For invasion probes, we deliberately chose not to use fluorescence-based assays to avoid potential interference from the attachment of fluorescent moieties. These labels could introduce electronic repulsion or steric hindrance that might influence the probe's affinity for its target. Therefore, the invasion efficiencies were quantified by analyzing the gel band intensities. Results were visualized by denaturing (8 M urea) 8% polyacrylamide gel electrophoresis (PAGE). Gels were stained afterwards with SYBR™ Gold Nucleic Acid Gel Stain. Images were captured with the FUJIFILM LAS-3000

Luminescent Image Analyzer (and MECAN PLBXG-G7XM3-LED470DF System) and analyzed using ImageJ v1.53k with global contrast adjustment. The band intensities of the 200-mer and 190-mer templates in the no-probe control group was normalized to 100%. The invasion efficiency of the Forward and Reverse probes was then calculated as the percentage reduction in the intensity of their respective target bands: the reduction in the 200-mer band intensity reflects the invasion efficiency of the Fw probe, while the reduction in the 190-mer band reflects that of the Rev probe. Data are presented as the mean ± SD from three independent experiments (n = 3).

## 2.5 Result and Discussion

### 2.5.1 pDDI towards 400-mer Template DNA

First, we examined the pDDI efficiency of the ODN KU probes using the 400-mer template. A mixture of 25 nM double-stranded 400-mer template DNA and 2.5 μM each (100-eq. with respect to its targeted template) of both Forward and Reverse probes in 10 mM Tris HCl buffer (pH 7.4) was incubated at 37°C for 60 minutes, then photo-irradiated under 385 nm wavelength for 1 minute. The 8% denaturing PAGE results in Figure 15 confirmed successful double-duplex invasion by both sets of probes. Set 2-KU probes has significantly higher overall invasion efficiency compared to the Set 1-KU probes. The overall invasion efficiency is calculated as decreased of the band intensity of the 400-mer Template DNA. Also, Set 2- KU probes showed 2 seperate band reflecting the Forward and Reverse invasion distinctly. And the band intensity showed slight difference indicating there might be a gap between the Forward and Reverse invasion efficiencies. This leads to our modification of the template DNA lengths in chapter 2.5.2. We aim to distinctly quantify the invasion efficiency of each probe with the shortened and distinct Template DNA.

To explain the difference of the invasion efficiencies in 2 sets of KU probes, we investigated their inter- and intra-probe cross linking rate. Figure 16 shows the cross-linking between Forward and Reverse invasion probes. As expected, in the high

concentration of the invasion probes, there are still some inter and intra probe cross-linking between the Forward and Reverse probes. However, Set 1 KU probes showed significantly higher inter- and intra-probe cross linking, which explained the low pDDI efficiency of Set 1 KU probes comparing to Set 2.

a).

| Lane | M | 1 | 2 | 3 | 4 |
|---|---|---|---|---|---|
| 400 mer dsDNA | | + | + | + | + |
| Invasion Probe | | Set1-KU probes | | Set2-KU probes | |
| UV-irradiation | | - | + | - | + |

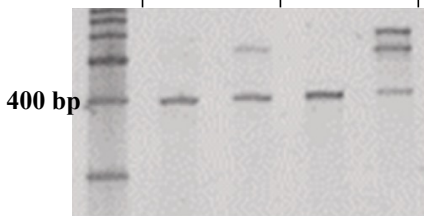


b).

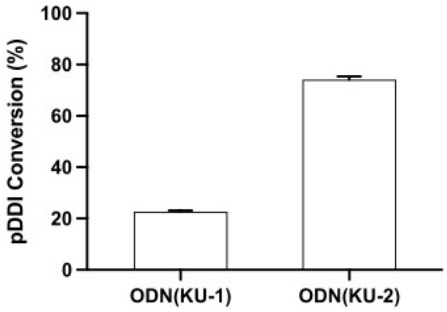


*Figure 15. pDDI efficiency of KU invading probes towards 400-mer template DNA. a). 8% denaturing PAGE reflecting the pDDI efficiency of both sets of probes. Lane M: 100-bp DNA ladder; lane 1: 400-mer template DNA with 100 molar access of Set1-KU-Fw and Set1-KU-Rev probes incubated at 37°C for 60 mins; lane 2: Lane 1 with photo-irradiation at 385 nm for 1 min; ; lane 3: 400-mer template DNA with 100 molar access of Set2-KU-Fw and Set2-KU-Rev probes incubated at 37°C for 60 mins; lane 4: Lane 3 with photo-irradiation at 385 nm for 1 min;. b). pDDI efficiency of the probes. Data are presented as the mean ± SD.*

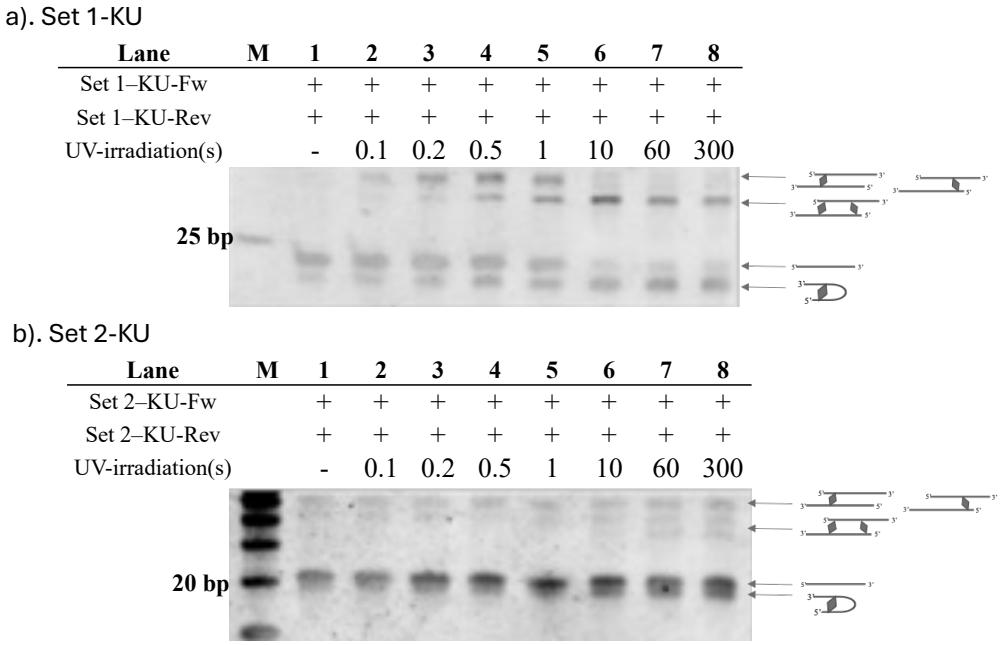


*Figure 16. Inter- and intra- probe cross-linking of the KU probes. a). Lane 1: Marker; Lane 2: Set 1-KU Fw and Set1-KU-Rev probes incubated at 37 ℃ for 60 min; Lane 3: lane 2 with 0.1 second photo-irradiation at 385 nm; Lane 4: lane 2 with 0.2 second photo-irradiation at 385 nm; Lane 5: lane 2 with 0.5 second photo-irradiation at 385 nm; Lane 6: lane 2 with 1 second photo-irradiation at 385 nm; Lane 7: lane 2 with 10 second photo-irradiation at 385 nm; Lane 8: lane 2 with 60 second photo-irradiation at 385 nm; Lane 9: lane 2 with 300 second photo-irradiation at 385 nm. b). same as a) of Set2-KU probes.*

Finally, with the relatively higher pDDI efficiency probes of Set 2, we investigated the ultra-fast kinetics of the $^{CNV}$K-incorporated invasion probes. The overall invasion efficiency is calculated with the decrease in band intensity of the 400-mer template DNA. A detailed photo-irradiation time-course analysis was conducted. The invasion progress was monitored over a discrete time interval: 0 s (no photo-irradiation), 0.1 s, 0.2 s, 0.5 s, 1s, 10 s, 60 s and 300 s after the 60 min incubation of the reaction mixture. Figure 17 confirmed that $^{CNV}$K facilitates the pDDI reaction to proceed within a second, the overall invasion efficiency reached 80% after 1 second of photo-irradiation.

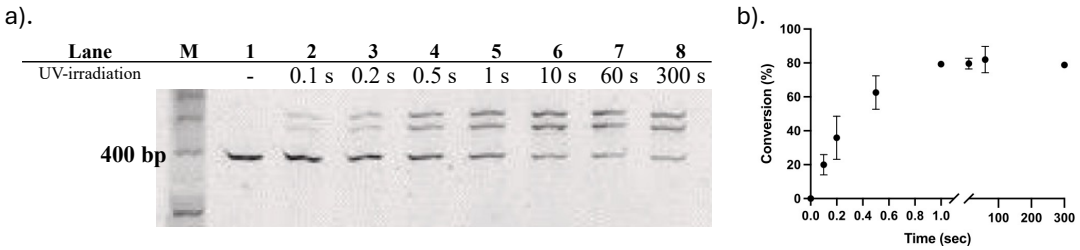


*Figure 17. Ultra-fast feature of pDDI with Set 2-KU probes. a). 8% denaturing PAGE reflecting the ultra-fast feature of pDDI using Set 2-KU probes with a photo-irradiation time-course analysis. Invasion conditions: [template DNA] = 25 nM, [probe ODN] = 2.5 μM (100-eq. relative to template DNA) at 37°C for 60 minutes then photo irradiated at 385 nm. b). Ultra-fast kinetics of the $^{CNV}$K-mediated pDI. The pDI reaction with Set 1-KT-Fw probe is monitored over a time interval of (0 s, 0.1 s, 0.2 s, 0.5 s, 1s, 10 s, 60 s and 300 s) with other conditions unchanged. The invasion efficiency is reflected by the conversion rate of 400- mer Template DNA. The result showed the invasion efficiency of Set 2-KU probes reached 80% after only 1 second of photo-irradiation. Data are presented as the mean ± SD.*

## 2.5.2 pDDI efficiency of the KU invasion probes

First, we examined the pDDI efficiency of the ODN KU probes using the 200-mer//190-mer template. A mixture of 100 nM double-stranded template DNA (200-mer//190-mer template) and 10 μM each (100-eq. with respect to its targeted template) of both Forward and Reverse probes in 10 mM Tris HCl buffer (pH 7.4) was incubated at 37°C for 60 minutes, then photo-irradiated under 385 nm wavelength for 1 minute. The 8% denaturing PAGE results in Figure 18 confirmed successful double-duplex invasion by both Set 1-KU and Set 2-KU probes. Normally, the strand displacement in the invasion process is supposed to be an equilibrium reaction. However, with the incorporation of $^{CNV}$K and upon photoirradiation, the formation of thermally irreversible probe-template cross-links shifts the reaction equilibrium forward, resulting in relatively

higher invasion efficiency. Ideally, with the suppression of probe self-duplexes, the molar concentration of active Forward and Reverse probes is expected to be equivalent. Consequently, a similar invasion rate is expected between the Forward and Reverse templates. Contrary to expectations, when quantifying the pDDI efficiency based on the decrease in template band intensity relative to the control group, the results revealed a more than 10% difference between the Forward and Reverse invasion efficiencies in both probe sets. Therefore, we hypnotized the paired invasion probes might be functioning independently instead of cooperating with each other.

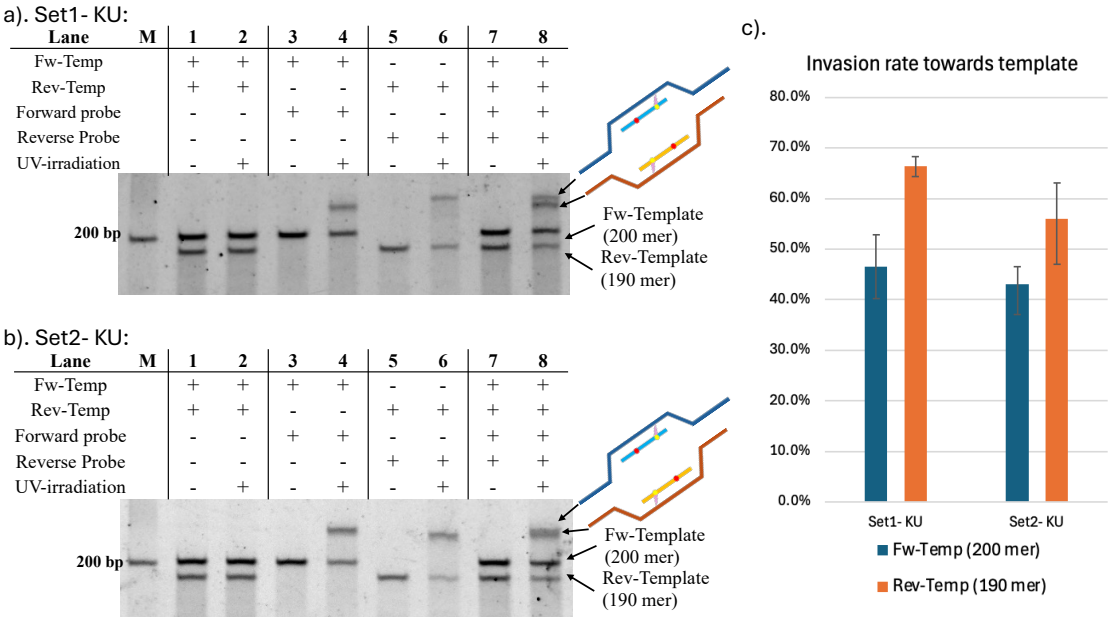


*Figure 18. pDDI efficiency of KU invading probes. a). 8% denaturing PAGE reflecting the pDDI efficiency of Set 1-KU probes. Lane M: 100-bp DNA ladder; lane 1-2: 200-mer//190-mer template only; lane 3-4: 200-mer template DNA with Set1-KU-Fw probe; lane 5-6: 190-mer template DNA with Set1-KU-Rev probe; lane 7-8: 200-mer//190-mer dsDNA with both Set1-KU-Fw and Set1-KU-Rev probes. Invasion conditions: [template DNA] = 100 nM, [probe ODN] = 10 µM (100-eq. with respect to the template DNA) at 37°C for 60 mins then photo-irradiated at 385 nm for 1 min. b). Same as (a), reflecting the pDDI efficiency of Set 2-KU probes. c). pDDI efficiency of the probes. Data are presented as the mean ± SD.*

### 2.5.3 Invasion independence of the probes in photo-induced double-duplex invasion (pDDI)

To address the gap between the Forward and Reverse invasion efficiency. The invasion independence of the probes was investigated using Job's Plots by systematically varying the Forward to Reverse probe ratio.

In particular, the total probe concentration was maintained at 100 molar equivalents relative to the target template, while the Forward:Reverse probe ratio was varied as 100:0, 75:25, 50:50, 25:75, and 0:100. In theory, when the probes were cooperating in the invasion process, pDDI efficiency should be dependent on the lowest concentration probe. Which means the highest invasion efficiency is expected at 50:50 Forward:Reverse ratio. Meaning the absence of either probe should result in the failure of pDDI. However, the result shows the pDDI efficiency of each probe is positively correlated with its concentration (Figure 19). The conversion rate of the template increased as the concentration of its corresponding probe increased. The discovery that a single Forward or Reverse probe can also achieve the invasion of double-stranded DNA confirms the invasion independence of the probes.

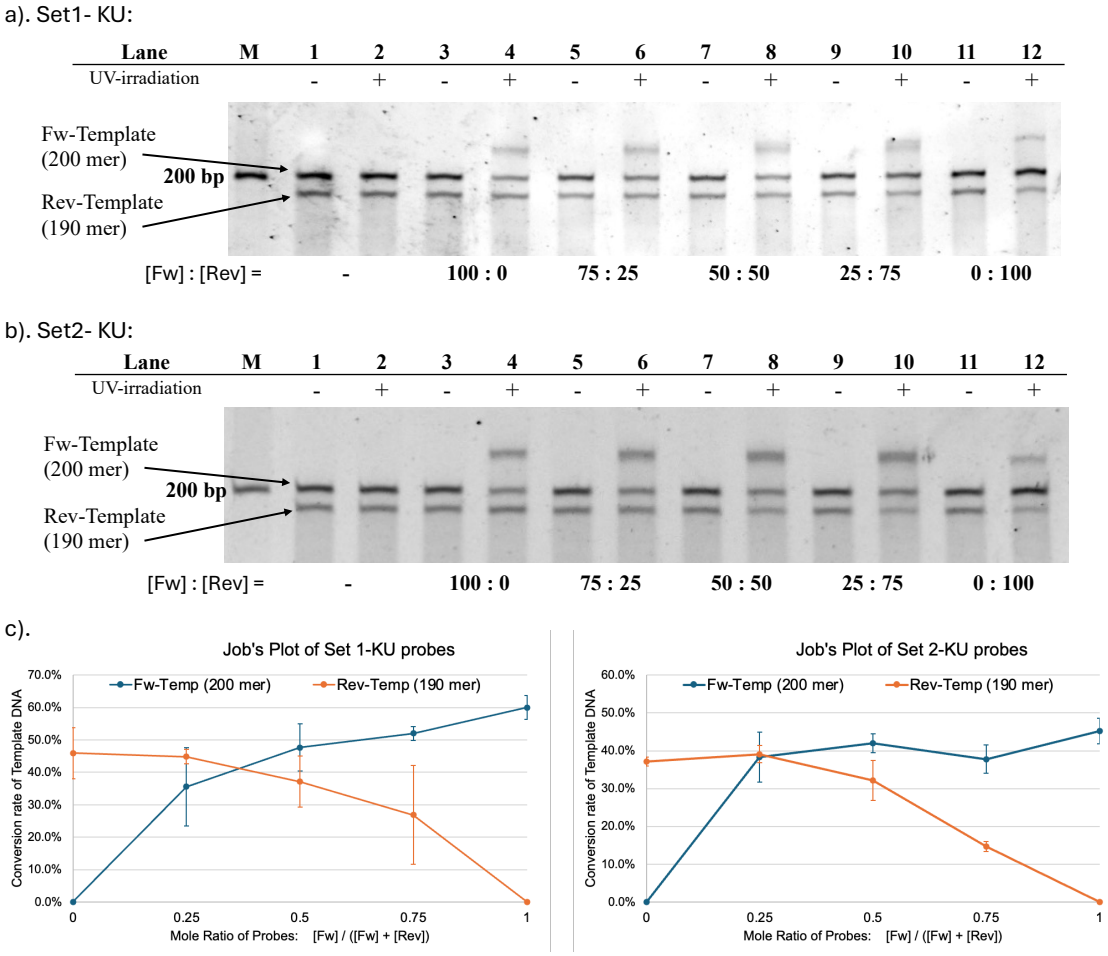


*Figure 19. Job's plot investigating the invasion independence of pDDI. a). 8% denaturing PAGE reflecting the invasion independence of the Set1-KU probes. Lane M: 100-bp DNA ladder; lane 1-2: 200-mer//190-mer template only; lane 3-4: 200-mer//190-mer dsDNA with Forward:Reverse probe at 100:0 ratio; lane 5-6: 200-mer//190-mer dsDNA with Forward:Reverse probe at 75:25 ratio; lane 7-8: 200-mer//190-mer dsDNA Forward:Reverse probe at 50:50 ratio; lane 9-10: 200-mer//190-mer dsDNA with Forward:Reverse probe at 25:75 ratio; lane 11-12: 200-mer//190-mer dsDNA with Forward:Reverse probe at 0:100 ratio. 100 nM ds template DNA incubated at 37°C for 60 minutes after adding the probes, then photo-irradiated at 385 nm for 1 min. b). Same as (a), reflecting that of Set2-KU probes. c). Job's plot reflecting the invasion independence of KU probes. Data are presented as the mean ± SD.*

## 2.5.4 Discussion

The development of the Photo-induced Double Duplex Invasion (pDDI) strategy was initiated with the goal of achieving sequence-specific recognition of long-range double-stranded DNA (dsDNA) under mild conditions. Our results successfully demonstrated that the paired probes, incorporating the ultra-fast photo-cross-linker $^{CNV}$K and the inter-probe photo-cross-linking inhibitor 5-cyanouridine ($^{C}$U), could effectively invade 200-mer//190-mer dsDNA targets. This is a significant advancement over traditional double-duplex invasion methods, such as those utilizing PNAs or LNAs, which often require prolonged incubation times or elevated temperatures to overcome the thermodynamic stability of the double helix. The pDDI method, driven by the formation of a covalent cross-link, stabilizes the invasion complex rapidly upon photo-irradiation, effectively shifting the equilibrium toward the invaded state.

However, a critical anomaly observed during the quantification of invasion efficiency provided the most significant insight of this chapter. Theoretically, in a cooperative double-duplex invasion model where two probes work synergistically to unwind the helix, the efficiencies of the Forward and Reverse probes should be closely aligned. Yet, our data revealed a consistent discrepancy of over 10% between the two. This suggested that the probes might not be functioning as a single cooperative unit. And The subsequent Job's plot analysis has confirmed the "invasion independence" of the pDDI probes. This discovery challenges the conventional assumption that "double" invasion is necessary to destabilize the dsDNA structure sufficiently for probe entry. Instead, it implies that the high affinity and cross-linking capability of $^{CNV}$K alone are sufficient to facilitate invasion. If the probes function independently, the necessity of using a paired system incorporated with $^{C}$U inhibitor becomes questionable. This realization is the driving force behind the simplification of our strategy, leading directly to the single-probe Photo-induced Duplex Invasion (pDI) methodology proposed in the following chapter.

## 2.6 Reference:


1. P. E. Nielsen, M. Egholm, R. H. Berg and O. Buchardt, “Sequence-Selective Recognition of DNA by Strand Displacement with a Thymine-Substituted Polyamide“ *Science*. **1991**, *254*, 1497–1500.
2. M. Egholm, O. Buchardt, L. Christensen, C. Behrens, S. M. Freier, D. A. Driver, R. H. Berg, S. K. Kim, B. Norden and P. E. Nielsen, “PNA hybridizes to complementary oligonucleotides obeying the Watson–Crick hydrogen-bonding rules“ *Nature*. **1993**, *365*, 566–568.
3. S. Obika, D. Nanbu, Y. Hari, K.-I. Morio, Y. In, T. Ishida and T. Imanishi, “Synthesis of 2‘-O, 4‘-C-methyleneuridine and -cytidine. Novel bicyclic nucleosides having a fixed C3, -endo sugar puckering“ *Tetrahedron Lett.* **1997**, *38*, 8735–8738.
4. S. Obika, K.-I. Morio, Y. Hari and T. Imanishi, “Preparation and properties of 2‘ ,5‘-linked oligonucleotide analogues containing 3‘-O, 4‘-C-methyleneribonucleosides“ *Bioorg. Med. Chem. Lett.* **1999**, *9*, 515–518.
5. A. A. Koshkin, P. Nielsen, M. Meldgaard, V. K. Rajwanshi, S. K. Singh and J. Wengel, “LNA (Locked nucleic acid): an RNA mimic forming exceedingly stable LNA:LNA duplexes“ *J. Am. Chem. Soc.* **1998**, *120*, 13252–13253.
6. A. A. Koshkin, S. K. Singh, P. Nielsen, V. K. Rajwanshi, R. Kumar, M. Meldgaard, C. E. Olsen and J. Wengel, “LNA (Locked Nucleic Acids): Synthesis of the adenine, cytosine, guanine, 5-methylcytosine, thymine and uracil bicyclonucleoside monomers, oligomerisation, and unprecedented nucleic acid recognition“ *Tetrahedron*. **1998**, *54*, 3607–3630.
7. S. K. Singh, A. A. Koshkin, J. Wengel and P. Nielsen, “LNA (locked nucleic acids): synthesis and high-affinity nucleic acid recognition“ *Chem. Commun.* **1998**, *4*, 455–456.
8. J. Wengel, A. Koshkin, S. K. Singh, P. Nielsen, M. Meldgaard, V. K. Rajwanshi, R. Kumar, J. Skouv, C. B. Nielsen, J. P. Jacobsen, N. Jacobsen and C. E. Olsen, “LNA (Locked nucleic acid)“ *Nucleosides Nucleotides*. **1999**, *18*, 1365–1370.

9. C. Wahlestedt, P. Salmi, L. Good, J. Kela, T. Johnsson, T. Hökfelt, C. Broberger, F. Porreca, J. Lai, K. Ren, M. Ossipov, A. Koshkin, N. Jakobsen, J. Skouv, H. Oerum, M. H. Jacobsen and J. Wengel, "Potent and nontoxic antisense oligonucleotides containing locked nucleic acids" *Proc. Natl. Acad. Sci. U.S.A.* **2000**, *97*, 5633–5638.
10. G. Felsenfeld, D. R. Davies and A. Rich, "FORMATION OF a THREE-STRANDED POLYNUCLEOTIDE MOLECULE" *J. Am. Chem. Soc.* **1957**, *79*, 2023–2024.
11. K. Hoogsteen, "The structure of crystals containing a hydrogen-bonded complex of 1-methylthymine and 9-methyladenine" *Acta Crystallogr.* **1959**, *12*, 822–823.
12. K. Hoogsteen, "The crystal and molecular structure of a hydrogen-bonded complex between 1-methylthymine and 9-methyladenine" *Acta Crystallogr.* **1963**, *16*, 907–916.
13. A. Morgan and R. Wells, "Specificity of the three-stranded complex formation between double-stranded DNA and single-stranded RNA containing repeating nucleotide sequences" *J. Mol. Biol.* **1968**, *37*, 63–80.
14. P. B. Dervan and M. M. Becker, "Molecular recognition of DNA by small molecules. Synthesis of bis(methidium)spermine, a DNA polyintercalating molecule" *J. Am. Chem. Soc.* **1978**, *100*, 1968–1970.
15. P. Dervan, "Molecular recognition of DNA by small molecules" *Bioorg. Med. Chem.* **2001**, *9*, 2215– 2235.
16. S. Obika, D. Nanbu, Y. Hari, K.-I. Morio, Y. In, T. Ishida and T. Imanishi, "Synthesis of 2'-O, 4'-C-methyleneuridine and -cytidine. Novel bicyclic nucleosides having a fixed C3, -endo sugar puckering" *Tetrahedron Lett.* **1997**, *38*, 8735–8738.
17. S. Obika, K.-I. Morio, Y. Hari and T. Imanishi, "Preparation and properties of 2' ,5'-linked oligonucleotide analogues containing 3'-O, 4'-C-methyleneribonucleosides" *Bioorg. Med. Chem. Lett.* **1999**, *9*, 515–518.
18. A. A. Koshkin, P. Nielsen, M. Meldgaard, V. K. Rajwanshi, S. K. Singh and J. Wengel, "LNA (Locked nucleic acid): an RNA mimic forming exceedingly stable LNA:LNA duplexes" *J. Am. Chem. Soc.* **1998**, *120*, 13252–13253.

19. A. A. Koshkin, S. K. Singh, P. Nielsen, V. K. Rajwanshi, R. Kumar, M. Meldgaard, C. E. Olsen and J. Wengel, "LNA (Locked Nucleic Acids): Synthesis of the adenine, cytosine, guanine, 5-methylcytosine, thymine and uracil bicyclonucleoside monomers, oligomerisation, and unprecedented nucleic acid recognition" *Tetrahedron*. **1998**, *54*, 3607–3630.
20. S. K. Singh, A. A. Koshkin, J. Wengel and P. Nielsen, "LNA (locked nucleic acids): synthesis and high-affinity nucleic acid recognition" *Chem. Commun.* **1998**, *4*, 455–456.
21. J. Wengel, A. Koshkin, S. K. Singh, P. Nielsen, M. Meldgaard, V. K. Rajwanshi, R. Kumar, J. Skouv, C. B. Nielsen, J. P. Jacobsen, N. Jacobsen and C. E. Olsen, "LNA (Locked nucleic acid)" *Nucleosides Nucleotides*. **1999**, *18*, 1365–1370.
22. C. Wahlestedt, P. Salmi, L. Good, J. Kela, T. Johnsson, T. Hökfelt, C. Broberger, F. Porreca, J. Lai, K. Ren, M. Ossipov, A. Koshkin, N. Jakobsen, J. Skouv, H. Oerum, M. H. Jacobsen and J. Wengel, "Potent and nontoxic antisense oligonucleotides containing locked nucleic acids" *Proc. Natl. Acad. Sci. U.S.A.* **2000**, *97*, 5633–5638.
23. B.-W. Sun, B. R. Babu, M. D. Sørensen, K. Zakrzewska, J. Wengel and J.-S. Sun, "Sequence and pH effects of LNA-Containing Triple Helix-Forming oligonucleotides: Physical chemistry, biochemistry, and modeling Studies" *Biochemistry*. **2004**, *43*, 4160–4169.
24. Y. V. Pabon-Martinez, Y. Xu, A. Villa, K. E. Lundin, S. Geny, C.- H. Nguyen, E. B. Pedersen, P. T. Jørgensen, J. Wengel, L. Nilsson, C. I. E. Smith and R. Zain, "LNA effects on DNA binding and conformation: from single strand to duplex and triplex structures" *Sci. Rep.* **2017**, *7*, 11043
25. R. Ge, J.E. Heinonen, M.G. Svahn, A.J. Mohamed, K.E. Lundin, C. I. E. Smith., "Zorro locked nucleic acid induces sequence-specific gene silencing". *The FASEB Journal*, **2007**, *21*, 1902-1914.
26. E. M. Zaghloul, A. S. Madsen, P. M. D. Moreno, I. I.bOprea, S. El-Andaloussi, B. Bestas, P. Gupta, E. B. Pedersen, K. E. Lundin, J. Wengel, C. I. E. Smith. "Optimizing anti-gene oligonucleotide 'Zorro-LNA' for improved strand invasion into duplex DNA" *Nucleic Acids Res*. **2011**, *39*, 1142–1154.

27. N. J. Peffer, J. C. Hanvey, J. E. Bisi, S. A. Thomson, C. F. Hassman, S. A. Noble and L. E. Babiss, “Strand-invasion of duplex DNA by peptide nucleic acid oligomers“ *Proc. Natl. Acad. Sci. U.S.A.* **1993**, *90*, 10648–10652.
28. J. Lohse, O. Dahl and P. E. Nielsen, “Double duplex invasion by peptide nucleic acid: A general principle for sequence-specific targeting of double-stranded DNA" *Proc. Natl. Acad. Sci. U.S.A.* **1999**, *96*, 11804–11808.
29. G. Lahoud, V. Timoshchuk, A. Lebedev, M. De Vega, M. Salas, K. Arar, Y.-M. Hou and H. Gamper, “Enzymatic synthesis of structure-free DNA with pseudo-complementary properties“ *Nucleic Acids Res.* **2008**, *36*, 3409–3419.
30. A. G. Olsen, O. Dahl, A. B. Petersen, J. Nielsen and P. E. Nielsen, “A novel pseudo-complementary PNA G-C base pair“ *Artificial DNA PNA XNA*. **2011**, *2*, 32–36.
31. T. Ishizuka, J. Yoshida, Y. Yamamoto, J. Sumaoka, T. Tedeschi, R. Corradini, S. Sforza and M. Komiyama, ”Chiral introduction of positive charges to PNA for double-duplex invasion to versatile sequences” *Nucleic Acids Res*. **2008**, *36*, 1464–1471.
32. M. Hibino, Y. Aiba and O. Shoji, “Cationic guanine: positively charged nucleobase with improved DNA affinity inhibits self-duplex formation” *Chem. Commun.* **2020**, *56*, 2546–2549.
33. Y. Yoshimura and K. Fujimoto, “Ultrafast Reversible Photo-Cross-Linking Reaction: toward in situ DNA manipulation” *Org. Lett*. **2008**, *10*, 3227–323
34. S. Sethi, H. Zumila, Y. Watanabe, J. Mo and K. Fujimoto, “UltraFast PhotoInduced double duplex DNA invasion into a 400-mer dsDNA target” *Bioorg. Med. Chem. Lett*. **2024**, *98*, 129597.
35. K. Fujimoto, A. Hirano, Y. Watanabe, A. Shimabara and S. Nakamura, “The Inhibition Effect of Photo-Cross-Linking between Probes in Photo-Induced Double Duplex Invasion DNA” *ChemBioChem.* **2021**, *22*, 3402–3405.

# Chapter 3 Photo-induced Duplex Invasion (pDI)

## 3.1 Background

In the previous chapter, we introduced the photo-induced double-duplex invasion (pDDI) that uses artificial nucleotides, 3-cyanovinylcarbazole nucleoside ($^{CNV}$K) as photo-cross-linker and 5-cyanouridine ($^{C}$U) as inter-probe photo-cross-linking inhibitor. While investigating the invasion mechanism of the pDDI, we discovered the invasion independence of pDDI probes and proposed a photo-induced duplex invasion (pDI) that achieves fast invasion using a single probe containing $^{CNV}$K. LNA-TFOs [1, 2] and Zorro-LNAs [3] are also double-stranded DNA recognition methods that utilize a single invasion probe. Zorro-LNA is a Z-shaped structure composed of LNA/DNA mixmers, its 2 arms bind to adjacent areas in the target duplex and achieve sequence-specific double-strand invasion. Optimized ssZorro replaced the hybridized bridge in the conventional 2-ON Zorro-LNA with non-nucleotide linker to achieve double-strand invasion with a single probe [4]. However, studies showed that its invasion takes place on a timescale range from hours to days. And as for the TFOs, The binding mechanism of TFOs restricts the binding to polypurine/polypyrimidine sequences and limits its application [5-12].

The pDI method we propose is sequence-specific, the photo-cross-linker $^{CNV}$K is tolerant of a wide range of experiment conditions. This rapid pDI approach provides a powerful new tool for site-specific manipulation of genomic DNA.

## 3.2 Schematic of photo-induced duplex invasion (pDI)

Figure 20 shows the schematic of photo-induced duplex invasion (pDI). A single $^{CNV}$K-incorporated invasion probe was used in pDI strategy. While $^{C}$U functioned as the

photo-cross-linking inhibitor in pDDI, pDI method does not require the incorporation of $^{C}U$.

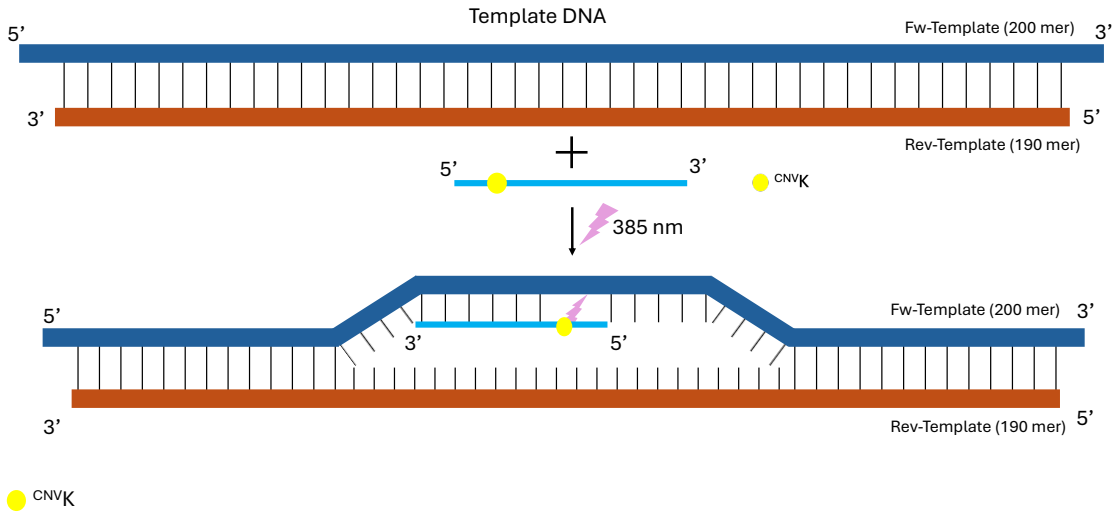


*Figure 20. Schematic of photo-induced duplex invasion (pDI) with single invading probe containing only the photo-cross-linker $^{CNV}K$.*

## 3.3 Material and methods

Template DNA strands are the same as in pDDI.

Table 3 listed the invasion probe sequence used in pDI. A total of 4 oligonucleotides (ODNs), organized into 2 Forward/Reverse probe sets, were utilized as invasion probes. The sequences are the same as in pDDI, but without the content of 5-cyanouridine ($^{C}U$). Within each set, Forward probes were designed to target the 200-mer Forward-Template strand, and Reverse probes target the 190-mer Reverse-Template strand. Figure 21. illustrates the recognition areas and photo-cross-linking sites. The KT probes (pDI probes) share the same recognition areas and cross-linking sites as of the KU probes (pDDI probes), $^{C}U$ in KU sets replaced by thymine in KT sets.

$^{CNV}K$ were synthesized, and probe oligonucleotides were prepared using DNA/RNA synthesis NTS M-Series. Probe ODNs were purified by High-Pressure Liquid Chromatography (HPLC). Purified ODNs are confirmed with MALDI-TOF

mass spectrometry analysis. And their concentrations were determined by spectroscopic methods using NanoDrop 1000.

*Table 3. pDI invading probe sequence.*

| Entry | Sequence 5'->3' | Target |
|---|---|---|
| Set 1-KT-Fw | GTTCCAA$^{CNV}$KGCGGGTTAATCCTC | Fw-Template |
| Set 1-KT-Rev | AGAGAGA$^{CNV}$KGATTAAACCCGCATT | Rev-Template |
| Set 2-KT-Fw | CTCTCGGCAGA$^{CNV}$KTCATTGGTC | Fw-Template |
| Set 2-KT-Rev | ATCTGCCGAGA$^{CNV}$KAGAGGATTA | Rev-Template |

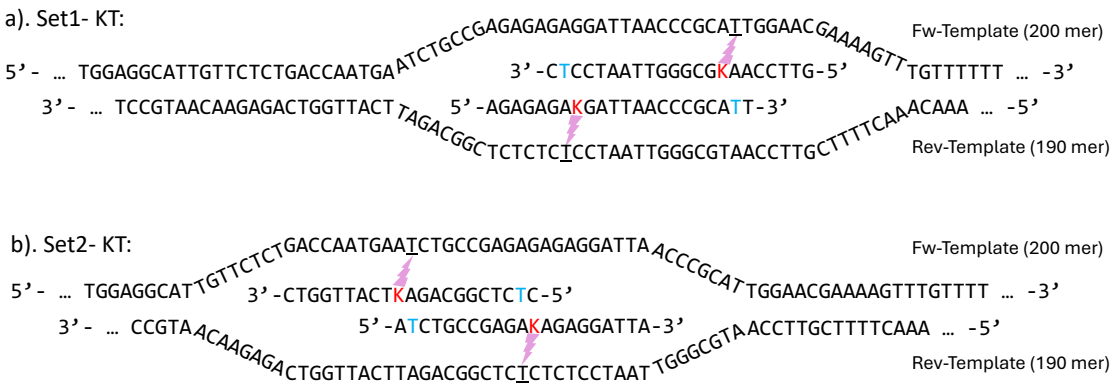


*Figure 21. The recognition areas and photo-cross-linking sites of KT invasion probes. KT probes share the same recognition area and cross-linking site as KU probes, $^{C}U$ in KU sets replaced by T in KT sets. K is $^{CNV}K$ and the lightening mark denotes photo-cross-linking, cross-linking site in the template strand is underlined.*

Target tubes are prepared by annealing 100 nM template DNAs (200-mer and 190-mer template DNA) in 10 mM Tris-HCl buffer, pH 7.4. Target tubes were heated to 90° C for 5 mins, then gradually lower to 37°C by -1°C/min to form double-strand. For invasion probes, we deliberately chose not to use fluorescence-based assays to avoid potential interference from the attachment of fluorescent moieties. These labels could introduce electronic repulsion or steric hindrance that might influence the probe's affinity for its target. Therefore, the invasion efficiencies were quantified by analyzing

the gel band intensities. Results were visualized by denaturing (8 M urea) 8% polyacrylamide gel electrophoresis (PAGE). Gels were stained afterwards with SYBR™ Gold Nucleic Acid Gel Stain. Images were captured with the FUJIFILM LAS-3000 Luminescent Image Analyzer (and MECAN PLBXG-G7XM3-LED470DF System) and analyzed using ImageJ v1.53k with global contrast adjustment. The band intensities of the 200-mer and 190-mer templates in the no-probe control group was normalized to 100%. The invasion efficiency of the Forward and Reverse probes was then calculated as the percentage reduction in the intensity of their respective target bands: the reduction in the 200-mer band intensity reflects the invasion efficiency of the Fw probe, while the reduction in the 190-mer band reflects that of the Rev probe. Data are presented as the mean ± SD from three independent experiments (n = 3).

## 3.4 Result and Discussion

### 3.4.1 pDI efficiency of the invasion probes

The observation that pDDI probes could function independently suggested the feasibility of duplex-invasion strategy using only a single probe. In the pDDI approach, $^{C}$U was initially incorporated to suppress the inter-probe cross-linking, thereby enhancing the invasion efficiency. Since the pDI approach aims to use only a single probe to achieve invasion, there is a possibility that $^{C}$U might not be in necessary. To test this hypothesis, we compared the invasion efficiencies of the KT probes with the KU probes (Figure 22). For each experiment, a 100-fold molar excess (10 μM) of the selected invasion probe was incubated with 100 nM of the target dsDNA (200-mer//190-mer template) in 10 mM Tris-HCl buffer (pH 7.4) at 37°C for 60 minutes, followed by photo-irradiation under 385 nm wavelength for 1 minute. The result revealed that KT probes, as well as the previous KU probes, showed the invasion capability of the double-stranded DNA. Set 1-KT-Fw probe was identified as most effective, achieving an invasion efficiency of more than 90%. More significantly, the

KT probes exhibited a markedly higher invasion rate in both probes sets compared to their KU counterparts. This enhanced performance is likely attributable to improved binding affinity of KT probes. Compared to the KT probes, the KU probes possess additional base-pair mismatches due to the presence of $^{C}$U, which would thermodynamically destabilize the probe-target interaction. We conducted Tm measurement to investigate the thermodynamic stability of the KT and KU invasion probes. And the result aligned with this theory (Figure 23).

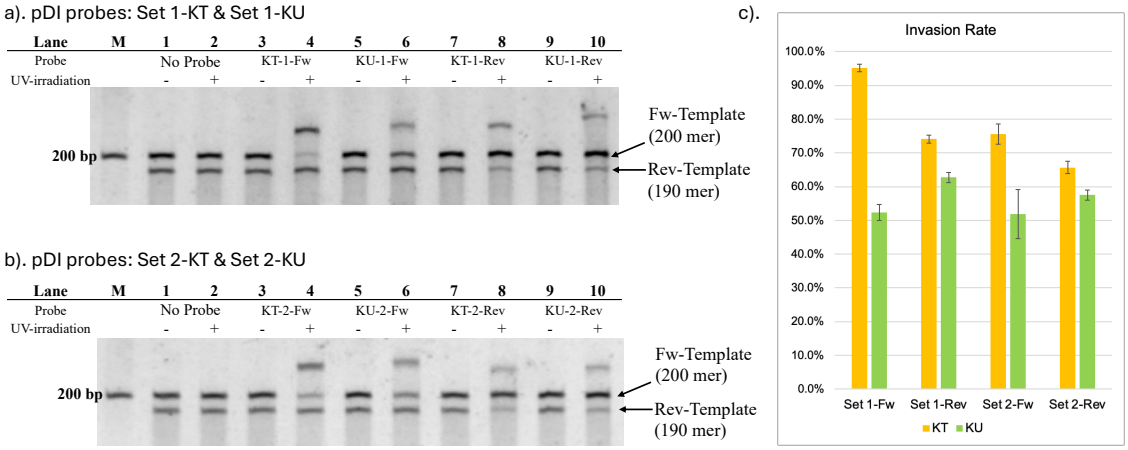


*Figure 22. pDI efficiency. a). 8% denaturing PAGE reflecting the pDI efficiency of Set 1-KT and Set 1-KU probes. Lane M: 100-bp DNA ladder; lane 1-2: 200-mer // 190-mer template only; lane 3-4: 200-mer // 190-mer ds DNA with Set1 KT-Fw probe; lane 5-6: 200-mer // 190-mer ds DNA with Set 1-KU-Fw probe; lane 7-8: 200-mer // 190-mer ds DNA with Set 1-KT-Rev probe; lane 9-10: 200-mer // 190-mer ds DNA with Set 1-KU-Rev probe. Invasion conditions: [template DNA] = 100 nM, [probe ODN] = 10 uM (100-eq. relative to template DNA) at 37°C for 60 minutes then photo irradiated at 385 nm for 1 min. b). Same as (a), reflecting the pDI efficiency of Set 2. c). pDI efficiency of the probes. Data are presented as the mean ± SD.*

a). Set1:

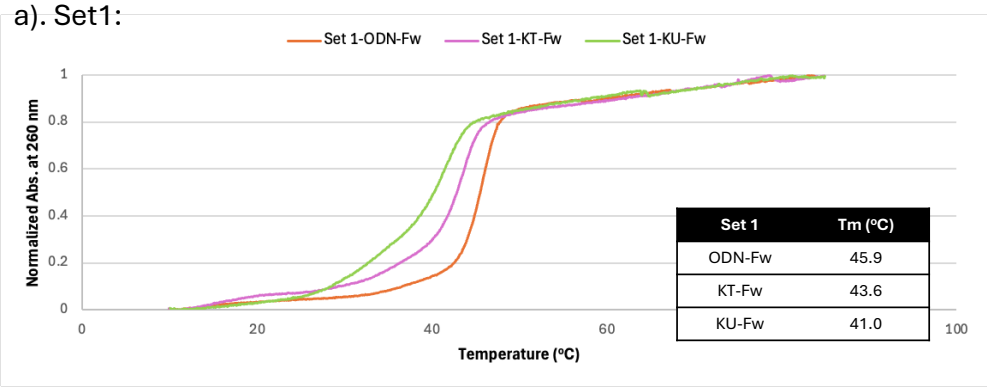


| Set 1 | Tm (°C) |
|---|---|
| ODN-Fw | 45.9 |
| KT-Fw | 43.6 |
| KU-Fw | 41.0 |

b). Set2:

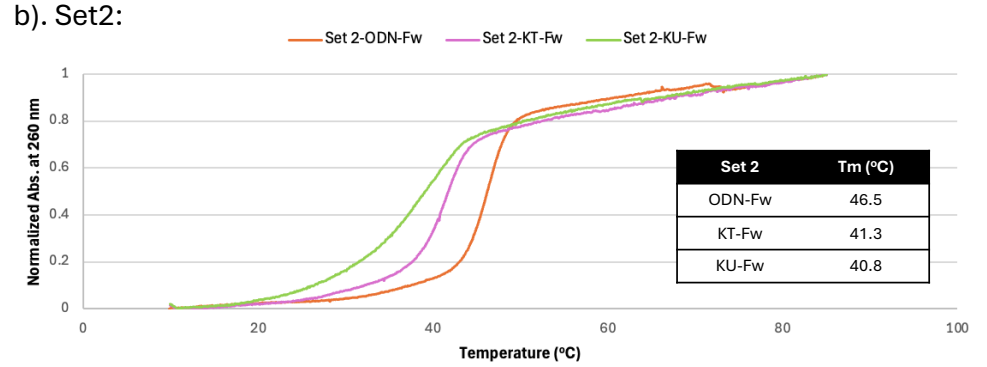


| Set 2 | Tm (°C) |
|---|---|
| ODN-Fw | 46.5 |
| KT-Fw | 41.3 |
| KU-Fw | 40.8 |

*Figure 23. Normalized Abs. at 260 nm and the calculated melting temperature of both sets. ODN-Fw is natural ODN that does not contain $^{CNV}K$ or $^{C}U$.*

## 3.4.2 The ultra-fast kinetics of pDI

A key advantage of $^{CNV}K$ is its capability for exceptionally rapid photo-cross-linking. To verify this feature in the context of our pDI approach, a detailed photo-irradiation time-course analysis, and incubation time-course analysis was conducted.

For the photo-irradiation time-course analysis, the invasion progress was monitored over a discrete time interval: 0 s (no photo-irradiation), 0.1 s, 0.2 s, 0.5 s, 1s, 10 s, 30 s, 60 s and 300 s after the 60 min incubation of the reaction mixture. Figure 24 and Figure 25 confirmed that the incorporation of $^{CNV}K$ facilitates the pDI reaction to proceed within a second. Especially with the Set 1-KT-Fw probe (Figure 24), the invasion efficiency surpassed 75% after 1 second of photo-irradiation and reached its maximum efficiency within 10 seconds. Even for the Set 2-KT-Fw probe, which exhibited relatively lower overall performance, the initial reaction was still impressively

rapid. Its invasion efficiency reached 40% within 1 second and approached its maximum after 30 seconds of photo-irradiation (Figure 25). Furthermore, the time-course analysis also revealed the optimal photo irradiation time of less than 30 seconds to achieve the maximum pDI efficiency.

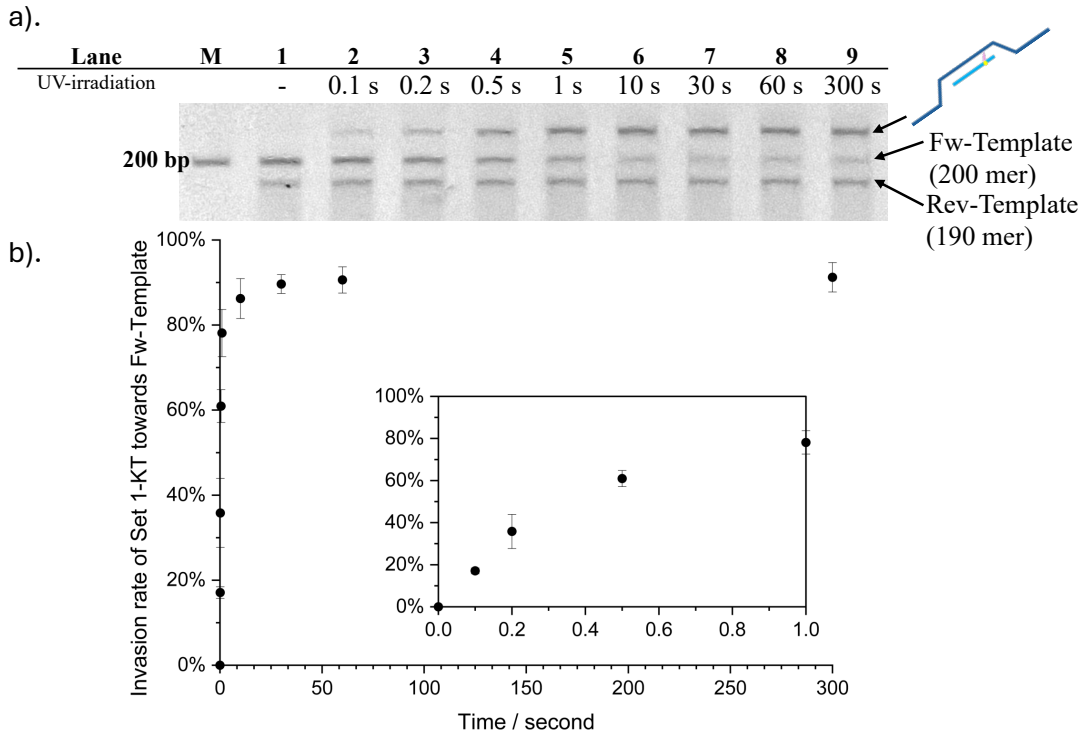


*Figure 24. Ultra-fast feature of pDI (Set 1-KT-Fw). a). 8% denaturing PAGE reflecting the ultra-fast feature of pDI using Set 1-KT-Fw probe with a photo-irradiation time-course analysis. Invasion conditions: [template DNA] = 100 nM, [probe ODN] = 10 μM (100-eq. relative to template DNA) at 37°C for 60 minutes then photo irradiated at 385 nm. b). Ultra-fast kinetics of the $^{CNV}$K-mediated pDI. The pDI reaction with Set 1-KT-Fw probe is monitored over a time interval of (0 s, 0.1 s, 0.2 s, 0.5 s, 1s, 10 s, 30 s, 60 s and 300 s) with other conditions unchanged. The invasion efficiency is reflected by the conversion rate of Fw-Template (200 mer). The result showed the invasion efficiency of Set 1-KT-Fw probe exceeded 75% after only 1 second of photo-irradiation. Data are presented as the mean ± SD.*

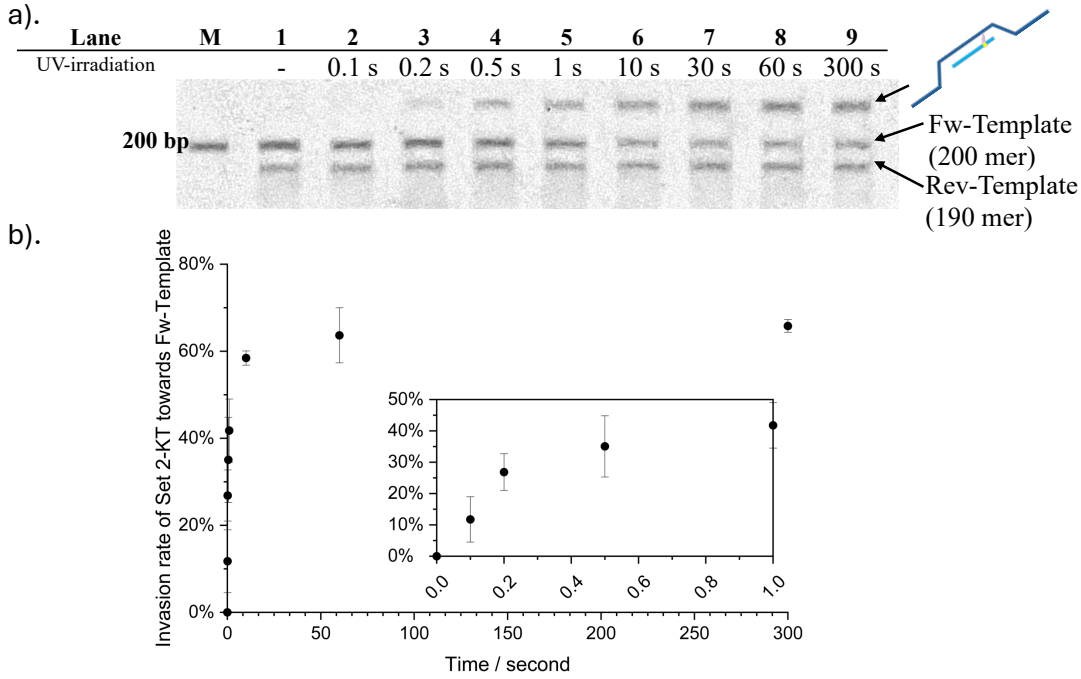


*Figure 25. Ultra-fast feature of pDI (Set 2-KT-Fw). a). 8% denaturing PAGE reflecting the ultra-fast feature of pDI using Set 2-KT-Fw probe with a photo-irradiation time-course analysis. Invasion conditions: [template DNA] = 100 nM, [probe ODN] = 10 μM (100-eq. relative to template DNA) at 37°C for 60 minutes then photo irradiated at 385 nm. b). Ultra-fast kinetics of the $^{CNV}$K-mediated pDI. The pDI reaction with Set 2-KT-Fw probe is monitored over a time interval of (0 s, 0.1 s, 0.2 s, 0.5 s, 1s, 10 s, 30 s, 60 s and 300 s) with other conditions unchanged. The invasion efficiency is reflected by the conversion rate of Fw-Template (200 mer). The result showed the invasion efficiency of Set 2-KT-Fw probe exceeded 40% after only 1 second of photo-irradiation. Data are presented as the mean ± SD.*

We have confirmed the invasion efficiency of Set 1-KT-Fw probe exceeds 75% after 60 min of incubation and 1 second of photo-irradiation. In the next step, we conducted the incubation time-course analysis using Set 1-KT-Fw. The photo-irradiation duration is fixed to 1 second. The incubation duration was varied over a discrete time interval of 0 min (no incubation), 1 min, 5 min, 10 min, 30 min and 60 min. Figure 26 confirmed that with Set 1-KT-Fw probe, the invasion efficiency exceeded 60% after 30 min of incubation when photo-irradiation is fixed to 1 s.

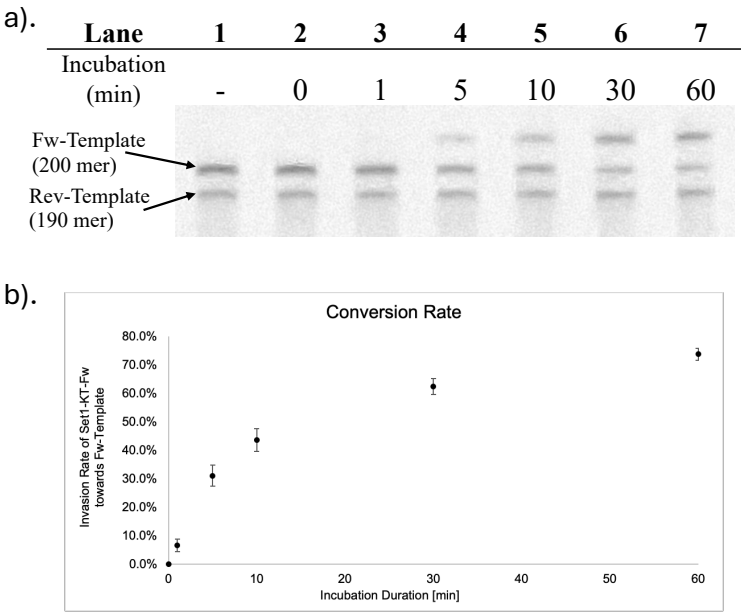


*Figure 26. Incubation time-course analysis using Set 1-KT-Fw. a). 8% denaturing PAGE reflecting the ultra-fast feature of pDI using Set 1-KT-Fw probe with incubation time-course analysis. Invasion conditions: [template DNA] = 100 nM, [probe ODN] = 10 μM (100-eq. relative to template DNA) at 37°C for a various time intervals, then photo irradiated at 385 nm for 1 s. b). Ultra-fast kinetics of the $^{CNV}$K-mediated pDI. The incubation duration after adding Set 1-KT-Fw probe is monitored over a time interval of (0 min, 1 min, 5 min, 10 min, 30 min and 60 min), following 1 s of photo-irradiation under 385 nm. The invasion efficiency is reflected by the conversion rate of Fw-Template (200 mer). Data are presented as the mean ± SD.*

## 3.4.3 Concentration analysis of pDI

A concentration analysis conducted with the best performing Set 1-KT-Fw probe. To a fixed 100 nM concentration of the target dsDNA (200-mer//190-mer template), varying amounts of Set 1-KT-Fw probe were added. the probe concentrations ranged from stoichiometric equivalence (1X) through intermediate excesses (5X, 10X, 20X, 50X), up to the maximum 100-fold molar excess (10 μM). These reaction mixtures were incubated at 37°C for 60 minutes following photo-irradiation at 385 nm for 1 second. The results derived from this study conclusively demonstrated the reliance of the pDI efficacy on probe concentration.

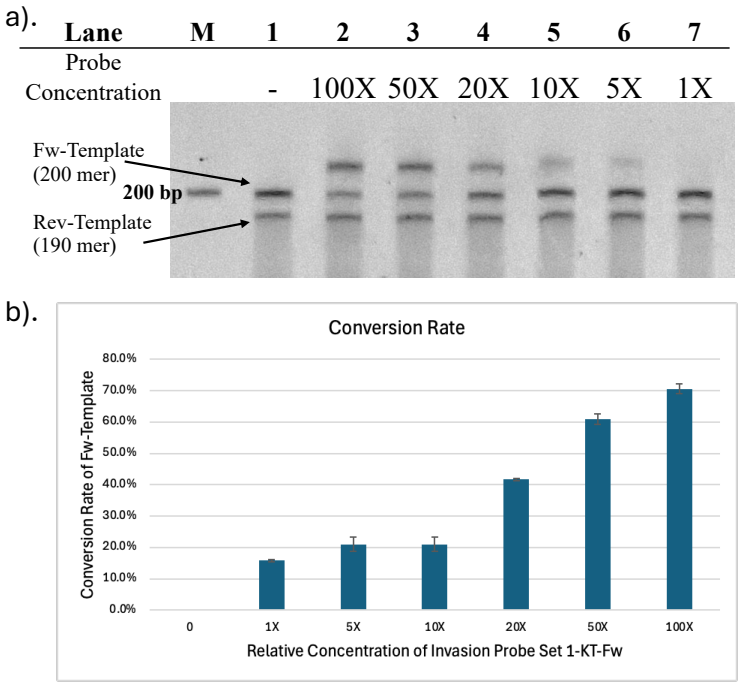


*Figure 27. pDI concentration analysis of Set 1-KT-Fw probe. a). 8% denaturing PAGE reflecting the pDI efficiency over a varies of probe concentration using Set 1-KT-Fw probe. Invasion conditions: [template DNA] = 100 nM, after adding the probe the mixture is incubated at 37°C for 60 min, then photo irradiated at 385 nm for 1 s. b). The invasion efficiency of Set 1-KT-Fw probe at different concentration condition. Invasion efficiency is reflected by the conversion rate of Fw-Template (200 mer). Data are presented as the mean ± SD.*

## 3.4.4 Probe Length

We investigated the effect of probe length (12-mer to 27-mer) on pDI efficiency. 3 new probe sequences were desighed based on the original Set 1-KT-Fw sequence, with the length of 12 mer, 17 mer and 27 mer (Table 4). The probe oligonucleotides were synthesized using DNA/RNA synthesis NTS M-Series and purified by High-Pressure Liquid Chromatography (HPLC). The purified ODNs are confirmed with MALDI-TOF mass spectrometry analysis. And their concentrations were determined by spectroscopic methods using NanoDrop 1000. For each experiment, a 100-fold molar excess (10 μM) of the selected invasion probe was incubated with 100 nM of the target dsDNA (200-mer//190-mer template) in 10 mM Tris-HCl buffer (pH 7.4) at 37°C for 60

minutes, followed by photo-irradiation under 385 nm wavelength for 1 minute. The result showed Set 1-KT-Fw (22 mer) has the highest invasion efficiency.

*Table 4. Probes used for comparison of probe length in pDI*

| Entry | Sequence 5'->3' | Length |
|---|---|---|
| 12 mer | TTCCAA$^{CNV}$KGCGGG | 12 |
| 17 mer | GTTCCAA$^{CNV}$KGCGGGTTAA | 17 |
| 22 mer (Set1-KT-Fw) | GTTCCAA$^{CNV}$KGCGGGTTAATCCTC | 22 |
| 27 mer | TTCGTTCCAA$^{CNV}$KGCGGGTTAATCCTCTC | 27 |

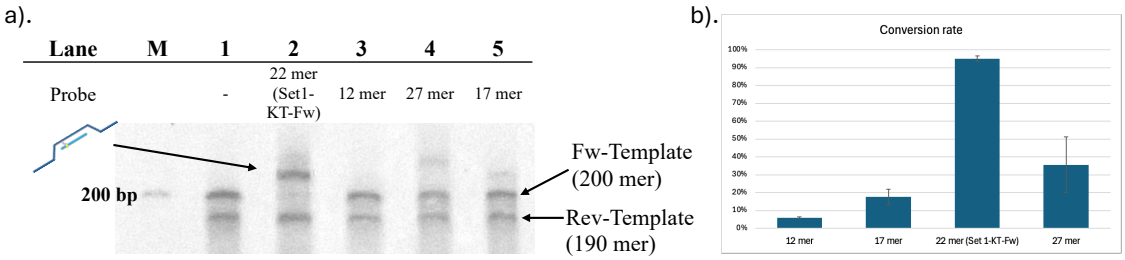


*Figure 28. Comparison of probe length in pDI. a). 8% denaturing PAGE result. Invasion conditions: [template DNA] = 100 nM, [probe ODN] = 10 μM (100-eq. of template DNA) at 37°C for 60 minutes then photo irradiated at 385 nm for 1 min. b). Conversion rate of invasion probes of different length. Data are presented as the mean ± SD.*

## 3.4.5 Reversibility and Reusability

As reversible photo-cross-linker, the covalent bond formed by $^{CNV}$K can be photo-split under 312 nm photo-irradiation. We have investigated the reversibility of pDI. After the successful invasion upon 1 min of 385 nm photo-irradiation, reaction mixture was photo-irradiated at 312 nm for 5 min, 20 min, 15 min and 20 min under 37°C. Figure 29. a. confirmed the reversibility of the pDI strategy. Moreover, we have

also tested the reusability of pDI by photo-irradiating the photo-split product again at 385 nm for 1 min. Figure 29. b. confirmed the reusability of pDI.

a).

| Lane | M | 1 | 2 | 3 | 4 | 5 | 6 |
|---|---|---|---|---|---|---|---|
| 385 nm photo-irradiation | | - | 1 min | 1 min | 1 min | 1 min | 1 min |
| 312 nm photo-irradiation | | - | - | 5 min | 10 min | 15 min | 20 min |

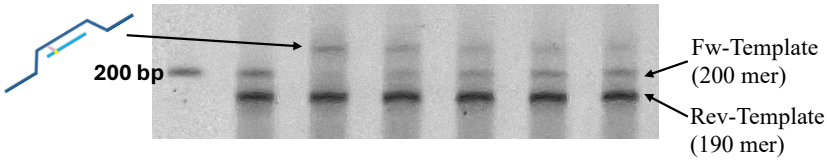


b).

| Lane | M | 1 | 2 | 3 | 4 |
|---|---|---|---|---|---|
| 385 nm photo-irradiation | | - | 1 min | 1 min | 1 min |
| 312 nm photo-irradiation | | - | - | 20 min | 20 min |
| 385 nm photo-irradiation | | - | - | - | 1 min |

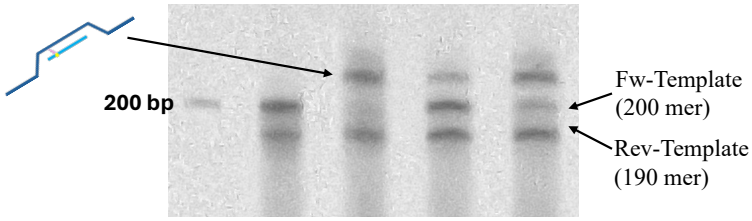


*Figure 29. 8% denaturing PAGE Demonstrating the reversibility of pDI. Concentration conditions: [template DNA] = 100 nM, [probe ODN] = 10 µM (100-eq. of template DNA). a). Invasion (photo-cross-linking) and photo-splitting condition: ds template DNA and probe ODN was incubated at 37°C for 60 minutes then photo irradiated at 385 nm for 1 min, photo-splitting group underwent 312 nm photo-irradiation after the photo-cross-linking. b). Invasion (photo-cross-linking) after photo-splitting. Lane 2: pDI procedure; Lane 3: 20 min of 312 nm photo-irradiation of Lane 2; Lane 4: 1 min of 385 nm photo-irradiation of Lane 3.*

## 3.4.6 Ion Dependence

Finally, we investigated the ion dependence of pDI in more biologically relevant buffer conditions (Table 5). With the increase of ion in the buffer, the stability of the double-stranded target is increased and the pDI efficiency dropped. pDI can barely proceeds under high salt condition such as 100 mM $Na^+$ (Figure 30). Although the pDI reaction exhibited salt-dependence which limits its immediate use in biological systems,

we hypothesize that the modification strategies previously developed to enhance the invasion affinity of double duplex invasion could also be applied to pDI, thereby facilitating its application under biological relevant buffer conditions.

*Table 5. Buffer Conditions.*

| | |
|---|---|
| **Buffer 0** | 10 mM Tris-HCl |
| **Buffer 1** | 10 mM Tris-HCl + 12.5 mM $MgCl_2$ |
| **Buffer 2** | 10 mM Tris-HCl + 10 mM NaCl |
| **Buffer 3** | 10 mM Tris-HCl + 100 mM NaCl |
| **Buffer 4** | TAE + 12.5 mM $MgCl_2$ |
| **Buffer 5** | 50 mM Sodium Cacodylate + 100 mM NaCl |

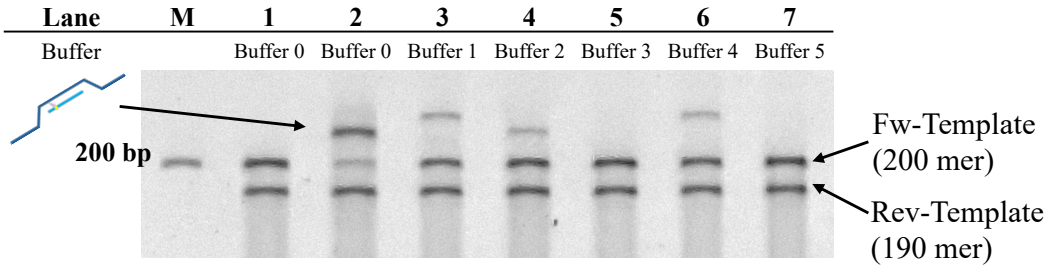


*Figure 30. Ion dependence of the probe. 8% denaturing PAGE demonstrating the pDI efficiency under different buffer condition using Set 2-KT-Fw probe. Invasion conditions: [template DNA] = 100 nM, [probe ODN] = 10 μM (100-eq. of template DNA) at 37°C for 60 minutes then photo irradiated at 385 nm for 1 min.*

## 3.4.7 Discussion

The 3-cyanovinylcarbazole nucleoside ($^{CNV}K$) has proven to be a highly effective artificial moiety for nucleic acid manipulation. It exhibits high sequence selectivity in forming site-specific covalent linkage. And the photo-induced cross-linking is exceptionally rapid. Moreover, it is tolerant of a wide range of reaction conditions, opening new possibilities for various biochemical applications. Photo-induced Double-

duplex and duplex invasion facilitated by the incorporation of $^{CNV}$K demonstrated high invasion efficiencies. The covalent photo-cross-link, being more robust than the hydrogen bond it replaces, stabilizes the invasion complex and drives the invasion process forward without changing the reaction conditions. Compared to other double-duplex invasion methods, which demand hours to days of incubation time and elevated temperature, which is not suitable for *in vivo* applications, our pDI method achieved its maximum invasion efficiency of over 90% with 60 minutes of incubation and 1 minute of photoirradiation under 37ºC. And the reaction time is expected to be further reduced with more refined probe sequence design. Furthermore, pDI requires only a single probe to successfully invade double-stranded DNA, which opens new avenues for genetic editing and manipulation. Our prior research has successfully established the efficacy of $^{CNV}$K-modified oligonucleotides in antisense approaches and Fluorescence In Situ Hybridization (FISH) detection[62-64]. The success of these methods confirmed that the $^{CNV}$K-modified oligonucleotides are functional within the complex environment of cultured cells. $^{CNV}$K-containing probe can be delivered into the cells and cross-link with its intracellular target. While these previous studies focused on targeting mRNA, the novel pDI method introduced here transitions from targeting mRNA to directly targeting the duplex DNA. Although the pDI reaction exhibited salt-dependence that limits its immediate use in biological systems, we hypothesize that the modification strategies previously developed to enhance the invasion affinity of double duplex invasion[31-35] could also be applied to pDI, thereby facilitating its application under biological relevant buffer conditions. Moreover, the reversibility of pDI opens unique opportunities for spatiotemporal control over its activity. Since pDI requires only a single probe to invade double-stranded DNA, we hope this new methodology might lay the essential groundwork for a new class of photo-induced antigene method. Future studies of the pDI method will be shifted from *in vitro* experiments to *in cellulo* systems. Future efforts will be directed towards efficient delivery of the $^{CNV}$K-modified probe to the nucleus and minimization of cytotoxicity.

## 3.5 Reference:


1. B.-W. Sun, B. R. Babu, M. D. Sørensen, K. Zakrzewska, J. Wengel and J.-S. Sun, "Sequence and pH effects of LNA-Containing Triple Helix-Forming oligonucleotides: Physical chemistry, biochemistry, and modeling Studies" *Biochemistry*. **2004**, *43*, 4160–4169.
2. Y. V. Pabon-Martinez, Y. Xu, A. Villa, K. E. Lundin, S. Geny, C.- H. Nguyen, E. B. Pedersen, P. T. Jørgensen, J. Wengel, L. Nilsson, C. I. E. Smith and R. Zain, "LNA effects on DNA binding and conformation: from single strand to duplex and triplex structures" *Sci. Rep.* **2017**, *7*, 11043
3. R. Ge, J.E. Heinonen, M.G. Svahn, A.J. Mohamed, K.E. Lundin, C. I. E. Smith., "Zorro locked nucleic acid induces sequence-specific gene silencing". *The FASEB Journal*, **2007**, *21*, 1902-1914.
4. E. M. Zaghloul, A. S. Madsen, P. M. D. Moreno, I. I.bOprea, S. El-Andaloussi, B. Bestas, P. Gupta, E. B. Pedersen, K. E. Lundin, J. Wengel, C. I. E. Smith. "Optimizing anti-gene oligonucleotide 'Zorro-LNA' for improved strand invasion into duplex DNA" *Nucleic Acids Res*. **2011**, *39*, 1142–1154.
5. G. Felsenfeld, D. R. Davies and A. Rich, "FORMATION OF a THREE-STRANDED POLYNUCLEOTIDE MOLECULE" *J. Am. Chem. Soc.* **1957**, *79*, 2023–2024.
6. K. Hoogsteen, "The structure of crystals containing a hydrogen-bonded complex of 1-methylthymine and 9-methyladenine" *Acta Crystallogr.* **1959**, *12*, 822–823.
7. K. Hoogsteen, "The crystal and molecular structure of a hydrogen-bonded complex between 1-methylthymine and 9-methyladenine" *Acta Crystallogr.* **1963**, *16*, 907–916.
8. A. Morgan and R. Wells, "Specificity of the three-stranded complex formation between double-stranded DNA and single-stranded RNA containing repeating nucleotide sequences" *J. Mol. Biol.* **1968**, *37*, 63–80.
9. Li, C., Zhou, Z., Ren, C., Deng, Y., Peng, F., Wang, Q., Zhang, H., & Jiang, Y. (2022). Triplex-forming oligonucleotides as an anti-gene technique for cancer

therapy. *Frontiers in Pharmacology*, *13*, 1007723. https://doi.org/10.3389/fphar.2022.1007723

10. J.-C. François, T. Saison-Behmoaras and C. Hélène, “Sequence-specific recognition of the major groove of DNA by oligodeoxynucleotides via triple helix formation. Footprinting studies“ *Nucleic Acids Res.* **1988**, *16*, 11431–11440.
11. P. B. Dervan and M. M. Becker, “Molecular recognition of DNA by small molecules. Synthesis of bis(methidium)spermine, a DNA polyintercalating molecule“ *J. Am. Chem. Soc.* **1978**, *100*, 1968–1970.
12. P. Dervan, “Molecular recognition of DNA by small molecules“ *Bioorg. Med. Chem.* **2001**, *9*, 2215– 2235.

# Chapter 4 Photo-induced DNA Memory Gate Transition

## 4.1 Background

Nucleic acids as a widely recognized biological material have been used increasingly for constructing the information processing compartments of the molecular robots. DNA is highly programmable for its predictability of following the Watson-Crick base pairing [1-4]. Hence been used increasingly in molecular engineering. Various DNA-based nano devices and logic circuits, such as DNA tweezers [5, 6], DNA memory devices [7, 8], DNA logic circuits [9] and DNA oscillators [10], have been designed over the last few decades. Those DNA-based molecular devices are functioned by toehold-mediated strand displacement or enzymatic reactions. However, enzymes come with restrictions on reaction conditions, such as reaction temperature, concentrations, or pH. Toehold-mediated strand displacement reaction has been widely studied and used to regulate the dynamic of DNA devices [11-13]. For an efficient molecular computing device, there are many requirements. For example, it should be scalable so that information can be processed in large scales. It should be stateful and time-responsive, input history should be stored in a certain state and the outputs should be re-computed every time receiving new input signals. It should be renew-able and reusable [14, 15]. It should be able to reset to its initial state, and with same input information, it should be able to compute a consistent output result. It should be energy-efficient. And it should have waste manage methods to eliminate the influence of waste products to the molecular computers system. There are a lot of studies published overcoming the challenges of the scalability of the simple logic gate [16], or the reusability of the system [16], etc.

## 4.2 Schematic of photo-induced DNA Memory Gate Transition

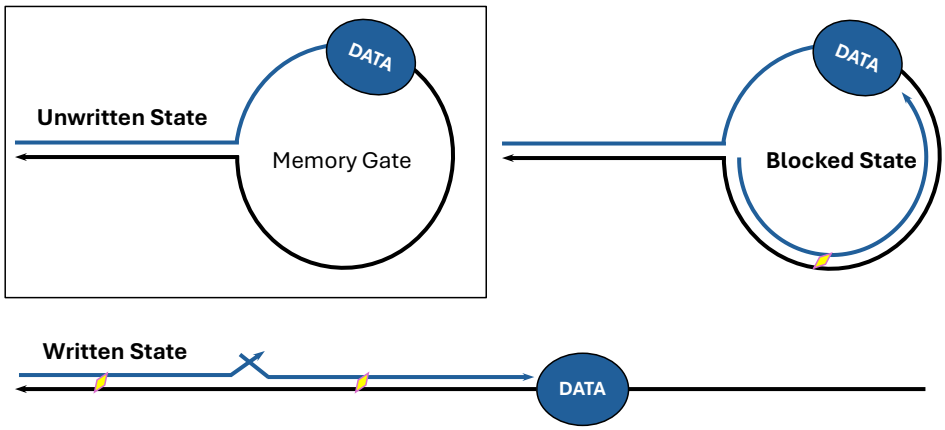


*Figure 31. Photo-induced DNA memory gate transition*

In this chapter, we propose a simple 2-input DNA memory gate motif using ultrafast photo-cross-linker $^{CNV}$K. Previous studies on DNA memory motifs are always limited to lower processing ability of single input data, and their regulation is dependent on physical parameters, such as temperature control. Our design employs two Data strands and can process its input orders. It functioned by the Toehold-mediated strand displacement reaction and is regulated by photo energy.

The toehold mediated strand displacement reaction is widely used in DNA molecular devices. It is composed of 2 steps: access of the toehold and the branch migration. As shown in this figure 32, accessing of invading strand A to the short overhang region of strand C, known as toehold, initiates the strand displacement reaction. Then, invading strand A starts back and forth branch migration competing with the complementary strand B, till it subsequently displaces strand B. It is required timewise because the branch migration is an equilibrium reaction. And because there is no toehold area in strand C for the complementary strand B to access to, the reverse reaction where the invading strand A is displaced by strand B operates significantly slower and can be considered ineffective.

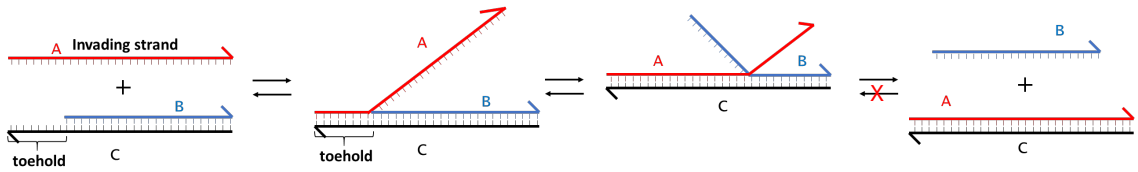


*Figure 32. Toehold mediated strand displacement reaction.*

Acceleration of the strand displacement reaction always requires changes in the design or the reaction conditions. For example, implementing toehold exchange mechanism, create drastic temperature change, creating concentration differences, etc. Previous studies have proven that in strand displacement reactions, inserting $^{CNV}K$ in invading strands can accelerate the strand displacement rate while stabilizing the DNA complex. The covalent bond formed by photo-cross-linking is thermally irreversible and inhibits the backward branch migration of the invading strand, hence accelerates the strand displacement reaction. Photo-cross-linking rate is an important factor in accelerating strand displacement reaction. Also, photo energy has been proven to be able to regulate the photo-cross-linking rate. Changing of photoirradiation wavelength or duration also has a strong impact on photo-cross-linking rate. Moreover, the insertion position of $^{CNV}K$ also has significant impact on strand displacement reaction, photo-cross-link in center position of branch migration proven to bring the optimal acceleration effect. These features of $^{CNV}K$ can contribute to a time-responsive DNA circuit.

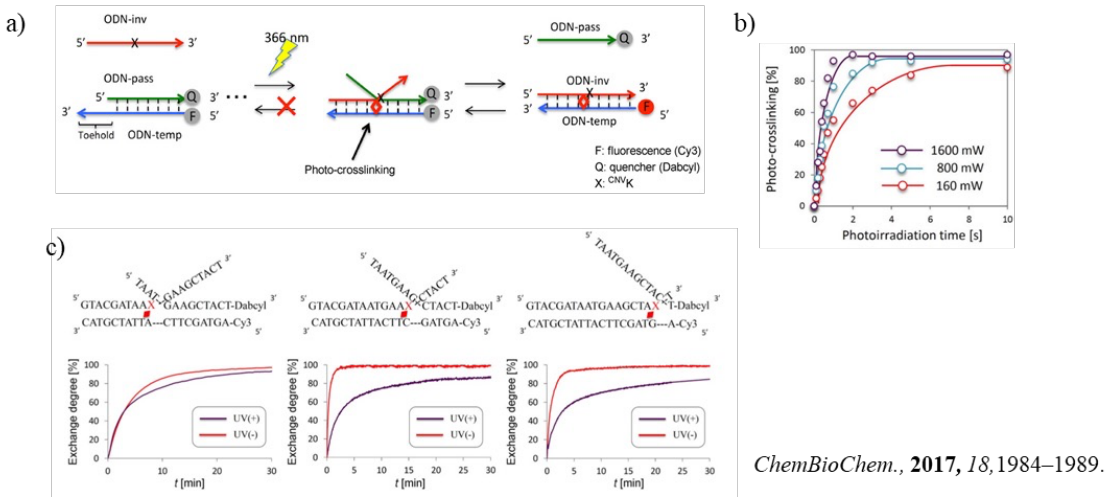


*ChemBioChem.*, **2017,** *18,*1984–1989.

*Figure 33.* $^{CNV}K$ *in accelerating toehold mediated strand displacement reaction. a). DNA strand displacement reaction accelerated by ultrafast DNA photo-cross-linking through inhibition of the backward branch migration. b). The effect of photo energy on photo-cross-linking rate. c). The effect of insertion position of* $^{CNV}K$ *on strand displacement reaction.*

As illustrated in the Figure 34, The photo-induced DNA memory gate motif is composed of a hairpin memory Gate DNA and two orthonormal DNA Data strands that are partially complementary to the memory Gate. State transition of the memory gate is functioned by toehold-mediated strand displacement reaction, and depend on the input order of the Data strands. When Data 1 was added first, it would access the toehold area in the gate and partially opens the hairpin. Data 2 added later would access the loop area of the gate, opens the hairpin completely and transit to the Written State. While in reverse order, if Data 2 was added first, it partially opens the hairpin gate and completely masks the toehold area of Data 1 and makes it hard for Data 1 to invade. Therefor Data 1 strand added later cannot bind to the memory gate, transit the memory gate from Unwritten State to the Blocked State.

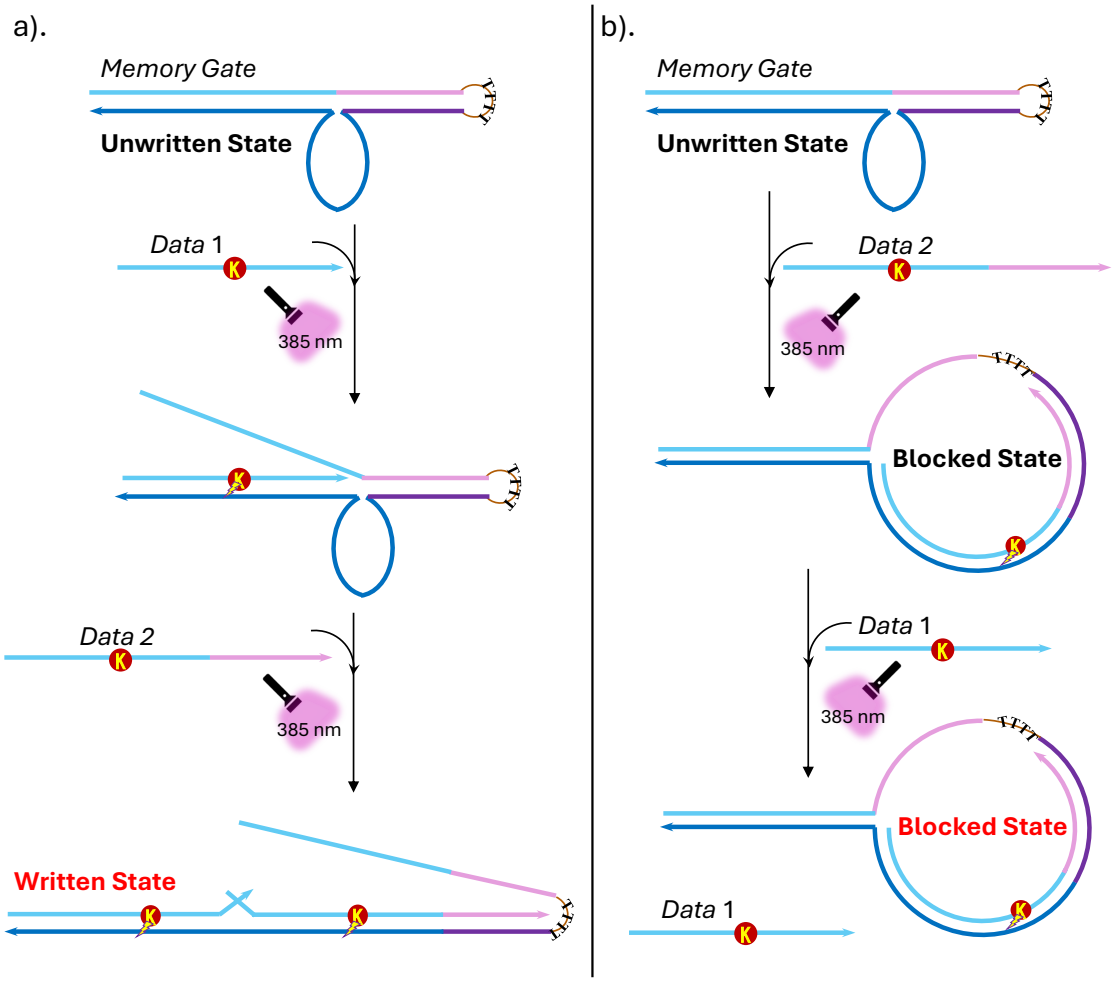


*Figure 34. Schematic of the simple 2-input photo-induced memory gate transition. a). When Data strands were added into the Memory gate in sequential order, both Data 1 and Data 2 cross-links with the hairpin structure under photo-irradiation, fully opens the hairpin gate and transit from the Unwritten State to the Written State. b). When Data strands were added into the Memory gate in reverse order, Data 2 cross-links with the hairpin structure and inhibits the cross-linking of Data 1 to the memory gate, transiting the gate to the Blocked State.*

## 4.3 Material and Methods

Memory gate sequence and input Data sequences listed in Table 6. The Data oligonucleotides were synthesized using DNA/RNA synthesis NTS M-Series and purified by High-Pressure Liquid Chromatography (HPLC). The purified ODNs are

confirmed with MALDI-TOF mass spectrometry analysis. And their concentrations were determined by spectroscopic methods using NanoDrop 1000.

*Table 6. Sequences used in this section.*

| Entry | Sequence 5'->3' |
|---|---|
| Memory Gate (124 nt) | GGCCAAGAAGCAGAAACGAACACACAACGCCGACAACCAAGGACA **TTTT**TGTCCTTGGTTGTCGTCTTGTCTGTGTCCCGGCTTTGTGCTCTCTGC GTTGTGTGTTCGTTTCTGCTTCTTGGCC |
| Data 1 (43 nt) | AAGACCGGCCAA$^{CNV}$**K**AAGCAGAAACGAACACACAACGCAGAGAGC |
| Data 2 (45 nt) | AGAGAGCACAAAGCCGGGACACA$^{CNV}$**K**ACAAGACGACAACCAAGGACA |

Target tubes are prepared by annealing 0.5 μM memory gate in 50 mM cacodylate buffer containing 100 mM NaCl. Target tubes were heated to 90° C for 5 mins, then gradually lower to 37°C by -1°C/min to form the hairpin structure. The experiments are conducted under 37°C. Result is evaluated with Polyacrylamide Gel Electrophoresis (PAGE) analysis. Gels were stained afterwards with SYBR™ Gold Nucleic Acid Gel Stain. Images were captured with the FUJIFILM LAS-3000 Luminescent Image Analyzer (and MECAN PLBXG-G7XM3-LED470DF System) and analyzed using ImageJ v1.53k with global contrast adjustment. And the state transition is concluded by the band signals.

## 4.4 Results and discussions

### 4.4.1 Photo-induced memory gate transition

Fig. 35 shows the 15% denaturing PAGE result of the memory gate transition at 1:1 Gate:Data molar ratio. Lane 1 indicates the band signal of the Unwritten State. Lane 2 and Lane 3 are controls showing the band position of the crosslinked complex of Data

1 to memory gate (Lane 2) and  of Data 2 to memory gate (Lane 3). Lane 5 shows the band shift after sequential addition of Data strands to the memory gate. First, Data 1 strand was added to the memory gate, the mixture is photo-irradiation under 385 nm for 10 min and further incubated at 37 °C for 20 min to fully hybridize to its target sequence. Subsequently, Data 2 was added to the same mixture, and the entire photo-irradiation and incubation procedure was repeated. The band signal indicates partial transition of the memory gate to both the Written State and the Blocked State. Lane 6 shows the result of adding the Data strands to the memory gate in reverse order, Data 2 followed by Data 1. The mixture is also photo-irradiated (385 nm) for 10 min and incubated (37 °C) for 20 min after each addition of Data strand. The band signal indicates successful transition from the Unwritten State to the Blocked State. This result is due to low invasion efficiency of Data 1 strand at 1:1 Gate:Data molar ratio. Therefor we increased the input Data strand concentration, and conducted the experiment at 1:2 Gate:Data molar ratio.

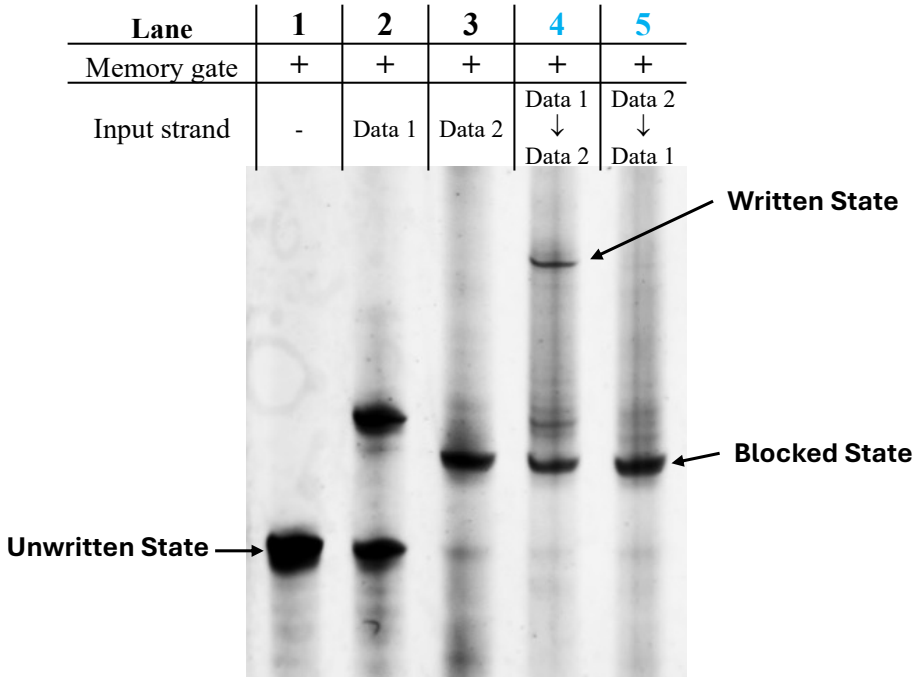


*Figure 35. 15% denaturing PAGE result of the photo-induced gate transition at 1:1 Gate: Data ratio. Lane 1: Memory gate only; Lane 2: Memory gate + Data 1; Lane 3: Memory gate + Data 2; Lane 4: Data strands added in sequential order; Lane 5: Data strands added in reverse order.*

Fig. 36 shows the 15% denaturing PAGE result of the memory gate transition at 1:2 Gate:Data molar ratio. Lane 1 indicates the band signal of the Unwritten State. Lane 2 and Lane 3 are controls showing the band position of the crosslinked complex of Data 1 to memory gate (Lane 2) and  of Data 2 to memory gate (Lane 3). Comparing Lane 2 in Figure 36 with Figure 35, Data 1 showed higher invasion efficiency. And in sequential input order, the memory gate successfully transited from the Unwritten State to the Written State (Lane 5). We also observed the state transition when a mixture of both two Data strands was added to the memory gate (Lane 4). The PAGE result shows a major band signal indicating transition to the Blocked State, with a nonsignificant noise band showing at the Written State position. We hypothesize that due to its longer toehold region, the binding of Data 2 strand to the memory gate is thermodynamically more favorable compared to that of Data 1 strand. And the covalent bound enhances the stability of the cross-linked complex of memory gate and Data 2, inhibiting the cross-links of the later added Data 1 strand. Overall, the memory gate can only transit to the Written State when the Data strands are added in sequential order. Otherwise, it transits to the Block State and prohibit the writing of Data 1.

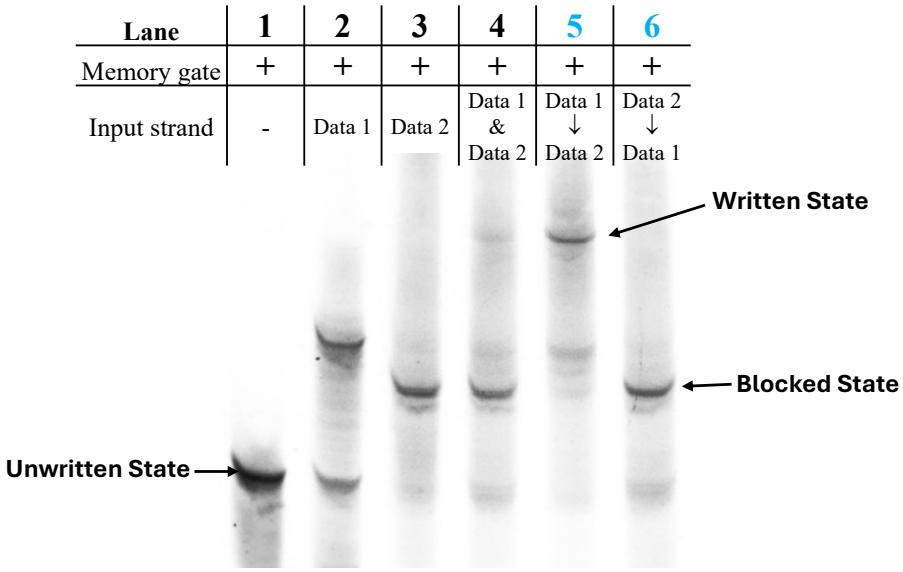


*Figure 36. 15% denaturing PAGE result of the photo-induced gate transition at 1:2 Gate: Data ratio. Lane 1: Memory gate only; Lane 2: Memory gate + Data 1; Lane 3: Memory gate + Data*

*2; Lane 4: Memory gate + mixture of both Data strands; Lane 5: Data strands added in sequential order; Lane 6: Data strands added in reverse order.*

### 4.4.2 The significance of $^{CNV}$K in memory gate transition

To investigate the significance of $^{CNV}$K in memory gate transition, the state transition was compared between photo-irradiated samples and non-irradiated controls with Native PAGE analysis. After adding the corresponding Data strand, reaction mixture was photo-irradiated at 385 nm for 10 min then incubated at 37°Cfor 20 min for the photo-irradiated (Photo-On) samples. The non-irradiation (Photo-OFF) sample mixtures are only incubated at 37°C for 30 min. Fig. 37 shows the 15% Native PAGE result comparing the Photo-ON and Photo-OFF products. The concentration of the Data strands was maintained at a two-fold molar excess relative to the memory gate. When Data strands were added to the memory gate in sequential order, both the photo-ON sample and Photo-OFF sample (Lane 5 and Lane 10) shows successful transition to the Written Sate. Conversely, when Data strands were added in reverse order, while Photo-OFF control (Lane 11) still exhibits a partial transition to the Written State, which is driven by the equilibrium toehold-mediated strand displacement reaction, Photo-ON sample (Lane 6) showed only Block State signal. This indicates that the cross-link of memory gate and Data 2 enhanced the stability of the resulting complex, forming a Blocked State resistant to the strand displacement reaction mediated by Data 1. Therefore, incorporation of $^{CNV}$K is crucial for the functioning of the memory gate.

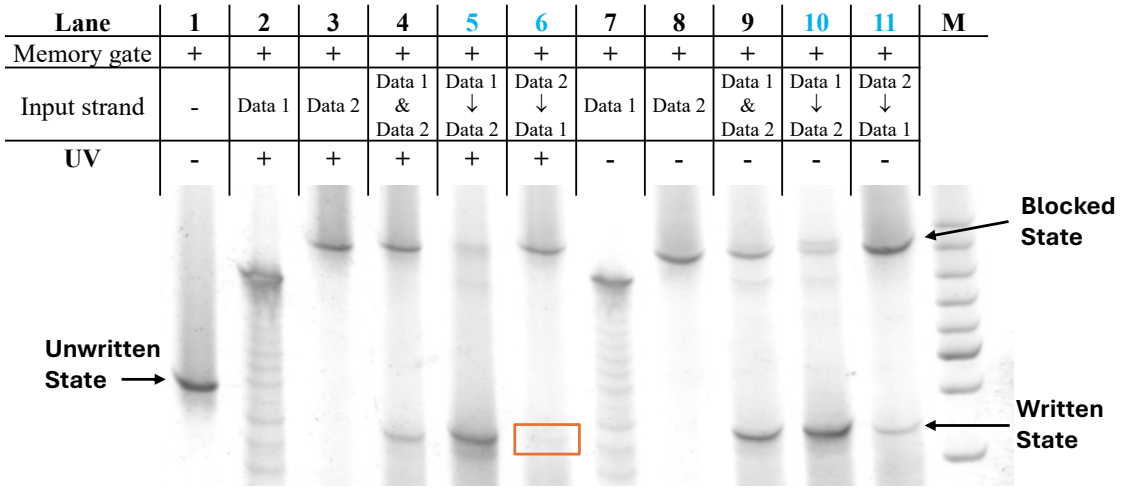


*Figure 37. 15% Native PAGE result of Photo-ON and Photo-OFF experiments. Lane 1: Memory gate only. Lane 2 ~ Lane 6 are Photo-ON condition. Lane 2: Memory gate + Data 1; Lane 3: Memory gate + Data 2; Lane 4: Memory gate + mixture of both Data strands; Lane 5: Data strands added in sequential order; Lane 6: Data strands added in reverse order. Lane 7 ~ Lane 11 are same as Lane 2 ~ Lane 6, under Photo-OFF condition.*

## 4.4.3 Ultra-fast kinetics of photo-induced memory gate transition

$^{CNV}$K-incorporated invading strands are proven to accelerate strand displacement reaction. Therefore, we conducted the state transition experiment under a controlled short photo-irradiation duration. After adding the Data strand, the reaction mixture was only photo-irradiated for 10s, 30 s, 60 s, and 300 s. The resulting products are evaluated by both Denaturing and Native PAGE analysis (Figure 38). When Data strands were added in sequential order, with the increase of photo-irradiation duration, the band signal of Written State also increased (Lane 4, 6, 8 and 10). While in reverse input order, 60 s photo-irradiation was sufficient to transit the gate to a robust Blocked State (Lane 9 in Figure 38. b). When photo-irradiation duration is less then 60 s, Native PAGE indicates slight noise band signal of Written State (Lane 5 and 6 in Figure 38. b).

a). 15% Denaturing PAGE

| Lane | 1 | 2 | 3 | 4 | 5 | 6 | 7 | 8 | 9 | 10 | 11 |
|---|---|---|---|---|---|---|---|---|---|---|---|
| Memory gate | + | + | + | + | + | + | + | + | + | + | + |
| Input strand | - | Data 1 ↓ Data 2 | Data 2 ↓ Data 1 | Data 1 ↓ Data 2 | Data 2 ↓ Data 1 | Data 1 ↓ Data 2 | Data 2 ↓ Data 1 | Data 1 ↓ Data 2 | Data 2 ↓ Data 1 | Data 1 ↓ Data 2 | Data 2 ↓ Data 1 |
| UV | - | 10 min | 10 min | 10 s | 10 s | 30 s | 30 s | 60 s | 60 s | 300 s | 300 s |

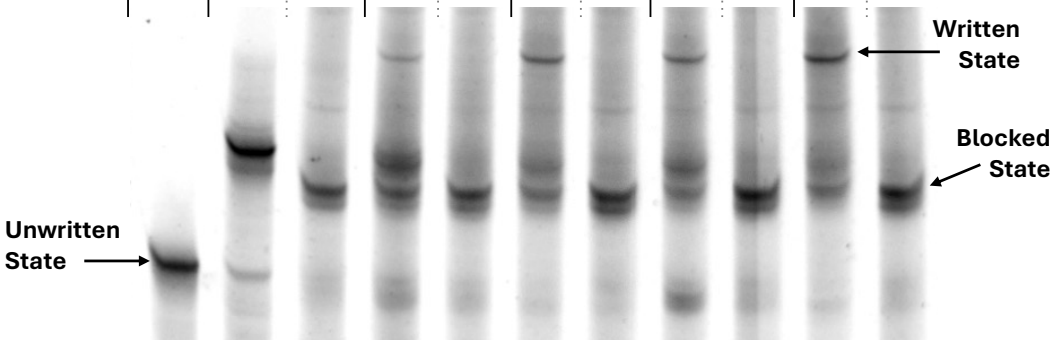


b). 15% Native PAGE

| Lane | 1 | 2 | 3 | 4 | 5 | 6 | 7 | 8 | 9 | 10 | 11 |
|---|---|---|---|---|---|---|---|---|---|---|---|
| Memory gate | + | + | + | + | + | + | + | + | + | + | + |
| Input strand | - | Data 1 ↓ Data 2 | Data 2 ↓ Data 1 | Data 1 ↓ Data 2 | Data 2 ↓ Data 1 | Data 1 ↓ Data 2 | Data 2 ↓ Data 1 | Data 1 ↓ Data 2 | Data 2 ↓ Data 1 | Data 1 ↓ Data 2 | Data 2 ↓ Data 1 |
| UV | - | 10 min | 10 min | 10 s | 10 s | 30 s | 30 s | 60 s | 60 s | 300 s | 300 s |

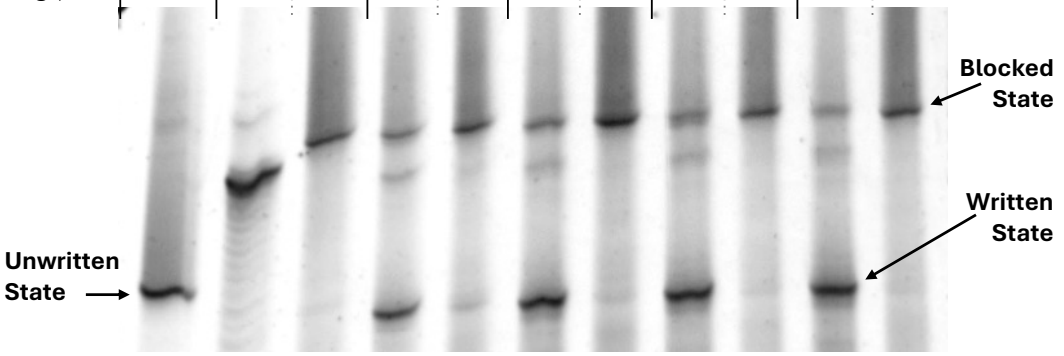


*Figure 38. Photo-induced memory gate transition under short photo-irradiation. a). 15% Denaturing PAGE result. Lane 1: Memory gate only; Lane 2: Memory gate + Data 1; Lane 3: Memory gate + Data 2; Lane 4: Data strands added in sequential order; Lane 6: Data strands added in reverse order. Same for Lane 6 and 7, Lane 8 and 9, Lane 10 and 11. Mixtures were photo-irradiated every time after adding the corresponding Data strand, photo-irradiation duration is noted on each lane. b). 15% Native PAGE result.*

## 4.4.4 Discussion

In this chapter, we successfully constructed a 2-input photo-induced DNA memory gate that utilizes the order of input signals to determine its final state. The

device operates on the principles of Toehold-Mediated Strand Displacement (TMSD), and innovated by incorporation of $^{CNV}$K to overcome the inherent reversibility of traditional DNA logic circuits. The significance of our design lies in its ability to lock in a specific state based on input history. As demonstrated in the sequential addition experiments (Data 1 followed by Data 2), the gate successfully transitions to the "Written State". Conversely, when the input order is reversed (Data 2 followed by Data 1), the system locks in a robust "Blocked State".

The crucial role of $^{CNV}$K is highlighted by the comparison between Photo-ON and Photo-OFF conditions (Figure 37). In standard TMSD systems without photo-cross-linking (Photo-OFF), the "Blocked State" is thermodynamically unstable; given enough time, Data 1 could still gradually invade the memory gate. However, our Photo-ON results show that $^{CNV}$K creates a thermally irreversible covalent bond upon photo-irradiation. This "locks" Data 2 into place, permanently effectively sealing the toehold and preventing any subsequent writing by Data 1. This transforms the system from a reversible equilibrium reaction into a kinetic trap, ensuring high fidelity in information storage.

Furthermore, the system demonstrates thermodynamic selectivity. When both data strands are introduced simultaneously, the system preferentially defaults to the Blocked State. This is attributed to the longer toehold sequence of Data 2, which provides a thermodynamic advantage over Data 1, allowing it to bind and lock the gate first.

Finally, the kinetics of this transition are notable. As shown in the time-course analysis (Figure 38), a robust memory state can be established with as little as 60 seconds of photo-irradiation. This speed, combined with the irreversibility provided by CNVK, suggests that this memory motif is highly suitable for integration into larger, time-responsive molecular robots or complex DNA logic circuits where transient signals must be permanently recorded.

## 4.5 Reference:


1. Ralf Dahm. Friedrich Miescher and the discovery of DNA. Dev Biol ., 2005, 278(2), 274-288.
2. M E Jones, Albrecht Kossel. A biographical sketch. Yale J Biol Med ., 1953, 26(1), 80-97.
3. D Elson, E Chargaff. On the desoxyribonucleic acid content of sea urchin gametes. Experientia , 1952, 8(4), 143-145.
4. J. D. Watson, F. H. C. Crick. Molecular Structure of Nucleic Acids: A Structure for Deoxyribose Nucleic Acid. Nature . 1953, 171, 737–738.
5. Yurke B, Turberfield AJ, Mills AP Jr, Simmel FC, and Neumann JL. A DNA-fuelled molecular machine made of DNA, *Nature*, 406, 605-608 (2000)
6. F. C. Simmel, and B. Yurke. A DNA-based molecular device switchable between three distinct mechanical states, *Appl. Phys. Lett.*, 80, 5, 883-885 (2002)
7. Shin, J. S., and Pierce, N. A. Rewritable memory by controllable nanopatterning of DNA, *Nano letters*, 4, 5, 905-909 (2004)
8. M. Takinoue, and A. Suyama. Hairpin-DNA memory Using Molecular Addressing, *small*, 2, 11, 1244-1247 (2006)
9. L. Qian, and E. Winfree. A simple DNA gate motif for synthesizing large-scale circuits, *J. R. Soc.*, 8, 1281-1297 (2011)
10. Montagne K, Plasson R, Sakai Y, Fujii T, and Rondelez Y. Programming an in vitro DNA oscillator using a molecular networking strategy. *Mol Syst Biol.*, 7, 466 (2011)
11. D. Y. Zhang, and E. Winfree. Control of DNA Strand Displacement Kinetics Using Toehold Exchange, *J. AM. CHEM. SOC.*, 131, 17303-17314 (2009)
12. G. Seelig, D. Soloveichik, D. Y. Zhang, and E. Winfree. Enzyme-free nucleic acid logic circuits, *Science*, 314, 5805, 1585-1588 (2006)
13. N. Srinivas, J. Parkin, G. Seelig, E. Winfree, and D. Soloveichik. Enzyme-free nucleic acid dynamical systems, *Science*, 358, 6369, eaal2052 (2017)
14. Hagiya, M., Aubert-Kato, N., Wang, S., and Kobayashi, S. Molecular computers for molecular robots as hybrid systems. *Theoretical Computer Science*., 632, 4-20 (2016)
15. L. Qian, and E. Winfree. Scaling up digital circuit computation with DNA strand displacement cascades, Science, 332, 6034, 1196-1201 (2011)

16. X. Song, A. Eshra, C. Dwyer, and J. Reif. Renewable DNA seesaw logic circuits enabled by photoregulation of toehold-mediated strand displacement, *RSC Adv*., 7, 28130-28144 (2017)

# Chapter 5 Conclusion

## 5.1 General Conclusion

This dissertation has focused on the development and application of novel DNA manipulation strategies utilizing the ultra-fast photo-cross-linker, 3-cyanovinylcarbazole nucleoside ($^{CNV}$K). The primary objective was to overcome the limitations of conventional double-stranded DNA (dsDNA) recognition methods, specifically the requirements for prolonged incubation times, elevated temperatures, and complex probe designs. Through the development of Photo-induced Double Duplex Invasion (pDDI), Photo-induced Duplex Invasion (pDI), and a Photo-induced DNA Memory Gate, we have demonstrated that $^{CNV}$K serves as a versatile and powerful tool for both genetic engineering and DNA nanotechnology.

In Chapter 2, we established the pDDI strategy, which employed a pair of Forward and Reverse probes containing $^{CNV}$K and the inhibitor 5-cyanouridine ($^{C}$U). The method successfully achieved sequence-specific invasion of long-range dsDNA targets (200-mer and 190-mer). The primary strength of this approach was its ability to target long dsDNA sequences with high specificity. The use of $^{C}$U successfully suppressed unwanted inter-probe cross-linking and maintain the concentration of efficient working probes. However, confirmed via Job's plot analysis, we discovered the invasion independence of the pDDI probes, indicating the possibility of achieving duplex-invasion.

In Chapter 3, building upon the discovery of invasion independence of pDDI, we streamlined the method into pDI, which utilizes a single $^{CNV}$K-containing probe. pDI represents a significant leap forward in reaction kinetics. Unlike PNA or LNA-based invasion, which often require hours to days, pDI achieved maximum invasion efficiency (>90%) with only 60 second of photo-irradiation after incubation. And the pDI is reversible via 312 nm irradiation, and reusable after the photo-splitting. The most significant limitation of pDI is its ion dependence. As demonstrated, the invasion efficiency drops in high-salt conditions (e.g., 100 mM $Na^+$) due to the stabilization of

the target double helix. This restricts the immediate application of pDI probes in physiological environments or standard biological buffers.

In Chapter 4, we expanded the application of $^{CNV}$K-incorporated invasion probe from simple invasion systems to dynamic DNA nanotechnology system by constructing a Photo-induced DNA Memory Gate. This Photo-induced DNA Memory Gate motif introduced "statefulness" to DNA logic. By using $^{CNV}$K to form a thermally irreversible covalent bond, the system can lock the memory gate in specific states (Written or Blocked States) based on the order of input Data signals. This overcomes the inherent thermodynamic reversibility and instability of traditional toehold-mediated strand displacement circuits.

In conclusion, this dissertation confirms that $^{CNV}$K-mediated photo-cross-linking is not merely a method for connecting strands, but a kinetic driver that enables ultra-fast, sequence-specific, and state-locking manipulations of DNA. These properties open new horizons for the control of genetic information and the construction of advanced molecular machinery.

## 5.2 Future Perspectives

The research presented in this dissertation lays the groundwork for several promising avenues of future investigation. Chemical Modification for Physiological Stability: To address the ion dependence limitation of pDI observed in Chapter 3, future work should focus on enhancing the binding affinity of the invasion probe. Integrating $^{CNV}$K into chemically modified backbones, such as Peptide Nucleic Acids (PNA) and Locked Nucleic Acids (LNA), or making charged modifications, could provide the necessary thermodynamic advantage to invade dsDNA under high-salt, physiological conditions. With these potential resolution of the salt-dependence issue, the next logical step is the transition from *in vitro* to *in cellulo* systems. The reversible nature of $^{CNV}$K offers a unique opportunity for spatiotemporal control of gene expression. Future studies will need to address the delivery of $^{CNV}$K probes into the cell nucleus and

evaluate cytotoxicity. If successful, pDI could evolve into a potent "photo-antigene" therapeutic strategy, capable of silencing specific genes with a flash of light. Regarding the photo-induced DNA Memory Gate state transition, future research should aim to scale this motif into larger, integrated logic circuits capable of processing more input signals. By combining the locking mechanism of $^{CNV}$K with other DNA logic gates (AND, OR, NOT), it may be possible to construct "sequential logic circuits" that can record complex biological events or environmental histories within a molecular robot.

# List of Publications

## Articles:

1. H. Zumila, S. Sethi, Y. Watanabe, & K. Fujimoto, “Photo-Induced Ultra-Fast duplex invasion targeting Long-Range Double-Stranded DNA using artificial nucleotide” *ChemBioChem*, **2025**, 0, e202500626.
2. S. Sethi, H. Zumila, Y. Watanabe, J. Mo and K. Fujimoto, “UltraFast PhotoInduced double duplex DNA invasion into a 400-mer dsDNA target” *Bioorg. Med. Chem. Lett*. **2024**, *98*, 129597.

## International Conferences (7 presentations):

**1. The International Symposium on Nucleic Acids Chemistry**

**2021**: Zumila Halili, Nanami Watanabe, Shigetaka Nakamura, Kenzo Fujimoto, “RNA FISH of 16S rRNA in *E. coli* using multiple probes containing ultrafast RNA photo-cross-linker”

**2023**: Zumila Hailili, Yasuha Watanabe, Toya Odai, Siddhant Sethi, Kenzo Fujimoto, “400 mer Double Duplex Invasion Via Ultra-Fast DNA Photo-Cross-Linking”

**2024**: Zumila Hailili, Mo Junling, Fujimoto Kenzo, “Towards chemical genomic manipulation: photochemical double-duplex invasion using ultra-fast photo-cross-linker”

**2025**: Zumila Hailili, Watanabe Yasuha, Nakamura Shigetaka, Fujimoto Kenzo, “Novel ultra-fast photo-triggered DNA manipulation for stable double-stranded nucleic acids such as genomic DNA”

**2. XXV International Round Table on Nucleosides, Nucleotides and Nucleic Acids**

**2024**: Zumila Hailili, Mo Junling, Fujimoto Kenzo, “Towards chemical genomic manipulation: photochemical double-duplex invasion using ultra-fast photo-cross-linker”

**3. The 84th Annual Meeting of the Japanese Cancer Association, International Cancer Meeting in Kanazawa**

**2025**: Zumila, Hailili, Huang Qingyuan, Fujimoto Kenzo, "Photochemical method inhibiting expression of c-myc gene by using photo-cross-linkable antisense oligonucleotides"

**4. The International Chemical Congress of Pacific Basin Societies**

**2025**: Zumila Hailili, Komeda Takeshi, Noda Tatsushi, Fujimoto Kenzo, "Photochemical double-duplex invasion (pDDI) and duplex-invasion (pDI) using 3-Cyanovinylcarbazole nucleoside ($^{CNV}$K)"

# Domestic Conferences (21 presentations):

**1. Hokuriku Area Annual Meeting of the Chemical Society of Japan, Kinki Branch**

**2019**: Zumila Hailili, 中村重孝, 藤本健造, "光照射時の DNA 情報を保存可能な光駆動型 DNA メモリーの開発"

**2020**: Zumila Hailili, Nakamura Shigetaka, Fujimoto Kenzo, "Photo-induced conformational change of hairpin memory dependent on the order of input DNA strands"

**2021**: Zumila Halili, Ichikawa Masakatsu, Nakamura Shigetaka, Fujimoto Kenzo, "Photo-induced aggregation and dispersion of liposomes using reversible ultrafast photo-cross-linking"

**2022**: Zumila Hailili, Sethi Siddhant, Fujimoto Kenzo, "Development of 3-Cyanovinylcarbazole Induced Ultra-fast Photocrosslinking Mediated DNA Circuits"

**2023**: Zumila Hailili, Hirano Ayumu, Watanabe Yasuha, Mo Junling, Sethi Siddhant, Fujimoto Kenzo, "Development of photo-triggered DNA double-strand invasion method targeting long chain oligonucleotides"

**2025**: Zumila Hailili, Fujimoto Kenzo, "Precise Regulation of DNA Circuits Using an Ultratast DNA Photocrosslinker"

**2. The Annual Meeting of the Chemical Society of Japan**

**2020**: Zumila Hailili, Kitamura Kanon, Nakamura Shigetaka, Fujimoto Kenzo, "Development of photo-induced gate transition using reversible DNA photo-cross-linking"

**2021**: Zumila Hailili, Kitamura Kanon, Nakamura Shigetaka, Fujimoto Kenzo, "Photo regulated DNA memory gate system using DNA photo-cross-linker"

**2023**: Zumila Hailili, Sethi Siddhant, Fujimoto Kenzo, "Development of DNA Circuits Using 3-cyanovinylcarbazole Induced Ultra-fast Photo-crosslinking"

**2024**: Zumila Hailili, Mo Junling, Fujimoto Kenzo, "Development of photo-triggered DNA double-strand invasion method targeting long chain oligonucleotides oriented to genome manipulation"

**3. The Annual Meeting of Japanese Society for Chemical Biology**

**2023**: Zumila Hailili, Nanami Watanabe, Siddhant Sethi, Kenzo Fujimoto, "Wash-free RNA FISH of 16S rRNA in E. coli using Multiple Ultrafast Photo-cross-linkable RNA Probes"

**2024**: Zumila Hailili, Mo Junling, Kenzo Fujimoto, "Development of photochemical double-strand invasion method targeting long-range DNA using artificial nucleic acids"

**4. The Symposium on Bio-Related Chemistry**

**2020**: Zumila Hailili, Nakamura Shigetaka, Fujimoto Kenzo, "Photo-driven conformational change of DNA reflecting the state during ultrafast DNA photo-cross-linking"

**2021**: Zumila Halili, Ichikawa Masakatsu, Nakamura Shigetaka, Fujimoto Kenzo, "Regulation of liposome aggregation using ultrafast DNA photocrosslinking"

**2022**: Zumila Hailili, Sethi Siddhant, Nakamura Shigetaka, Fujimoto Kenzo, "Construction of DNA circuits by ultra-fast DNA photo-cross-linking for photo-induced DNA memory"

**2023**: Zumila Hailili, Huang Qingyuan, Mo Junling, Fujimoto Kenzo, "A Novel Biological Method for Cryptographic DNA Using Ultrafast DNA Photo-cross-linker"

**2024**: Zumila Hailili, Fujimoto Kenzo, “Photochemical invasion of long DNA duplex using artificial nucleic acid probes for genome manipulation”

**5. The Annual Meeting of Nucleic Acids Therapeutics Society of Japan**

**2023**: Zumila Hailili, Watanabe Nanami, Sethi Siddhant, Fujimoto Kenzo, “Multi-probe RNA FISH of 16S rRNA in E. coli using Photo-cross-linker D-threoninol”

**2024**: Zumila Hailili, Mo Junling, Watanabe yasuha, Fujimoto Kenzo, “Photo-responsive Oligonucleic Acid double strand DNA Invasion Method for Long DNA Strands toward Genome Manipulation”

**2025**: Zumila Hailili, Huang Qingyuan, Fujimoto Kenzo, “Photochemical antisense method inhibiting c-Myc expression using ultra-fast photocrosslinker”

**6. The 11th Molecular Cybernetics and 55th Molecular Robotics Regular Meeting**

**2024**: (invited oral presentation) Zumila Hailili, “Photo-chemical duplex invasion method towards genome manipulation”

# Appendix

## I. Experiment Instruments

**DNA Synthesis**

NIHON TECHNO SERVICE CO., LTD, NTS M-2-MX DNA/RNA Synthesizer

**High-Pressure Liquid Chromatography (HPLC)**

JASCO, PU-980, Intelligent HPLC Pump

JASCO, UV-970, Intelligent UV-VIS Detector

JASCO, HG-980-31, Solvent Mixing Module

JASCO, DG-980-50, 3-Line Degasser

Nacalai Tesque, COSMOSIL 5C18:AR-II (4.6x 150), HPLC Column

**UV-LED**

OmniCure, LX405S, 9500 mW/cm$^2$, 385 nm LED light

**Polyacrylamide Gel Electrophoresis (PAGE) Equipment**

BIO-RAD, Power Pac Basic

FUJIFILM, LAS-3000 Luminescent Image Analyzer

**Constant Temperature Incubator (for PAGE Analysis)**

TAITEC Corp., BioShaker BR-21FH

**UV-Vis Spectrophotometer**

JASCO, V-630 Bio UV-Vis Spectrophotometer

**Thermal Cycler**

Eppendorf, Mastercycler® gradient

**Low temperature Bath**

EYELA, NCB-1200, Low temperature Bath

**Concentrator**

Thermo Scientific, The SAVANT DNA 120 SpeedVac Concentrator

**Freeze Dryer**

Labconco, FreeZone Legacy 2.5 L Benchtop Freeze Dry System

Asahi Life Science, Vacuum Pump ALS-50AC

# II. Experiment Reagents

**Glen Research Corp.**

dA-CE phosphoramidite

dmf-dG-CE phosphoramidite

Ac-dC-CE phosphoramidite

dT-CE phosphoramidite

Acetonitrile, anhydrous

Cap mix A (Tetrahydrofuran/Pyridine/Acetic Anhydride)

Cap mix B (10% 1 -Methylimidazole in Tetrahydrofuran)

Activatior (5-(Benzylthio)-1H-Tetrazole in Anhydrous Acetonitrile)

Oxidizing Solution (0.02 M Iodine in Tetrahydrofuran/Pyridine/Water)

**FUJIFILM Wako Pure Chemical Corp.**

Distilled water

Acrylamide

N, N’-Methylenebis (acrylamide)-HG

Ammonium Peroxodisulfate

Boric Acid

N, N, N’, N’-Tetramethyl-ethylenediamine

2-Amino-2-hydroxymethyl-1,3-propanediol

Sodium chloride

Formamide

Ammonia solution

50 mM Ammonium format

Deblocking Solution-1 (3w/v% Trichloroacetic Acid, Dichloromethane Solution)

Triethylamine

Dichloromethane, Super Dehydrated

**DOJINDO LABORATORIES**

2Na (EDTA·2Na)

**Nacalai Tesque, Inc.**

0.2 mol/L-Cacodylate Buffer Solution (pH 7.4)

Urea

**Sigma-Aldrich Japan, Inc.**

Acetonitrile

**Promega, Corp.**

Blue/Orange 6X Loading Dye

10 bp DNA step ladder

25 bp DNA step ladder

100 bp DNA step ladder

**Thermo Fisher Scientific Inc.**

SYBR™ Gold Nucleic Acid Gel Stain (10,000X Concentrate in DMSO)

**Hirano junyaku**

Forward-Template (200 mer):

5’-

TTTGGAATCCTAGTTGGCAGTATGGAGGCATTGTTCTCTGACCAATGAATCTG
CCGAGAGAGAGGATTAACCCGCATTGGAACGAAAAGTTTGTTTTTTATGAGC
CAGCCTTCGGTTGTCGATATGAGGATCTCGCGATTGAAAAGTTCATGTCTCCG
TCTAATCACGATGTGAGTGGTGGGGGGTACTTCATACAAGAT-3’

Reverse-Template (190 mer):

5’-

GTATGAAGTACCCCCCACCACTCACATCGTGATTAGACGGAGACATGAACTT
TTCAATCGCGAGATCCTCATATCGACAACCGAAGGCTGGCTCATAAAAAACA
AACTTTTCGTTCCAATGCGGGTTAATCCTCTCTCTCGGCAGATTCATTGGTCA
GAGAACAATGCCTCCATACTGCCAACTAGGATT-3’

**Fasmac Co., Ltd**

Memory Gate (124 nt):

5’-GGCCAAGAAGCAGAAACGAACACACAACGCCGACAACCAAGGACA
TTTTTGTCCTTGGTTGTCGTCTTGTCTGTGTCCCGGCTTTGTGCTCTCTGCGTT
GTGTGTTCGTTTCTGCTTCTTGGCC -3’

*10X TBE Buffer*

2-Amino-2-hydroxymethyl-1,3-propanediol (108.0 g), Boric Acid (55.0 g), 0.5 M EDTA·2Na(2H2O) (3.7 g) were dissolved and diluted to 1.0 L with distilled water.

*10% APS*

Ammonium Peroxodisulfate (0.1 g) dissolved in 0.9 mL distilled water.

*Denaturant*

Urea (2.0 g) was dissolved in 10 mL Formamide.

*8% AA Stock Containing 8 M Urea (1000 mL)*

Acrylamide (77.3 g), N, N'-Methylenebis(acrylamide) (2.7 g), and urea (480.0 g) was dissolved in 100 mL 10X TBE buffer and diluted to 1000 mL with distilled water.

*8% AA Stock (1000 mL)*

Acrylamide (77.3 g) and N, N'-Methylenebis(acrylamide) (2.7 g) was dissolved in 100 mL 10X TBE buffer and diluted to 1000 mL with distilled water.

*8% AA Denaturing Gel*

5 mL of 8% AA solution Containing 8 M Urea mixed with 25 µL 10% APS, TEMED (N, N, N', N'-Tetramethylethy lene diamine) 2.5 µL was added and swirled to mixed. Cast the gel solution and let it polymerize for 1 - 2 hours.

*8% AA NATIVE Gel*

5 mL of 8% AA solution mixed with 25 µL 10% APS, TEMED (N, N, N', N'-Tetramethylethy lene diamine) 2.5 µL was added and swirled to mixed. Cast the gel solution and let it polymerize for 1 - 2 hours.

*15% AA Stock Containing 8 M Urea (1000 mL)*

Acrylamide (145.0 g), N, N'-Methylenebis(acrylamide) (5.0 g), and urea (480.0 g) was dissolved in 100 mL 10X TBE buffer and diluted to 1000 mL with distilled water.

*15% AA Stock (1000 mL)*

Acrylamide (145.0 g) and N, N'-Methylenebis(acrylamide) (5.0 g) was dissolved in 100 mL 10X TBE buffer and diluted to 1000 mL with distilled water.

*15% AA Denaturing Gel*

5 mL of 15% AA solution Containing 8 M Urea mixed with 25 µL 10% APS, TEMED (N, N, N', N'-Tetramethylethy lene diamine) 2.5 µL was added and swirled to mixed. Cast the gel solution and let it polymerize for 1 - 2 hours.

*15% AA NATIVE Gel*

5 mL of 15% AA solution mixed with 25 µL 10% APS, TEMED (N, N, N', N'-Tetramethylethy lene diamine) 2.5 µL was added and swirled to mixed. Cast the gel solution and let it polymerize for 1 - 2 hours.

# III. Scheme for synthesizing of $^{CNV}$K-amidite

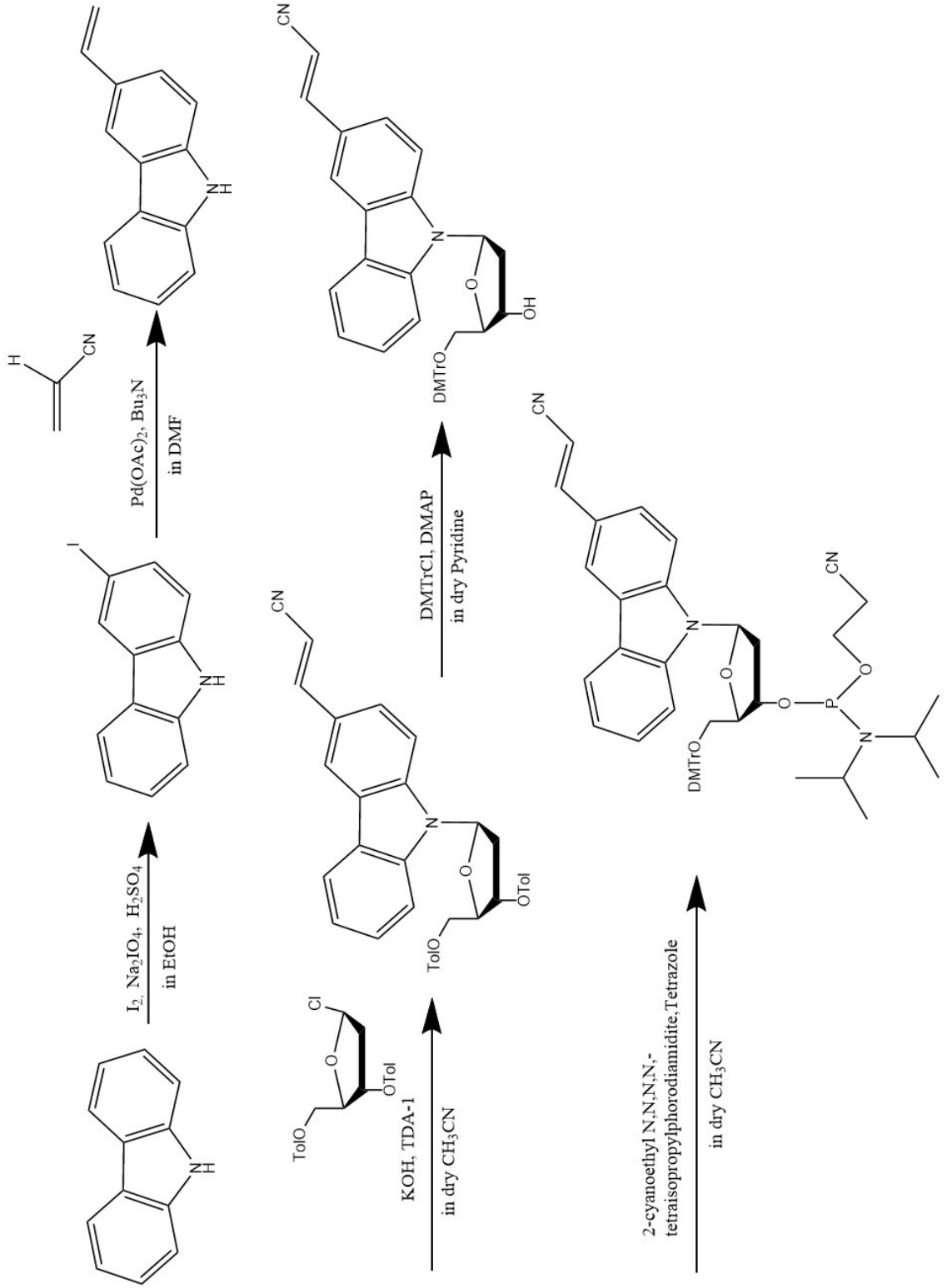

# IV. Scheme for synthesizing of Trifluorothymidine ($^{TF}$T) / $^{C}$U-amidite

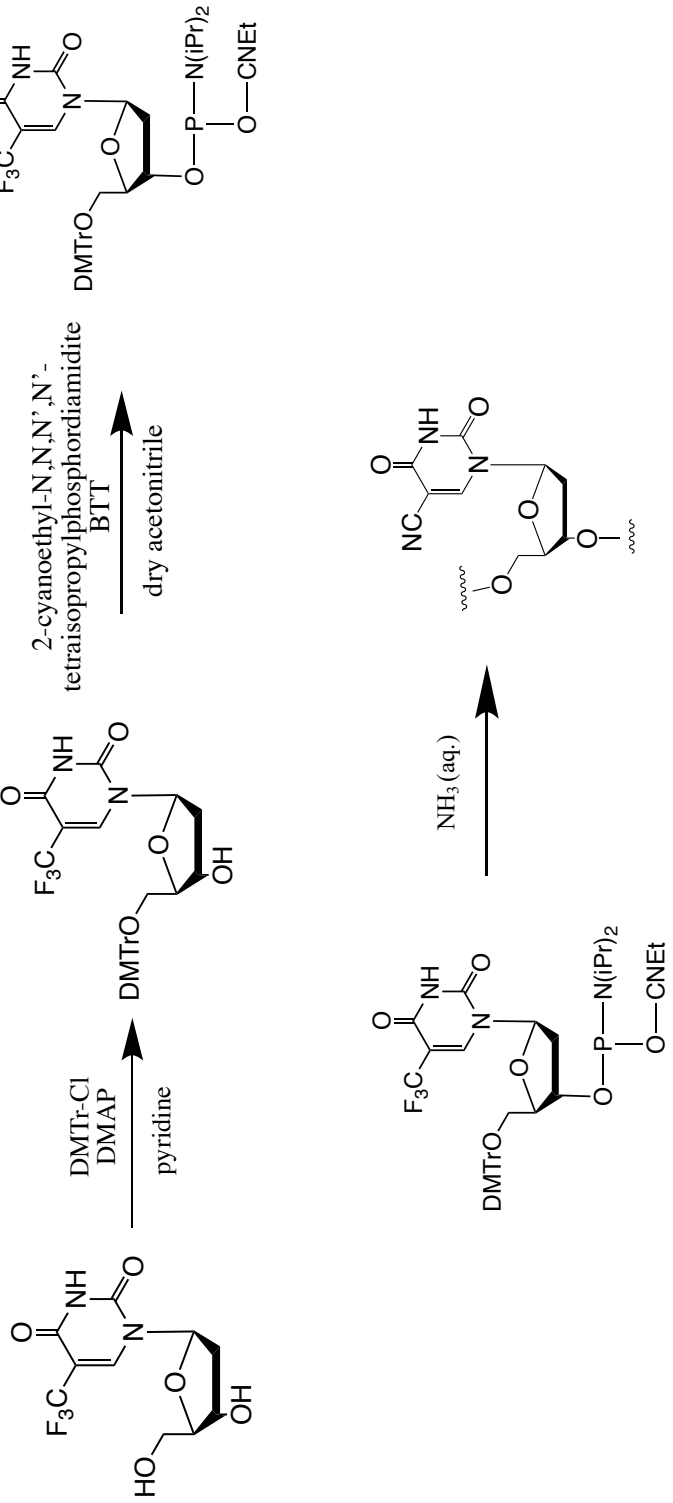

# V. ODN Purification

i). Cleavage and Deprotection

Cleavage from the solid support was performed with 2 mL 28% Ammonium Format under room temperature for 1 hour. Following the deprotection process by 4 h incubation under 65℃. Samples are concentrated via 2 hours Speed Vac. Crude ODNs, with 4,4′-dimethoxytrityl (DMTr) protecting group on its 5'-end, obtained after Speed Vac was further purified with high-pressure liquid chromatography (HPLC).

ii). HPLC Purification of Crude ODN

HPLC condition is as follows.

Flow rate: 1.0 mL/min

Wavelength setting: 260 nm

Column temperature: room temperature

Buffer A: 50 mM Ammonium format

Buffer B: Acetonitrile (Sigma-Aldrich Japan, Inc.)

Injection: 50 μL

Buffer gradient: Buffer A 90%, Buffer B 10% → Buffer A 60%, Buffer B 40% in 30 min

Peak fractions were collected and freeze-dried for removing DMTr protecting Group.

iii). Detritylation

Detritylation was carried out by adding deblocking solution 50 μL/tube on ice. Tubes that turned orange indicating presence of DMTr protective group were kept, and let stand for 15 min. 50 μL of dichloromethane : Triethylamine = 1 : 1 solution was added to each kept tubes to remove the free DMTr from the solution. Tubes were let stand under room temperature for 10 min before concentrated to dryness with Speed Vac in 30 min.

iv). HPLC Purification of ODN (DMT-OFF)

ODNs (DMT-OFF) were dissolved in distilled water and HPLC purification was performed. HPLC condition is as follows.

Flow rate: 1.0 mL/min

Wavelength setting: 260 nm

Column temperature: room temperature

Buffer A: 50 mM Ammonium format

Buffer B: Acetonitrile (Sigma-Aldrich Japan, Inc.)

Injection: 50 μL

Buffer gradient: Buffer A 98%, Buffer B 2% → Buffer A 65%, Buffer B 35% in 30 min

Peak fractions were collected and freeze-dried for MALDI-TOF mass spectrometry analysis.